12-2011

Quantification of stochastic uncertainty propagation for Monte Carlo depletion methods in reactor analysis

Quentin Thomas Newell
University of Nevada, Las Vegas

QUANTIFICATION OF STOCHASTIC UNCERTAINTY PROPAGATION FOR MONTE CARLO DEPLETION METHODS IN REACTOR ANALYSIS

by

Quentin Thomas Newell

Bachelor of Science in Mechanical Engineering
University of Texas at Austin
2003

Master of Science Engineering in Mechanical Engineering
University of Texas at Austin
2005

A dissertation submitted in partial fulfillment
of the requirements for the

Doctor of Philosophy in Mechanical Engineering

Mechanical Engineering Department
Howard R. Hughes College of Engineering
The Graduate College

University of Nevada, Las Vegas
December 2011

THE GRADUATE COLLEGE

We recommend the dissertation prepared under our supervision by

Quentin Thomas Newell

entitled

Quantification of Stochastic Uncertainty Propagation for Monte Carlo Depletion Methods in Reactor Analysis

be accepted in partial fulfillment of the requirements for the degree of

Doctor of Philosophy in Mechanical Engineering
Department of Mechanical Engineering

Robert Boehm, Committee Chair

Denis Beller, Committee Member

Charlotta Sanders, Committee Member

Gary Cerefice, Committee Member

Mark Williams, Committee Member

Julie Staggers, Graduate College Representative

Ronald Smith, Ph. D., Vice President for Research and Graduate Studies
and Dean of the Graduate College

December 2011

ABSTRACT

Quantification of Stochastic Uncertainty Propagation for Monte Carlo Depletion Methods in Reactor Analysis

by

Quentin Thomas Newell

Dr. Robert Boehm, Examination Committee Chair
Professor of Mechanical Engineering
University of Nevada, Las Vegas

The Monte Carlo method provides powerful geometric modeling capabilities for large problem domains in 3-D; therefore, the Monte Carlo method is becoming popular for 3-D fuel depletion analyses to compute quantities of interest in spent nuclear fuel including isotopic compositions. The Monte Carlo approach has not been fully embraced due to unresolved issues concerning the effect of Monte Carlo uncertainties on the predicted results.

Use of the Monte Carlo method to solve the neutron transport equation introduces stochastic uncertainty in the computed fluxes. These fluxes are used to collapse cross sections, estimate power distributions, and deplete the fuel within depletion calculations; therefore, the predicted number densities contain random uncertainties from the Monte Carlo solution. These uncertainties can be compounded in time because of the extrapolative nature of depletion and decay calculations.

The objective of this research was to quantify the stochastic uncertainty propagation of the flux uncertainty, introduced by the Monte Carlo method, to the number densities for the different isotopes in spent nuclear fuel due to multiple depletion time steps. The research derived a formula that calculates the standard deviation in the nuclide number

densities based on propagating the statistical uncertainty introduced when using coupled Monte Carlo depletion computer codes. The research was developed with the use of the TRITON/KENO sequence of the SCALE computer code.

The linear uncertainty nuclide group approximation (LUNGA) method developed in this research approximated the variance of ψ_N term, which is the variance in the flux shape due to uncertainty in the calculated nuclide number densities.

Three different example problems were used in this research to calculate of the standard deviation in the nuclide number densities using the LUNGA method. The example problems showed that the LUNGA method is capable of calculating the standard deviation of the nuclide number densities and k_{inf}. Example 2 and Example 3 demonstrated a percent difference of much less than 1 percent between the LUNGA and the exact methods for calculating the standard deviation in the nuclide number densities.

The LUNGA method was capable of calculating the variance of the ψ_N term in Example 2, but unfortunately not in Example 3. However, both Example 2 and 3 showed the contribution from the ψ_N term to the variance in the number densities is minute compared to the contribution from the ψ_S term and the variance and covariances of the number densities themselves.

This research concluded with validation and verification of the LUNGA method. The research demonstrated that the LUNGA method and the statistics of 100 different Monte Carlo simulations agreed with 99 percent confidence in calculating the standard deviation in the number densities and k_{inf} based on propagating the statistical uncertainty in the flux introduced by using the Monte Carlo method in coupled Monte Carlo depletion calculations.

To, In Loving Memory, Grandma

ACKNOWLEDGMENT

I have a number of people I would like to thank for their technical and personal support. I want to thank Oak Ridge National Laboratory (ORNL) for the opportunity to be an intern at the laboratory and have access to the facility and staff. I want to thank the staff at ORNL, of which there are to many to list, for their support with the SCALE computer code, and general insights and recommendations for this project. I want to especially thank Dr. Mark Williams for his direction and instruction during this project. I want also like to thank Dr. Mark DeHart for his guidance, Dr. Matthew Jessee for his insights and programming assistance, and Mr. Ian Gauld for his aid with SCALE.

I want to thank the University of Nevada, Las Vegas for giving me the opportunity to start this research. I want to thank Dr. Denis Beller and Dr. Charlotta Sanders for their advice during this project. I would also like to thank all of my committee members for their time.

I want to thank my extended family for their support and encouragement during this time in my life. Finally, I want to thank Mom and Dad for all their love and support during these years; they helped make this possible believing in me. They inspire me to do my best and taught me to strive for excellence.

I have dedicated this dissertation to my Grandma, who passed away earlier this year.

TABLE OF CONTENTS

LIST OF TABLES

LIST OF FIGURES

CHAPTER 1

INTRODUCTION

The increasing complexity in reactor designs suggests a need to reexamine methods applied to spent fuel characterization. The ability to accurately predict the nuclide composition of depleted reactor fuel is important in a wide variety of applications including, but not limited to, design, licensing, operation of commercial/research reactors, and spent fuel transport/storage systems. Some of the new complex design projects like the Generation IV power reactors [5] or space reactors might also require calculational methods that provide accurate prediction of the isotopic inventory [17, 1]. Coupled depletion calculations are typically applied in characterization of fuel performance, lattice design, and spent fuel source terms for high-fidelity reactor analysis [15]. Such methods apply a detailed neutron transport solution for a core or assembly lattice as a function of burnup, while changes in isotopic inventories are estimated using a numerical approximation for the Bateman equations for radioactive transmutation [15, 19, 1]. Coupled Monte Carlo (MC) depletion calculations use a Monte Carlo computer code to solve the transport equation and another computer code to perform the depletion of the isotopic inventories. These depletion calculations are solved in an iterative process (over the depletion period) where the flux (solved with the Monte Carlo method) is used as input to the depletion program that solves and updates the isotopic inventories for the next transport calculation [19].

Deterministic solutions are generally favored over Monte Carlo solutions for the transport phase of such depletion analyses because of their ability to generate an accurate

spatial distribution of fluxes over a complete problem domain. The Monte Carlo method; however, can provide powerful geometric modeling capabilities for large problem domains in three dimensions (3-D) and usually involve less approximation of energy and geometry than deterministic solutions [22]; therefore, the Monte Carlo method is becoming more popular for 3-D fuel depletion analyses to compute various quantities of interest including isotopic compositions of spent nuclear fuel. Such approaches have not yet been fully embraced due to unresolved issues relative to the effect of Monte Carlo uncertainties on predicted results.

Use of the Monte Carlo method to solve the transport equation introduces stochastic uncertainty in computed fluxes. These fluxes are used to collapse cross sections, estimate power distributions, and deplete the fuel within depletion calculations; therefore, the predicted number densities contain random uncertainties from the Monte Carlo solution. These uncertainties can be compounded in time because of the extrapolative nature of depletion and decay calculations. Additionally, such errors are known to have a spatial component. The flux errors will be smallest in the most reactive regions of the fuel (where greater sampling occurs) and will be larger in the lower flux regions of the fuel. There is a need to determine and understand statistical uncertainties and their propagation in Monte Carlo depletion calculations.

According to a 2006 workshop on simulation and modeling for advanced nuclear energy systems, co-sponsored by the Department of Energy (DOE), one of the key needs of the Global Nuclear Energy Partnership (GNEP) program is to have available predictive simulation tools that include a sound and credible prediction of uncertainties and biases [17]. These are particularly important for the design of new technologies and facilities

based on novel processes. The attendees at the workshop discussed uncertainty propagation for systems as one of three primary research challenges in the subject of predictive estimation for application in GNEP [17]. Also, in a presentation at the Monte Carlo user's group meeting in the UK, the Monte Carlo N-Particle eXtended (MCNPX) team from Los Alamos National Laboratory (LANL) discussed a new feature in MCNPX for burnup and depletion calculations. In this meeting, they also acknowledged, as part of future work, the need for calculating number density error and error propagation during the depletion process. The MCNPX team also discussed the need for benchmarking Monte Carlo depletion calculations [10].

Monte Carlo methods are a powerful and proven tool for the nuclear engineering community. Coupled Monte Carlo depletion methods add the power of the Monte Carlo method with a depletion code. This allows for the analysis of isotopic inventories, fuel performance, lattice design and spent fuel source terms [15]. Monte Carlo methods are based on probabilities and therefore have stochastic uncertainties and propagated uncertainties in the results of a Monte Carlo depletion calculation. However, these propagated uncertainties are not reported to the user. Understanding and quantification of the stochastic uncertainty propagation in Monte Carlo depletion methods will give users more confidence in the results of this method and will also give users the ability to use this method in addition to deterministic depletion methods. Quantification of the stochastic uncertainty propagation in Monte Carlo depletion methods will produce better predictions of isotopic compositions, which are essential to optimize transmutation, recycling and waste disposal.

CHAPTER 2

LITERATURE REVIEW

Monte Carlo calculations work well for eigenvalues because these are global quantities that converge much faster than local spatial quantities [15, 13]. For example, the average flux over the entire problem domain is a relatively easy quantity to estimate because every particle history contributes to this value [13]. However, if the quantity of interest is the flux in a particular region (volume), then only the particles passing through that region will contribute to the estimate of the flux in that region [15, 27]. Fewer particles mean less sampling in that region, which leads to higher uncertainties as well as slower convergence [15, 27]. The flux is a quantity that is not directly calculated in a Monte Carlo calculation but is rather computed based on some form of estimator. For example, Monte Carlo N-Particle (MCNP), MCNPX, and KENO V.a use a track-length estimator to compute the fluxes in a Monte Carlo simulation [15, 27]. The track-length estimator is favored over the collision estimator for the flux because with the track length estimator every particle that passes through the volume contributes to the flux, whereas with the collision estimator only those particles that collide in the volume will contribute to the flux [13]. The track-length estimator is usually reliable because there are frequently many tracks in a volume (compared to the number of collisions), which leads to many contributions to the estimator [27]. The flux in a given volume (cell) is estimated by summing the product of track lengths and weight of each particle in that volume and then dividing by the given volume, or $\bar{\phi}_v = WT_l / V$ where W is the weight of

the particles, T_l is the track lengths, V is the volume, and $\bar{\phi}_v$ is the average flux in the given volume [15, 27].

The nature of Monte Carlo simulations makes it extremely difficult to obtain accurate fluxes in locations that are far removed from the most reactive region of an analysis domain. Since the accuracy of the neutron flux is therefore a function of position in Monte Carlo simulations, the accuracy of the depletion solution (isotopic predictions) is also spatially distributed [4]. For axially long rods, such as those used in commercial light water reactors (LWR), the axial variation in the neutron flux produces a non-uniform burnup distribution along the axial length of nuclear reactor fuel assemblies. The axial distribution is typically characterized by the end regions of the fuel, which have a significantly lower burnup value with respect to the assembly-average burnup value. Figure 1 shows an example of the axial burnup distribution of a fuel assembly [24]. The under-burned regions are dominant in terms of reactivity and must be represented correctly to ensure subcritical margins for fuels that have a moderate to high burnup (beyond 20 gigawatt-days/metric ton uranium – GWd/MTU). Numerous studies have been done to quantify the reactivity effect associated with axial burnup distributions [24]. In general, the authors of these studies have shown that assuming a uniform axial burnup is conservative for fuels with low burnups but becomes increasingly non-conservative for fuels as the burnup increases [24]. This means that for moderate to high burnups, the uniform axial burnup distribution assumption underestimates the reactive in the system, and as an approximate rule-of-thumb the effect is on the order of 1%Δk/10 GWd/MTU [25].

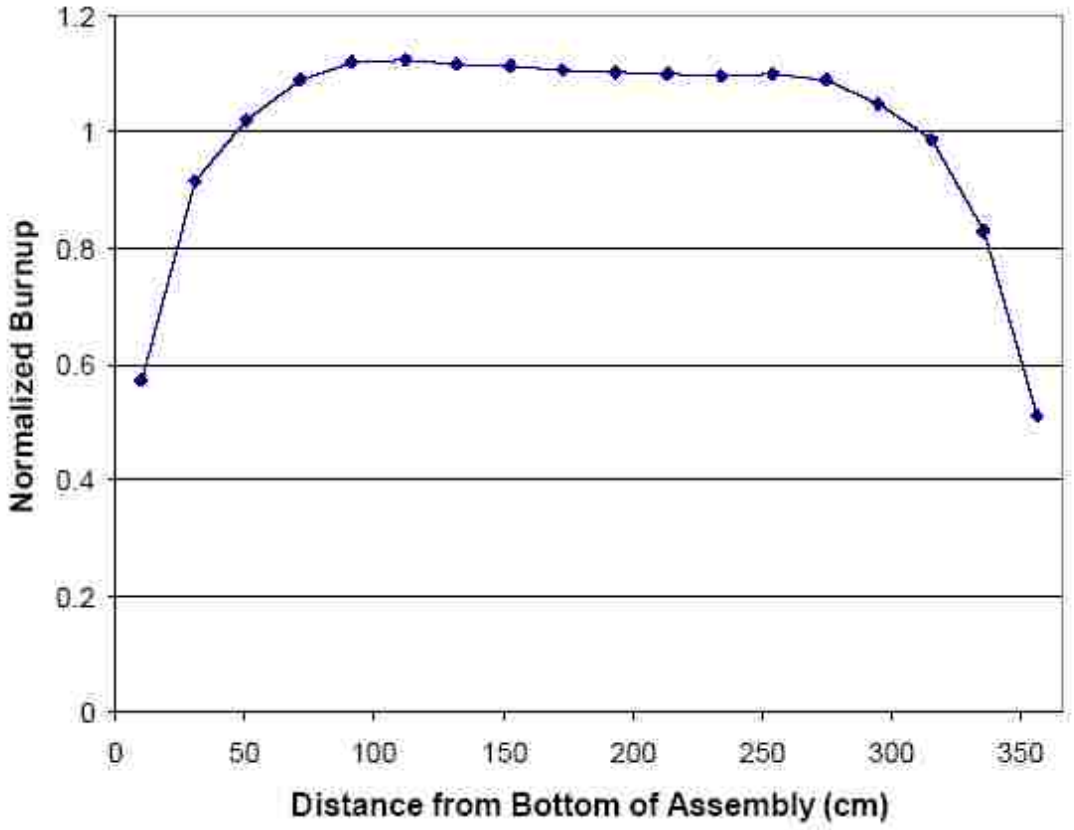

Figure 1. Example of a PWR fuel assembly axial burnup distribution [24].

Like the burnup, the neutron flux has an axially distribution along the fuel assemblies in a reactor, which produces a neutron flux that is not spatially uniform for typical reactor systems. This results in non-uniform statistical uncertainties in the computed reaction rates in Monte Carlo simulations. For regions where the flux is low (axial ends of LWR fuel assemblies), computed quantities like isotopic compositions may have large statistical uncertainties. However, in currently available Monte Carlo depletion codes these statistical uncertainties are not calculated or reported to the user. Consequently,

users have no indication of the reliability of their results in such regions. This can be a significant obstacle to the effective use of Monte Carlo methods for design and optimization studies of advanced fuel designs. Additionally, for applications like criticality safety for spent nuclear fuel, the under-depleted end regions of the fuel tend to dominate [2] the reactivity (negatively – meaning a higher reactivity) and must be accurately represented [2, 24, 25].

Coupled Monte Carlo point-depletion methods have been developed to varying degrees. An early implementation was the MOCUP package that was based on MCNP and the Oak Ridge Isotope GENeration 2 (ORIGEN2) computer code. This package has never been fully coupled and automated, thereby requiring limited user intervention in completing a sequence of calculations. An improved implementation of this code coupling was accomplished with MONTEBURN, which uses scripts to couple MCNP calculations with ORIGEN2. Both of these codes suffer from limitations due to the selection of codes they use. ORIGEN2 has a more significant limitation because it uses fixed cross section libraries selected based on user selection appropriate for the intended application. MONTEBURN provides for cross section updates of the ORIGEN2 data, but it is limited to nuclides and temperatures in MCNP and cannot propagate uncertainties. KENOREST is another package (developed in Germany) based on a coupled arrangement between KENO V.a from the modular code system for performing Standardized Computer Analyses for Licensing Evaluations (SCALE) and the GRS OREST package. KENOREST has been developed for LWR lattice analysis and makes geometric assumptions that limit its general applicability, and has shown to perform well relative to other codes for OECD computational depletion benchmarks [4]. The TRITON

control module, part of the SCALE 5.1 package, can perform 3-D depletion calculations using the KENO Monte Carlo transport code and can also perform 2-D deterministic depletion calculations using the NEWT discrete ordinates code [15]. Some other Monte Carlo depletion codes include: MCNPX/CINDER90, ALEPH, MCB1C, SWAT2, McCARD and MVP-BURN. MCNPX/CINDER90 is the MCNPX team's version of a Monte Carlo depletion code and couples MCNPX with CINDER90, which is used to perform the isotopic depletion with a "burn card" added to the MCNPX input deck [9]. ALEPH is a Monte Carlo burnup code that couples any version of MCNP or MCNPX (neutron transport) to ORIGEN2.2 (depletion) [18]. MCB1C is a code that integrates MCNP4C (transport) to a novel Transmutation Trajectory Analysis (TTA) code (depletion) for Monte Carlo depletion analysis [14]. SWAT2 couples the Monte Carlo code MVP with ORIGEN2.1 to perform depletion analysis by the Monte Carlo method [11]. However, none of the above code packages address the issues that are most relevant for Monte Carlo driven depletion, which are determination of propagated uncertainties in ORIGEN results (depletion calculation) or improved performance in resolving fluxes in low-importance regions [4].

Calculating and quantifying the uncertainty propagation in Monte Carlo methods will not be a simple task. There have been few studies that have considered theoretical formulations developed to quantify the uncertainties of the Monte Carlo tallies, nuclide number density estimates, and their propagation behavior with the iterative advancement of a depletion calculation. A burnup matrix method (by Takeda) was developed and aimed at estimating the effect of uncertainty propagation on the nuclide number densities in Monte Carlo burnup calculations. Since then, an equation that can predict the variance

(var) of nuclide number densities after burnup calculations was presented [19]. The method was used to examine effects of uncertainty propagation of nuclide number densities on Monte Carlo burnup calculations [19].

Takeda et al. [21] derived a formula that evaluates the variance of nuclide number densities at the end of a burnup period. This is accomplished using the burnup matrix method [19] which considers the change in number densities with burnup for a given time step. The derived formula evaluated the error propagation in the number densities of individual nuclides over a burnup period. The equation considered the uncertainties in cross sections and the statistical error in the Monte Carlo calculation as error sources. The method used a burnup matrix which was composed of reaction rates and decay constants. The reaction rates were calculated using the Monte Carlo method; therefore, error in the reaction rates came from the following three terms: errors in cross sections, errors in number densities, and the Monte Carlo statistical error. The authors focused on a simplified fast reactor core and concluded that the error in the number densities due to the statistical error was very small in comparison to the error in the cross sections [21].

Tohjoh [22] investigated the effects of error propagation on Monte Carlo burnup calculations of an 8x8 boiling water reactor (BWR) fuel assembly. The author proposed a rather simplified equation that predicted the variance of the nuclide number densities after burnup calculations and verified the equation with numerous separate Monte Carlo simulations. The formula used in the article was set up as a ratio in the number densities between the i^{th} burnup point and the previous burnup point (i^{th}-1 point). The equation focused on the number densities of nuclides after the burnup calculation when the variation of the nuclides was dominated by absorption reactions. The formula also

evaluated the changes in errors in the number densities with a change in the number of burnup calculation points (steps) in a simulation. The method demonstrated that the effects of error propagation on Monte Carlo burnup calculations of an 8x8 BWR fuel assembly were low up to 60 GWd/MTU [22].

Shim et al. [19] researched the development of a formula for uncertainty propagation in Monte Carlo depletion analysis and examined quantitatively the propagation trend of uncertainties in Monte Carlo tallies for important reactor parameters, which included reaction rates and nuclide number density estimates from solutions to the depletion equation as a function of depletion time steps [19]. The authors expressed the uncertainties involved in Monte Carlo estimates on reaction rates (or tallied parameters) and the nuclide number density estimates in terms of the covariance (cov) of random parameters that contribute to the uncertainties [19]. The method by Shim [19] was more general than the method by Tohjoh [22] in that it did not limit the variation in number densities to when they were dominated by absorption reactions, but included any reaction that lead to the number density of the nuclide of interest and also the decay of the nuclide. In this sense the methodology developed by Shim [19] was like a compilation of the journal articles by Tohjoh [22] and Takeda [21]. To verify the formula presented, the authors conducted a Monte Carlo depletion analysis for a simplified 7x7 fuel assembly and a 17x17 PWR fuel assembly, and found that the formula produced results in good agreement with those from the McCARD routine, which is a Monte Carlo depletion analysis computer code [19].

Garcia-Herranz et al. [7] developed a hybrid method for uncertainty propagation in Monte Carlo depletion calculations. The authors based the method on combining aspects

of two different methodologies to propagate the uncertainties of the nuclide inventory in combined Monte Carlo and burnup calculations: one methodology based on sensitivity/uncertainty analysis and the other methodology based on random sampling techniques (uncertainty Monte Carlo method). The authors investigated the influence of uncertainties in the activation cross section and statistical errors in the neutron flux spectrum on the calculated actinide inventory along consecutive spectrum-depletion steps. The authors focused on examining a benchmark problem of a high temperature gas-cooled reactor (HTGR) for plutonium burning applications, and the results showed that there are large uncertainties found at high burnup (80 GWd/MTU). The authors noted that the statistical errors are negligible compared to the effect of the cross section uncertainties but state that if the flux relative errors are higher than ten percent, then the impact of the statistical errors is not negligible on some isotopes even if the contribution is mainly due to the cross section errors [7].

The methods developed different formulas to investigate the propagation of uncertainty in the nuclide number densities in Monte Carlo depletion calculations. However, the equations in the articles used the same techniques in order to do so, namely developing covariance matrixes by applying some kind of sensitivity method, except the equation by Tohjoh, which looked at ratios in the nuclide concentration between time steps [77, 19, 21, and 22]. The authors of the articles took into account other sources of uncertainty besides the statistical uncertainty from using the Monte Carlo method. Therefore, the methods can not develop a complete understanding of the propagation of the statistical uncertainty in the fluxes calculated by the Monte Carlo method.

CHAPTER 3

METHODOLOGY

The objective of this research is to develop an understanding and expression for the quantification of stochastic uncertainty propagation of the flux uncertainty introduced by the Monte Carlo method in the number densities for the different isotopes in spent nuclear fuel due to multiple time steps. The research derives a formula calculates the standard deviation (sd) in the nuclide number densities based on propagating the statistical uncertainty introduced when using the Monte Carlo method to solve the neutron transport equations in coupled Monte Carlo depletion computer codes. The research was developed with the use of the TRITON/KENO sequence of the SCALE computer code. After the methodology is proven, it could possibly be adopted and integrated into the TRITON/KENO sequence of the SCALE computer code by the SCALE development team at Oak Ridge National Laboratory (ORNL). In particular, the work focuses on development of an approach to determine the uncertainty in isotopic predictions based on the compounded effects of multiple calculations (depletion time steps) with stochastic uncertainties in each time step from the fluxes calculated by the Monte Carlo method. To help validate uncertainty estimates for isotopic concentration predictions from Monte Carlo depletion calculations, results can be compared to isotopic concentrations from a deterministic calculation. Note that both Monte Carlo and deterministic methods are subject to biases and uncertainties in data and modeling approximations. This research seeks only to estimate the stochastic uncertainty not present in deterministic methods. The statistical development for propagated statistical

uncertainties in the isotopic concentrations involves developing a formula that determines the uncertainties in the isotopic concentrations and presents these uncertainties to the user in the output of the computer code.

This research investigated the propagation of the stochastic uncertainty by propagating the uncertainty of the flux to the uncertainty in the cross sections, power distribution, and nuclide number densities. The uncertainty was also propagated in time by using multiple time steps during the calculation. The research involved a detailed tracking and calculation of the uncertainty in the different quantities the flux effects through the flow of the program. In doing so, this work should develop an understanding of the propagation of the stochastic uncertainties with the effects of power density, cycle length, and number of libraries per cycle.

The approach pursued in this research was to develop a complete mathematical expression for the standard deviation of the nuclide number densities based on the stochastic uncertainty in the fluxes. The study involved a very detailed tracking of how and where any information in the fluxes was used for the calculation of the number densities. The method propagated the uncertainty of the flux to the number densities considering that the flux will produce uncertainties in the cross sections and power distribution. Since uncertainties in the flux cause uncertainties in the power distributions, which were used to balance the power distribution between different mixtures (when depleting more than one mixture), the expression developed needed to account for uncertainty in the power distribution. The research first focused on only one mixture to develop an understanding of the phenomena that govern uncertainties in the isotopics. Then the research added in the effect of the uncertainties calculated in the power

distribution caused by the uncertainties in the flux. These topics were believed to represent the primary issues to be resolved in the propagation of stochastic uncertainty.

The initial step was to develop a clear understanding of how the TRITON sequence operates and more specifically how information was transferred between the different SCALE modules in the TRITON sequence. The output quantities and the algorithms that calculate those quantities from the individual modules were also required. For example, how the program collapses the cross sections and determines the reaction rates were essential to propagating the stochastic uncertainty to the number densities.

The next step in this process was to calculate the standard deviation in the number densities for one time step, which gave the standard deviation at the end of that time step. Next a study of sequential time steps was performed to determine if and what correlations existed in the standard deviations of the number densities from one time step to the next. This lead to being able to calculate the standard deviation in the number densities for any number of time steps in a calculation. Calculating and understanding the standard deviation in the number densities at each time step could also lead to the possibility of being able to fit the standard deviation in the number densities to some kind of mathematical expression (linear or polynomial). It was anticipated that the standard deviation in the number densities will increase with each time step because each sequential time step will have the stochastic uncertainty plus the uncertainty in the nuclide number densities. The uncertainty in the nuclide number densities was caused by the standard deviation of the nuclide number densities from the previous time step. However, the rate of increase could be small, which means that each time step adds uncertainty but only a small amount of uncertainty.

The formulas developed in this research are based on first order perturbation theory. Therefore, the effects of using first order perturbation theory were investigated to determine if it was appropriate for the equations that were derived in this research. Three example problems were used in this research to investigate the approximation that was developed in the research and to examine the use of first order perturbation theory. Two analytical examples, adopted from an ORNL paper by Williams [26], are: 1) Example 1 which is a one-group, single nuclide infinite medium system, and 2) Example 2 which is a two-group, two nuclide infinite medium system. Additionally, Example 3, which is developed herein, is a three-group, four nuclide infinite fuel pin lattice system. The time-dependent behavior of the nuclides is found with the equations given in chapter 4.

Linear algebra and a suite of mathematical techniques are used to develop the expressions. Variances and covariances are determined using standard statistical methods and definitions. Chapter 5 discusses the results of this research, and includes a section on the effects of first order perturbation theory, which confirms that first order perturbation theory is appropriate for this application and is capable of accurately describing changes in the quantities of interest. Nuclide number densities, standard deviation and variance values are reported with two to three decimal places. All calculations in SCALE and MathCad are conducted with double precision, therefore two to three decimal places are considered accurate in this research. This also follows the convention used in the SCALE computer code [15]. The fluxes calculated with SCALE also generally have a percent deviation of under 0.5 percent, thus making the values very reliable.

3.1 SCALE Computer Code Package

The research was conducted with the SCALE computer code, which is made up of many different code modules (or sequences). The control modules used in this research are the T5-DEPL and CSAS modules for the Monte Carlo simulations and the T-DEPL module for the deterministic calculations. These control modules call other modules to perform specific calculations and are briefly discussed in the next section. Readers can refer to the SCALE manual for an in-depth discussion of the SCALE computer code [15]; section 3.1.1 gives readers a general overview of the flow of information in the T5-DEPL sequence.

3.1.1 Simplified View of How SCALE Operates

This research was based on the T5-DEPL sequence of the TRITON module in SCALE, which uses the Monte Carlo method to solve the neutron transport equation via KENO V.a. In the calculational sequence, TRITON first reads the problem input, checks geometries and problem parameters, and prepares input information for the calculation. Cross section processing is then performed using either CENTRM, WORKER and PMC, or NITAWL. The KENO V.a module then solves the transport equation using the isotopic concentrations at the beginning of the time step, either the time zero concentrations or the concentrations from the previous time step after the depletion calculation. KMART reads the KENO restart file and creates three-group cross sections within each mixture in the problem that are averaged over each mixture. The COUPLE module then uses those cross sections, creates one-group effective cross sections, and uses them to update burnup dependent cross sections in the ORIGEN-S library.

ORIGEN-S performs point depletion/decay calculations for each mixture. The results of the post-processing by KMART also provide power distributions that are normalized by TRITON to match a specified local power. ORIGEN-S uses the updated cross section library to predict the isotopic inventory in the future (next depletion time step). The isotopic inventory is then passed back, as an input, to the beginning of the program flow (cross section processing program), and the process is iterated for all depletion time steps. TRITON uses a predictor-corrector approach in which cross sections estimated for a mid-step (predictor phase) are used in a full step depletion (corrector phase). Once all depletion steps have been completed, the OPUS module is invoked to extract specific information requested by the user. Figure 2 illustrates the execution path for a Monte Carlo depletion calculation using the TRITON/KENO sequence of the SCALE computer code.

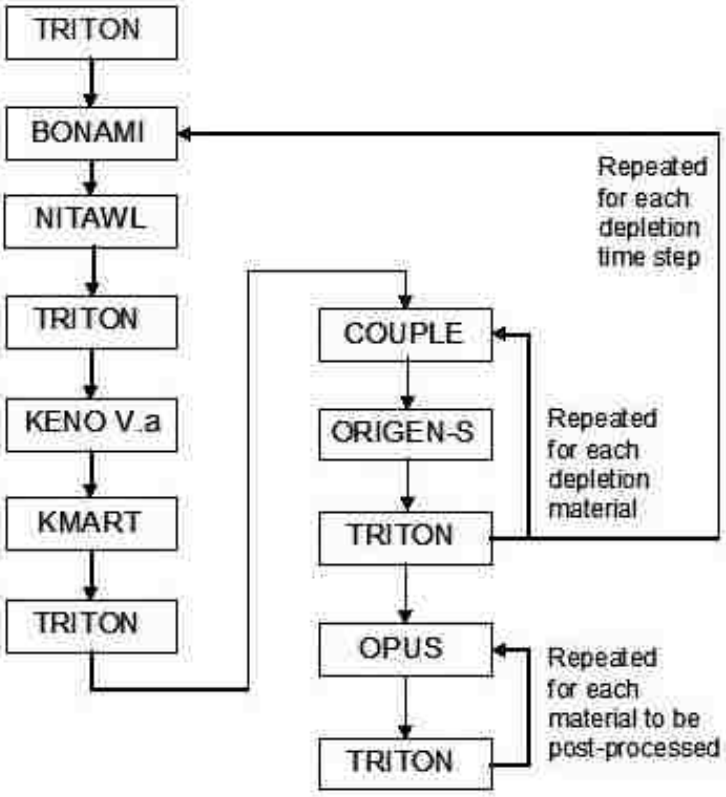

Figure 2. Execution path for the TRITON/KENO sequence in SCALE.

3.1.2 Verification of SCALE Computer Code

The research was conducted with the release version of SCALE 6.0 (RSICC code number C00750MNYCP00). The SCALE computer code was installed and was verified on a personal computer according to the SCALE manual. All computer simulations were preformed on the same computer.

3.2 Assumptions Used in Research

- There is no uncertainty in the initial nuclide concentrations. Knowledge of the isotopes in fresh nuclear fuel assemblies is considered very accurate.
- There is no uncertainty in the nuclide decay constants (λ_i). The half-lives of nuclides are considered well known; therefore, their decay constants are well known.
- There is no uncertainty in the fission yields. These are accepted as well known values.
- There is no uncertainty in the multi-group cross section values (σ_i). For the purpose of this study, the multi-group cross sections have no uncertainty. The uncertainty in the cross sections caused by the uncertainty in the flux is accounted for, but no uncertainty is considered in the multi-group cross section values themselves.
- There are no correlations between energy groups. For this to be done, it would require massive tracking in the Monte Carlo code. Since neutrons generally lose most of their energy in a couple of collisions before being absorbed, this is not an unrealistic assumption.
- There are no correlations between the statistical uncertainty in the current time step and the statistical uncertainty in the previous time step, because each time step is an independent Monte Carlo simulation [21].
- The statistical uncertainty is independent of the nuclide number density. This assumption was also used by the authors of previous literature [19].

- The parameters (cross sections, flux, etc.) are constant during a time step. During a given time step, parameters are constant but can be updated after each time step.
- Depletion is done under constant power which means the power does not change during a time step ($\Delta P = 0$ during any time step). Reactors operate at nearly a constant power; thereby making this reasonable.
- There is no uncertainty considered in the number densities of the ^{239}U and ^{239}Np isotopes, when these isotopes are included in the extended equations of Example 3. The isotopes decay quickly to ^{239}Pu, compared to the 30 day time step used in this research; therefore there is no accumulation of these isotopes in the calculations performed with this research. The half-lives of ^{239}U and ^{239}Np are 23.47 minutes and 2.355 days, respectively.

3.3 General Equations and Variance Terms

The general equations are presented for a change in variables and the variance in these variables. The general equations were developed with first order perturbation theory. The equations are used to investigate how a change in the flux shape affects and propagates to the other parameters affected by the flux shape; namely, the cross sections, the power distribution, and the nuclide number densities of the system. These are the terms that are affected by the propagation of the statistical uncertainty in the flux from the Monte Carlo simulation. The discussion starts with the uncertainty in the flux shape, which is the source of uncertainty in Monte Carlo calculations and continues with the terms affected by the flux shape.

In this research the uncertainty in the flux shape is made up of two terms: the statistical uncertainty in the flux shape (ψ_S) and the uncertainty in the flux shape due to uncertainty in the number densities (ψ_N). The change in the flux shape is $\Delta\psi = \Delta\psi_s + \Delta\psi_N$ where $\Delta\psi_S$ is a change in the statistical uncertainty in the flux shape and $\Delta\psi_N$ is a change in the uncertainty in the flux shape due to a change in the number density. The $\Delta\psi_N$ term can be evaluated by $\Delta\psi_N = \frac{\partial\psi}{\partial\overline{N}}\Delta\overline{N}$ where $\overline{N}$ is a vector of all nuclides in the system. The variance of the $\Delta\psi_S$ term is $\mathrm{var}(\psi_S) = E\left[(\Delta\psi_S)^2\right]$ where E is the expectation operator and $E[(\Delta X)^2]$ is the expected value of $(\Delta X)^2$. The variance of the $\Delta\psi_N$ term is $\mathrm{var}(\psi_N) = E\left[(\Delta\psi_N)^2\right] = \left(\frac{\partial\psi}{\partial\overline{N}}\right)^T COV\left[\overline{N},\overline{N}^T\right]\left(\frac{\partial\psi}{\partial\overline{N}}\right)$ where $COV\left[\overline{N},\overline{N}^T\right]$ is the nuclide covariance matrix. The variance of ψ is then $\mathrm{var}(\psi) = E\left[(\Delta\psi)^2\right] = \mathrm{var}(\psi_s) + \mathrm{var}(\psi_N)$ where correlations between energy groups are assumed equal to zero and the statistical uncertainty is independent of the uncertainty due to a change in the number density.

The effective cross section (σ_{eff}) is defined by

$\sigma_{eff} = \frac{\sum_g \sigma_g\psi_g}{\sum_g \psi_g}$, or with thermal normalization of the cross sections $\sigma_{eff} = \frac{\sum_g^G \sigma_g\psi_g}{\sum_{g'}^G \psi_{g'}}$,

where g' is the first thermal group of the flux. The change in the effective cross section is $\Delta\sigma_{eff} = \frac{\partial\sigma_{eff}}{\partial\psi_g}\Delta\psi_g$ and the variance in the effective cross section is

$\mathrm{var}(\sigma_{eff}) = E\left[(\Delta\sigma_{eff})^2\right] = \sum_g \left[\left(\frac{\partial\sigma_{eff}}{\partial\psi_g}\right)^2 * \mathrm{var}(\psi_g)\right]$ where covariances between groups are neglected.

The power of the system is defined by $P = \beta\Phi\sum_{ij} Q_{ij} N_i \sigma_{ij}$ where β equals $1.6\text{x}10^{-19}$ (a constant conversion factor), and is obtained from the SCALE manual [15]. The change in the flux normalization that results from the power constraint defined above is:

$$\Delta P = \frac{\partial P}{\partial \Phi}\Delta\Phi + \frac{\partial P}{\partial N_i}\Delta N_i + \frac{\partial P}{\partial \sigma_{ij}}\Delta\sigma_{ij}$$

constant power $\Rightarrow$ no change in P $\Rightarrow \Delta P = 0$

$$0 = \frac{\partial P}{\partial \Phi}\Delta\Phi + \frac{\partial P}{\partial N_i}\Delta N_i + \frac{\partial P}{\partial \sigma_{ij}}\Delta\sigma_{ij}$$

$$\Delta\Phi = -\left(\frac{\partial P}{\partial N_i}\Delta N_i + \frac{\partial P}{\partial \sigma_{ij}}\Delta\sigma_{ij}\right) * \frac{1}{\frac{\partial P}{\partial \Phi}}$$

The variance in the flux normalization is

$$\mathrm{var}(\Phi) = E\left[(\Delta\Phi)^2\right] = \left[-\left(\frac{\partial P}{\partial N_i}\Delta N_i + \frac{\partial P}{\partial \sigma_{ij}}\Delta\sigma_{ij}\right) * \frac{1}{\frac{\partial P}{\partial \Phi}}\right]^2$$

The equation for the change in the nuclide number density is

$\Delta N_F^j = \sum_i \frac{\partial N_F^j}{\partial N_0^i}\Delta N_0^i + \left(\frac{\partial N_F^j}{\partial \bar{A}}\right)\Delta\bar{A} + \sum_g \frac{\partial N_F^j}{\partial \psi_g}\Delta\psi_g$ where N_F^j is the final number density of the j[th] nuclide (at end of time step) and N_0^i is the initial number density of the i[th] nuclide (at beginning of time step), and $\bar{A}$ is the transition matrix containing rate coefficients for radioactive decay and neutron absorption [15]. The equation for the variance of the j[th] nuclide number density is given by the following equation

$$\mathrm{var}(N_F^j) = E\left[\left(\Delta N_F^j\right)^2\right] = \left[\frac{\partial N_F^j}{\partial \overline{N}_0^i} \quad \frac{\partial N_F^j}{\partial \overline{A}} \quad \frac{\partial N_F^j}{\partial \psi_g}\right]\left[C_N\right]\left[\frac{\partial N_F^j}{\partial \overline{N}_0^i} \quad \frac{\partial N_F^j}{\partial \overline{A}} \quad \frac{\partial N_F^j}{\partial \psi_g}\right]^T$$

where C_N is the covariance matrix of $\overline{N}_0$, $\overline{A}$, and ψ_g.

3.4 Problem Formulated

The uncertainties in the isotopic number densities are produced by the statistical uncertainty in the flux shape from the Monte Carlo simulation, and the propagation of the statistical uncertainty in the flux shape to the cross sections, flux normalization (the power constraint), and finally the number densities themselves. These effects are also propagated in time as the simulation progresses from one time step to the next time step.

The preceding section showed that one source of uncertainty in the isotopic number densities comes from the uncertainty in the flux shape. A change in the flux shape comes from a change in the statistical uncertainty and a change in the nuclide number densities. A change in the flux shape due to a change in the nuclide number densities can be evaluated by taking the derivate of the flux shape with respect to the nuclide number densities times a change in the nuclide number densities or mathematically

$\Delta\psi = \Delta\psi_s + \Delta\psi_N$ where $\Delta\psi_N = \frac{\partial\psi}{\partial\overline{N}}\Delta\overline{N}$. The variance of ψ_N is

$\mathrm{var}(\psi_N) = \left(\frac{\partial\psi}{\partial\overline{N}}\right)^T COV\left[\overline{N}, \overline{N}^T\right]\left(\frac{\partial\psi}{\partial\overline{N}}\right)$ where $\overline{N}$ is a vector of all the nuclides in the system, which is the exact equation for a change in the flux shape. As seen in the equation, one must know or calculate the derivative of the flux shape with respect to the nuclide number density for each nuclide in the system to exactly calculate the uncertainty in the isotopic number densities. The research here uses the Monte Carlo method, which

means running separate Monte Carlo simulations for each nuclide in the system to accurately describe the change in the flux shape due to a change of the nuclides in the system, or the $\Delta\psi_N$ term. This is not very practical when the number of nuclides in the system is large. If needed, ORIGEN can track close to 2,000 different isotopes; therefore, calculating these derivates can quickly become extremely time consuming and computationally inefficient. A method that could reduce the number of Monte Carlo simulations needed to describe the ψ_N term would be desirable and could solve these issues. The next section describes an approach taken that evaluates the ψ_N term while reducing the computational load needed to describe the ψ_N term.

3.5 The Linear Uncertainty Nuclide Group Approximation (LUNGA) Method

The previous section showed a few problems arise when trying to accurately describe the ψ_N term. The LUNGA method is developed to approximate the ψ_N term in this research. The LUNGA method appears to approximate the $\Delta\psi_N$ term in a way that reduces the number of Monte Carlo simulations needed to describe the ψ_N term and only requires one additional simulation per area of interest or material being depleted. The equation being used to approximate the ψ_N term in the LUNGA method is $\sigma_{\psi_N} \approx \Delta\psi_N = \psi' - \psi$ where ψ' and ψ are the fluxes of the perturbed and unperturbed systems, and the solutions for the fluxes come from using the Monte Carlo method to solve the neutron transport equation. The neutron transport equation is

$$\frac{1}{\mathrm{v}}\frac{\partial}{\partial t}\psi(\hat{\rho}) + \hat{\Omega} * \nabla\psi(\hat{\rho}) + N(\hat{r},t) * \sigma_t(\hat{r},E) * \psi(\hat{\rho}) = N(\hat{r},t) * \left[\sigma_s(\hat{r},E',\Omega' \to E,\Omega)\psi(\hat{\rho}) + \frac{\chi(E)}{4\pi}\upsilon\sigma_f(E')\psi(\hat{\rho})\right]_{E',\Omega'}$$

where $\psi(\hat{\rho}) = \psi(\hat{r}, E, \hat{\Omega}, t)$. Defining the Boltzman operator as B by $B = B[\overline{N}(\hat{r}, t), \overline{\sigma}(\hat{r}, E)]$ where $\overline{N}$ is a vector of all the nuclides in the system, $\overline{\sigma}$ is the cross section vector with entries corresponding to the elements of $\overline{N}$, and the notation is adopted from Williams [26]; the neutron transport equation becomes $\frac{1}{\mathrm{v}}\frac{\partial}{\partial t}\psi(\hat{\rho}) = B(\overline{N}, \sigma)\psi(\hat{\rho})$ [26]. The steady state neutron transport equation is $B(\overline{N} + \Delta\overline{N})\psi' = 0$ for the perturbed system and $B(\overline{N})\psi = 0$ for the unperturbed system.

The results of initial calculations showed that the LUNGA method will over predict the standard deviation in the isotopic number densities; however, this would be a bounding value for the standard deviations, and the true standard deviations would be smaller than the values calculated with the LUNGA method. The results of these calculations also demonstrate that the LUNGA method will incorporate some of the covariance terms present in the exact equation. The LUNGA method was initially investigated with a simple pin cell model in XSDRN and KENO V.a for a system containing either 2 or 15 nuclides. Table 1 only shows the standard deviation of the ψ_N term, so the value calculated using the LUNGA solution could be compared directly to the value calculated using the exact solution. The results in Table 1 indicate that the approximation of the ψ_N term using the LUNGA method can calculate the standard deviation of the ψ_N term accurately and therefore should be investigated further.

Table 1. Preliminary comparison of sd(ψ_N) between exact and LUNGA methods.

Standard deviation in the total flux (n/cm^2*s)					
XSDRN					
	LUNGA solution	Exact solution (no COV terms)	Percent difference (LUNGA and exac - no COV)	Exact solution (with COV terms)	Percent difference (LUNGA and exact with COV)
2 nuclide system	1.09E+00	8.18E-01	3.3E+01	1.09E+00	-1.2E-01
15 nuclide system	6.80E-01	4.27E-01	5.9E+01	6.86E-01	-9.2E-01
KENO					
	LUNGA solution	Exact solution (no COV terms)	Percent difference (LUNGA and exac - no COV)	Exact solution (with COV terms)	Percent difference (LUNGA and exact with COV)
2 nuclide system	1.92E-03	1.45E-03	3.2E+01	1.94E-03	-1.4E+00
15 nuclide system	1.20E-03	7.49E-04	6.0E+01	1.22E-03	-1.5E+00

There was an interesting side discovery when conducting the research to examine the differences between the LUNGA and exact methods using the pin cell model. Some of the derivatives of the flux shape with respect to the nuclides (found using the central difference method) are equal to zero, which means a change in a particular isotopic number density does not affect the flux shape. The derivatives of the flux shape with respect to the nuclides are shown in Table 2 for a system containing 15 nuclides. This is an interesting discovery because it means that a number of the covariance terms in the $\partial\psi/\partial N$ covariance matrix will be equal to zero. This could lead to being able to group some nuclides together and take the derivative of the flux shape with respect to that group, which could lead to a more accurate answer than the LUNGA method developed in this research. There is also the potential that separate Monte Carlo simulations only have to be executed for the nuclides where the derivative of the flux shape with respect to number density is not equal to zero, which would greatly reduce the number of separate Monte Carlo runs needed to calculate the solution using the exact method.

Table 2. Derivatives of the flux shape with respect to number density.

	Change in flux from perturbation (n/cm^2*s)		Change of flux shape with respect to change in number density
Nuclide	pert. up	pert. down	dΨ/dN
u-235	3.48E+01	3.50E+01	-7.0E+03
u-238	3.47E+01	3.52E+01	-2.6E+02
zr-93	3.49E+01	3.49E+01	0.0E+00
sr-90	3.49E+01	3.49E+01	0.0E+00
tc-99	3.49E+01	3.49E+01	0.0E+00
xe-135	3.49E+01	3.49E+01	-3.0E+07
sm-149	3.49E+01	3.49E+01	0.0E+00
pu-239	3.49E+01	3.50E+01	-1.5E+04
pu-240	3.49E+01	3.50E+01	-1.1E+04
pu-241	3.49E+01	3.49E+01	-1.2E+04
pu-242	3.49E+01	3.49E+01	0.0E+00
am-241	3.49E+01	3.49E+01	0.0E+00
cm-244	3.49E+01	3.49E+01	0.0E+00

CHAPTER 4

EXAMPLE PROBLEMS

The research uses two analytic example problems that are described in the following sections and are adopted from a report by Williams [26]. Example 1 is a single group, single nuclide infinite medium system, and Example 2 is a two-group, two nuclide infinite medium system. These example problems provide two different systems in which equations for the variance in the number densities can be derived for each system. Since both of these example problems have analytic solutions, the examples allow for the equations for a change in the number densities to be checked and compared with the direct perturbation of the analytic equations for the two systems in order to determine if using first order perturbation theory is acceptable. Example 2 allows for the derived equations of the LUNGA method (method developed in this research) to be compared to the exact equations (the exact method) for finding the change in the number densities.

A final example system, Example 3, is developed herein to further compare the LUNGA and exact methods. Example 3 is a three-group, four nuclide infinite fuel pin lattice system that contains an isotope from neutron capture and a fission product. Example 3 is a semi-analytic example, which can be solved analytically with the aid of mathematical software or with using the flux shape values calculated with the Monte Carlo method (SCALE computer code). This means the Monte Carlo solution can be compared to the analytic solution for the exact and LUNGA methods for finding the standard deviation in the number densities. Example 3 is also used to further investigate

the use of first order perturbation theory in this research and could serve as a benchmark problem for the SCALE computer code.

4.1 Governing Equations

The governing equations for Example 1, Example 2, and Example 3 are presented next. The equations for a change in the variables and the variance of the variables for the example problems are derived from these governing equations.

4.1.1 Single Group, Single Nuclide Infinite Medium System (Example 1)

Example 1 provides an analytical example to investigate the variance of a single nuclide and to investigate the use of first order perturbation theory.

The equations for this example [26] include: the flux shape equation, the flux normalization equation, the transmutation equation, and the initial condition. Those equations are:

$$0 = N_0\left(\sigma_a - \lambda\upsilon\sigma_f\right)\psi$$

$$\psi N_0 \Phi \sigma_f = P$$

$$\frac{dN}{dt} = -\sigma_a \psi \Phi N_0$$

The initial condition of the system is N(0)=2.232E+24 atoms/cm^3. The equations can be solved analytically and yield the following solutions [26]

$$\lambda = \frac{\lambda}{k_\infty} = \frac{\sigma_a}{\upsilon\sigma_f}$$

$$\Phi = \frac{P}{\psi N_0 \sigma_f}$$

$$N = N(t) = N_0 e^{-\sigma_a \Phi t}$$

where λ can be found independently of N_0 and ψ_0, and ψ_0 is taken to be unity.

4.1.2 Two-group, Two Nuclide Infinite Medium System (Example 2)

Example 2 still considers an infinite medium, but the system is expanded to include two nuclides and two energy groups. The example allows for some additional effects to be investigated in the system, such as having multiple nuclides and multiple energy groups. The example is also used to investigate the use of first order perturbation theory and the acceptability of using the LUNGA method. The solution is slightly more involved than the previous example but can still be solved analytically [26]. The equations for the flux shape [26] are:

$$\begin{bmatrix} N_1(t)\sigma^1_{r1} & 0 \\ -N_1(t)\sigma^1_{s1-2} & N_1(t)\sigma^1_{a2}+N_2(t)\sigma^2_{c2} \end{bmatrix} * \begin{bmatrix} \psi_1 \\ \psi_2 \end{bmatrix} - \lambda \begin{bmatrix} 0 & N_1(t)\upsilon\sigma^1_{f2} \\ 0 & 0 \end{bmatrix} * \begin{bmatrix} \psi_1 \\ \psi_2 \end{bmatrix} = 0$$

The flux normalization equation is $P = N_1\sigma^1_{f2}\psi_2\Phi$ [26]. The nuclide transmutation equations are $\begin{bmatrix} -\left(\sigma^1_{a1}\psi_1+\sigma^1_{a2}\psi_2\right)*\Phi & 0 \\ \gamma\sigma^1_{f2}\psi_2\Phi & -\left(\sigma^2_{c2}\psi_2\Phi+\Lambda\right) \end{bmatrix} * \begin{bmatrix} N_1 \\ N_2 \end{bmatrix} = \frac{d}{dt}\begin{bmatrix} N_1 \\ N_2 \end{bmatrix}$

where γ is the yield of N_2 from fission, and Λ is the decay constant of N_2 [26]. The initial conditions of the system include $N_1(0)$=1.00E+24 atoms/cm^3 and $N_2(0)$=0.00E+24 atoms/cm^3. The solutions to the above equations after one time step are

$$\lambda = \frac{\sigma^1_{r1}\left(\sigma^1_{a2}+\frac{N_2(t)}{N_1(t)}\sigma^2_{c2}\right)}{\nu\sigma^1_{f2} * \sigma^1_{s1-2}}$$

$$\frac{\psi_1}{\psi_2} = \frac{\left(\sigma^1_{a2}+\frac{N_2(t)}{N_1(t)}\sigma^2_{c2}\right)}{\sigma^1_{s1-2}}$$

$$\Phi = \frac{P}{N_1\sigma^1_{f2}\psi_2}$$

$$N_1(t) = N_1(0)e^{-a_{11}t}$$

$$N_2(t) = N_2(0)e^{-a_{22}t} + \frac{N_1(0)a_{21}}{a_{22}-a_{11}}\left[e^{-a_{11}t} - e^{-a_{22}t}\right]$$

where a_{ij} are the coefficients of the matrix in the nuclide transmutation equations [26]. After substitution of the coefficients, the nuclide transmutation equations yield

$$N_1(t) = N_1(0)e^{-\left(\sigma_{a1}^1\psi_1+\sigma_{a2}^1\psi_2\right)\Phi t}$$

$$N_2(t) = N_2(0)e^{-\left(\sigma_{c2}^2\psi_2\Phi+\Lambda\right)t} + \frac{N_1(0)\gamma\sigma_{f2}^1\psi_2\Phi}{\left(\sigma_{c2}^2\psi_2\Phi+\Lambda\right)-\left(\sigma_{a1}^1\psi_1+\sigma_{a2}^1\psi_2\right)\Phi} * z$$

$$\textit{where} \quad z = \left[e^{-\left(\sigma_{a1}^1\psi_1+\sigma_{a2}^1\psi_2\right)\Phi t} - e^{-\left(\sigma_{c2}^2\psi_2\Phi+\Lambda\right)t}\right]$$

4.1.3 Three-group, Four Nuclide Infinite Fuel Pin Lattice System (Example 3)

Example 3 expands on Example 2 to include four nuclides and three energy groups. The example allows for additional effects to be investigated in the system, like having multiple energy groups and multiple nuclides. Example 3 examines how the system behaves with an isotope from neutron capture and a fission product. The example is developed to further examine how the approximation performs and could be used as a benchmark problem for testing the SCALE computer code. The example is also used to further examine the use of first order perturbation theory.

The system considers ^{235}U (N_1), ^{238}U (N_2), a capture reaction product ^{239}Pu (N_3), and a fission product ^{155}Eu (N_4). In the example, N_1, N_2, and N_3 are fissionable nuclides. N_3 is an isotope produced from the neutron capture of N_2 and it can decay. N_4 is a fission product produced from the fission of N_1, N_2, and N_3 that can also decay and has a large neutron capture cross section. The solution is more involved than the previous example, but can be solved semi-analytically with the aid of mathematical software. The flux shape equations are:

$$\begin{bmatrix} N_1(t)\sigma_{r1}^1 + N_2(t)\sigma_{r1}^2 & 0 & 0 \\ +N_3(t)\sigma_{r1}^3 + N_4(t)\sigma_{r1}^4 & & \\ -\begin{pmatrix} N_1(t)\sigma_{s,1-2}^1 + N_2(t)\sigma_{s,1-2}^2 \\ +N_3(t)\sigma_{s,1-2}^3 + N_4(t)\sigma_{s1-2}^4 \end{pmatrix} & N_1(t)\sigma_{r2}^1 + N_2(t)\sigma_{r2}^2 & 0 \\ & +N_3(t)\sigma_{r2}^3 + N_4(t)\sigma_{r2}^4 & \\ -\begin{pmatrix} N_1(t)\sigma_{s,1-3}^1 + N_2(t)\sigma_{s,1-3}^2 \\ +N_3(t)\sigma_{s,1-3}^3 + N_4(t)\sigma_{s1-3}^4 \end{pmatrix} & -\begin{pmatrix} N_1(t)\sigma_{s,2-3}^1 + N_2(t)\sigma_{s,2-3}^2 \\ +N_3(t)\sigma_{s,2-3}^3 + N_4(t)\sigma_{s2-3}^4 \end{pmatrix} & N_1(t)\sigma_{a3}^1 + N_2(t)\sigma_{a3}^2 \\ & & +N_3(t)\sigma_{a3}^3 + N_4(t)\sigma_{a3}^4 \end{bmatrix} * \begin{bmatrix} \psi_1 \\ \psi_2 \\ \psi_3 \end{bmatrix}$$

$$-\lambda \begin{bmatrix} \chi_{11}\nu_{11}N_1(t)\sigma_{f1}^1 & \chi_{11}\nu_{12}N_1(t)\sigma_{f2}^1 & \chi_{11}\nu_{13}N_1(t)\sigma_{f3}^1 \\ +\chi_{21}\nu_{21}N_2(t)\sigma_{f1}^2 & +\chi_{21}\nu_{22}N_2(t)\sigma_{f2}^2 & +\chi_{21}\nu_{23}N_2(t)\sigma_{f3}^2 \\ +\chi_{31}\nu_{31}N_3(t)\sigma_{f1}^3 & +\chi_{31}\nu_{32}N_3(t)\sigma_{f2}^3 & +\chi_{31}\nu_{33}N_3(t)\sigma_{f3}^3 \\ \chi_{12}\nu_{11}N_1(t)\sigma_{f1}^1 & \chi_{12}\nu_{12}N_1(t)\sigma_{f2}^1 & \chi_{12}\nu_{13}N_1(t)\sigma_{f3}^1 \\ +\chi_{22}\nu_{21}N_2(t)\sigma_{f1}^2 & +\chi_{22}\nu_{22}N_2(t)\sigma_{f2}^2 & +\chi_{22}\nu_{23}N_2(t)\sigma_{f3}^2 \\ +\chi_{32}\nu_{31}N_3(t)\sigma_{f1}^3 & +\chi_{32}\nu_{32}N_3(t)\sigma_{f2}^3 & +\chi_{32}\nu_{33}N_3(t)\sigma_{f3}^3 \\ 0 & 0 & 0 \end{bmatrix} * \begin{bmatrix} \psi_1 \\ \psi_2 \\ \psi_3 \end{bmatrix} = 0$$

The cross sections in the above equations come from the following definitions of the cross sections: $\sigma_t = \sigma_s + \sigma_a$ and $\sigma_{rg} = \sigma_{tg} - \sigma_{sgg'}$ where $\sigma_{sgg'}$ is the in-group scattering cross section. The fission spectrum for the system is $\chi_1 = \int_{E_2}^{E_1} \chi(E)dE$, $\chi_2 = \int_{E_3}^{E_2} \chi(E)dE$, and $\chi_3 = \int_{E_4}^{E_3} \chi(E)dE = 0$. The flux normalization equation is, following the ORIGENS manual [15],

$$P = 1.6\text{x}10^{-19}\Phi\sum_{ij} Q_{ij}N_i\sigma_{ij}$$

$$\Rightarrow P = 1.6\text{x}10^{-19}\Phi\begin{bmatrix} Q_{1f}N_1\sigma_{1f} + Q_{1\gamma}N_1\sigma_{1\gamma} + Q_{2f}N_2\sigma_{2f} + Q_{2\gamma}N_2\sigma_{2\gamma} \\ +Q_{3f}N_3\sigma_{3f} + Q_{3\gamma}N_3\sigma_{3\gamma} + Q_{4\gamma}N_4\sigma_{4\gamma} \end{bmatrix}$$

where Q_{ij} is the recoverable energy released from fission and capture [15].

The nuclide transmutation equations are:

$$\begin{bmatrix} -\Phi\sigma_a^1 & 0 & 0 & 0 \\ 0 & -\Phi\sigma_a^2 & 0 & 0 \\ 0 & \Phi\sigma_c^2 & -\left(\Phi\sigma_a^3+\Lambda_3\right) & 0 \\ \gamma_4^1\Phi\sigma_f^1 & \gamma_4^2\Phi\sigma_f^2 & \gamma_4^3\Phi\sigma_f^3 & -\left(\Phi\sigma_c^4+\Lambda_4\right) \end{bmatrix} * \begin{bmatrix} N_1 \\ N_2 \\ N_3 \\ N_4 \end{bmatrix} = \frac{d}{dt}\begin{bmatrix} N_1 \\ N_2 \\ N_3 \\ N_4 \end{bmatrix}$$

where Λ_3 and Λ_4 are the decay constants of N_3 and N_4 respectively. γ_4^1, γ_4^2, and γ_4^3 are the fission product yields of N_4 from N_1, N_2, and N_3 respectively. The initial condition of the system is fresh fuel with an enrichment of 5 weight percent ^{235}U. The cross sections are the effective one-group cross sections and are calculated using the following formula:

$$\sigma_{eff} = \frac{\sum_g \sigma_g \psi_g}{\sum_g \psi_g}$$

With substitution of the one-group effective cross sections, the nuclide transmutation equations are written as shown on the following page.

$$\begin{bmatrix} -\Phi\dfrac{\begin{pmatrix}\sigma_{a1}^{1}\psi_1+\sigma_{a2}^{1}\psi_2\\+\sigma_{a3}^{1}\psi_3\end{pmatrix}}{(\psi_1+\psi_2+\psi_3)} & 0 & 0 & 0 \\ 0 & -\Phi\dfrac{\begin{pmatrix}\sigma_{a1}^{2}\psi_1+\sigma_{a2}^{2}\psi_2\\+\sigma_{a3}^{2}\psi_3\end{pmatrix}}{(\psi_1+\psi_2+\psi_3)} & 0 & 0 \\ 0 & \Phi\dfrac{\begin{pmatrix}\sigma_{c1}^{2}\psi_1+\sigma_{c2}^{2}\psi_2\\+\sigma_{c3}^{2}\psi_3\end{pmatrix}}{(\psi_1+\psi_2+\psi_3)} & -\left(\Phi\dfrac{\begin{pmatrix}\sigma_{a1}^{3}\psi_1+\sigma_{a2}^{3}\psi_2\\+\sigma_{a3}^{3}\psi_3\end{pmatrix}}{(\psi_1+\psi_2+\psi_3)}+\Lambda_3\right) & 0 \\ \gamma_4^1\Phi\dfrac{\begin{pmatrix}\sigma_{f1}^{1}\psi_1+\sigma_{f2}^{1}\psi_2\\+\sigma_{f3}^{1}\psi_3\end{pmatrix}}{(\psi_1+\psi_2+\psi_3)} & \gamma_4^2\Phi\dfrac{\begin{pmatrix}\sigma_{f1}^{2}\psi_1+\sigma_{f2}^{2}\psi_2\\+\sigma_{f3}^{2}\psi_3\end{pmatrix}}{(\psi_1+\psi_2+\psi_3)} & \gamma_4^3\Phi\dfrac{\begin{pmatrix}\sigma_{f1}^{3}\psi_1+\sigma_{f2}^{3}\psi_2\\+\sigma_{f3}^{3}\psi_3\end{pmatrix}}{(\psi_1+\psi_2+\psi_3)} & -\left(\Phi\dfrac{\begin{pmatrix}\sigma_{c1}^{4}\psi_1+\sigma_{c2}^{4}\psi_2\\+\sigma_{c3}^{4}\psi_3\end{pmatrix}}{(\psi_1+\psi_2+\psi_3)}+\Lambda_4\right) \end{bmatrix} * \begin{bmatrix} N_1 \\ N_2 \\ N_3 \\ N_4 \end{bmatrix} = \frac{d}{dt}\begin{bmatrix} N_1 \\ N_2 \\ N_3 \\ N_4 \end{bmatrix}$$

The solutions to the nuclide transmutation equations are:

$$N_1(t) = N_1(0)e^{-a_{11}t}$$

$$N_2(t) = N_2(0)e^{-a_{22}t}$$

$$N_3(t) = N_3(0)e^{-a_{33}t} + \frac{a_{32}N_2(0)}{a_{22}-a_{33}}\left[e^{-a_{33}t} - e^{-a_{22}t}\right]$$

$$N_4(t) = N_4(0)e^{-a_{44}t} + \frac{a_{41}N_1(0)}{a_{11}-a_{44}}\left[e^{-a_{44}t} - e^{-a_{11}t}\right] + \frac{a_{42}N_2(0)}{a_{22}-a_{44}}\left[e^{-a_{44}t} - e^{-a_{22}t}\right]$$
$$+ \frac{a_{43}N_3(0)}{a_{33}-a_{44}}\left[e^{-a_{44}t} - e^{-a_{33}t}\right]$$
$$+ a_{43}a_{32}N_2(0) * z$$

$$\textit{where} \quad z = \left[\frac{e^{-a_{44}t}}{(a_{33}-a_{44})(a_{22}-a_{44})} + \frac{e^{-a_{33}t}}{(a_{44}-a_{33})(a_{22}-a_{33})} + \frac{e^{-a_{22}t}}{(a_{44}-a_{22})(a_{33}-a_{22})}\right]$$

where a_{ij} refers to elements in the matrix of the nuclide transmutation equations. After substitution of the elements in the matrix, the solutions to the nuclide transmutation equations become:

$$N_1(t) = N_1(0)e^{-\Phi\sigma_a^1 t}$$

$$N_2(t) = N_2(0)e^{-\Phi\sigma_a^2 t}$$

$$N_3(t) = N_3(0)e^{-\left(\Phi\sigma_a^3+\Lambda_3\right)t} + \frac{\Phi\sigma_c^2 N_2(0)}{\Phi\sigma_a^2 - \left(\Phi\sigma_a^3+\Lambda_3\right)}\left[e^{-\left(\Phi\sigma_a^3+\Lambda_3\right)t} - e^{-\Phi\sigma_a^2 t}\right]$$

$$N_4(t) = N_4(0)e^{-\left(\Phi\sigma_c^4+\Lambda_4\right)t} + \frac{\gamma_4^1\Phi\sigma_f^1 N_1(0)}{\Phi\sigma_a^1 - \left(\Phi\sigma_c^4+\Lambda_4\right)}\left[e^{-\left(\Phi\sigma_c^4+\Lambda_4\right)t} - e^{-\Phi\sigma_a^1 t}\right]$$
$$+ \frac{\gamma_4^2\Phi\sigma_f^2 N_2(0)}{\Phi\sigma_a^2 - \left(\Phi\sigma_c^4+\Lambda_4\right)}\left[e^{-\left(\Phi\sigma_c^4+\Lambda_4\right)t} - e^{-\Phi\sigma_a^2 t}\right]$$
$$+ \frac{\gamma_4^3\Phi\sigma_f^3 N_3(0)}{\left(\Phi\sigma_a^3+\Lambda_3\right) - \left(\Phi\sigma_c^4+\Lambda_4\right)}\left[e^{-\left(\Phi\sigma_c^4+\Lambda_4\right)t} - e^{-\left(\Phi\sigma_a^3+\Lambda_3\right)t}\right]$$
$$+ \gamma_4^3\Phi^2\sigma_f^3\sigma_c^2 N_2(0)\left[\frac{1}{x}e^{-\left(\Phi\sigma_c^4+\Lambda_4\right)t} + \frac{1}{y}e^{-\left(\Phi\sigma_a^3+\Lambda_3\right)t} + \frac{1}{z}e^{-\Phi\sigma_a^2 t}\right]$$

where $x = \left[\left(\Phi\sigma_a^3+\Lambda_3\right) - \left(\Phi\sigma_c^4+\Lambda_4\right)\right] * \left[\left(\Phi\sigma_a^2\right) - \left(\Phi\sigma_c^4+\Lambda_4\right)\right]$

$$y = \left[\left(\Phi\sigma_c^4+\Lambda_4\right) - \left(\Phi\sigma_a^3+\Lambda_3\right)\right] * \left[\left(\Phi\sigma_a^2\right) - \left(\Phi\sigma_a^3+\Lambda_3\right)\right]$$

$$z = \left[\left(\Phi\sigma_c^4+\Lambda_4\right) - \left(\Phi\sigma_a^2\right)\right] * \left[\left(\Phi\sigma_a^3+\Lambda_3\right) - \left(\Phi\sigma_a^2\right)\right]$$

4.1.4 Three-group, Four Nuclide Infinite Fuel Pin Lattice System (Example 3) with Multiple Materials

Example 3 with multiple materials is an extension of Example 3 that includes having different fuel pin types (multiple materials) in the system. The equations presented here are a continuation of the equations for Example 3, and show how multiple materials are incorporated into the equations. Most of the equations for Example 3 apply to multiple materials; however, there are a few changes that need to be made to some of the equations.

The equations for the flux shape stay the same, but the power of the system is now defined by multiple materials, so changes are needed in the power normalization equation. The power of the system is defined by $P = \beta \sum_{m} \Phi_{m} \sum_{ij} Q_{ijm} N_{im} \sigma_{ijm}$, where β equals 1.6×10^{-19} (constant conversion factor) and the summation over m is over the pin types (different materials) in the system. The equations for the cross sections and the nuclide transmutation equations remain unchanged, except that the materials are depleted with their respective flux values (Φ_1 flux used for material 1 and Φ_2 flux used for material 2, etc.).

4.2 Derived Variance Equations

The equations presented in this section are the derived equations of the LUNGA method that are used to calculate the variance in the number densities and are derived from the governing equations that are shown in the previous section. The equations for the variance in the number densities are represented in general form for each example problem.

4.2.1 Example 1 Variance Equations

The equations for the variance in the number density for Example 1 are simplistic in nature. Since Example 1 is a single nuclide, the example is well suited for showing the approach taken in this research.

A change in the flux shape comes from the statistical uncertainty in the flux shape as $\Delta\psi = \Delta\psi_s$. A change in the flux comes from a change in the flux normalization equation as follows (ψ is fixed to be unity):

$$\Phi = \frac{P}{\psi N_0 \sigma_f} \Rightarrow P = N_0 \Phi \sigma_f \psi$$

$$\Delta P = 0 = \frac{\partial P}{\partial N_0}\Delta N_0 + \frac{\partial P}{\partial \Phi}\Delta\Phi + \frac{\partial P}{\partial \sigma_f}\Delta\sigma_f + \frac{\partial P}{\partial \psi}\Delta\psi$$

$$\Rightarrow \Delta\Phi = -\left(\frac{\partial P}{\partial N_0}\Delta N_0 + \frac{\partial P}{\partial \sigma_f}\Delta\sigma_f + \frac{\partial P}{\partial \psi}\Delta\psi\right) * \frac{1}{\left(\frac{\partial P}{\partial \Phi}\right)}$$

Transmutation is done under a constant power restraint; therefore, there is no change in the power during a time step (i.e. $\Delta P = 0$). The equation for the change in the nuclide number density is given by the following equation:

$$\Delta N = \frac{\partial N}{\partial N_0}\Delta N_0 + \frac{\partial N}{\partial \Phi}\Delta\Phi + \frac{\partial P}{\partial \sigma_a}\Delta\sigma_a = \frac{\partial N}{\partial N_0}\Delta N_0 + \frac{\partial P}{\partial \sigma_a}\Delta\sigma_a$$
$$+ \frac{\partial N}{\partial \Phi}\left(-\left(\frac{\partial P}{\partial N_0}\Delta N_0 + \frac{\partial P}{\partial \sigma_f}\Delta\sigma_f + \frac{\partial P}{\partial \psi}\Delta\psi\right) * \frac{1}{\left(\frac{\partial P}{\partial \Phi}\right)}\right)$$

$$\Rightarrow \Delta N = \left(e^{-\Phi\sigma_a t} + \Phi\sigma_a t e^{-\Phi\sigma_a t}\right)\Delta N_0 + \frac{N_0 \Phi t \sigma_a e^{-\Phi\sigma_a t}}{\psi}\Delta\psi$$
$$+ \frac{N_0 \Phi t \sigma_a e^{-\Phi\sigma_a t}}{\sigma_f}\Delta\sigma_f + \left(-N_0 \Phi t e^{-\Phi\sigma_a t}\right)\Delta\sigma_a$$

The variance of the nuclide is given by $\text{var}(N) = E[(\Delta N)^2]$.

4.2.2 Example 2 Variance Equations

The equations for the variance in the number densities for Example 2 are slightly more complicated than the equations for Example 1. The equations are awkward because there are numerous terms in the equations; therefore, the equations are presented here in a condensed form. Readers can refer to the Appendix for the expanded equations for Example 2.

A change in the flux shape comes from the statistical uncertainty in the flux shape and the uncertainty in the flux shape due to uncertainty in the number densities given by the equation $\Delta\psi = \Delta\psi_s + \Delta\psi_N = \Delta\psi_s + \frac{\partial\psi}{\partial\overline{N}}\Delta\overline{N}$. A change in the flux comes from a change in the flux normalization equation as follows:

$$\Phi = \frac{P}{N_{10}\sigma_{f2}^{1}\psi_2} \Rightarrow P = N_{10}\sigma_{f2}^{1}\psi_2\Phi$$

$$\Delta P = 0 = \frac{\partial P}{\partial \psi_2}\Delta\psi_2 + \frac{\partial P}{\partial N_{10}}\Delta N_{10} + \frac{\partial P}{\partial \Phi}\Delta\Phi$$

$$\Rightarrow \Delta\Phi = -\left(\frac{\partial P}{\partial \psi_2}\Delta\psi_2 + \frac{\partial P}{\partial N_{10}}\Delta N_{10}\right) * \frac{1}{\left(\frac{\partial P}{\partial \Phi}\right)}$$

There is no uncertainty in σ_{f2}^{1} since the parameter is a group cross section value and not an effective cross section value (see assumptions). Solving for the change in the number densities after a time step is a very time consuming task.

The equations for the change in the nuclide number densities are given by the following equations (shown with the derivatives for readability):

$$\Delta N_1 = \frac{\partial N_1}{\partial \psi_1}\Delta\psi_1 + \frac{\partial N_1}{\partial \psi_2}\Delta\psi_2 + \frac{\partial N_1}{\partial N_{10}}\Delta N_{10} + \frac{\partial N_1}{\partial \Phi}\Delta\Phi$$

$$= \frac{\partial N_1}{\partial \psi_1}\Delta\psi_1 + \frac{\partial N_1}{\partial \psi_2}\Delta\psi_2 + \frac{\partial N_1}{\partial N_{10}}\Delta N_{10} + \frac{\partial N_1}{\partial \Phi}\left(-\left(\frac{\partial P}{\partial \psi_2}\Delta\psi_2 + \frac{\partial P}{\partial N_{10}}\Delta N_{10} \right) * \frac{1}{\left(\frac{\partial P}{\partial \Phi} \right)} \right)$$

$$\Delta N_2 = \frac{\partial N_1}{\partial \psi_1}\Delta\psi_1 + \frac{\partial N_1}{\partial \psi_2}\Delta\psi_2 + \frac{\partial N_2}{\partial N_{20}}\Delta N_{20} + \frac{\partial N_2}{\partial N_{10}}\Delta N_{10} + \frac{\partial N_2}{\partial \Phi}\Delta\Phi$$

$$= \frac{\partial N_1}{\partial \psi_1}\Delta\psi_1 + \frac{\partial N_1}{\partial \psi_2}\Delta\psi_2 + \frac{\partial N_2}{\partial N_{20}}\Delta N_{20} + \frac{\partial N_2}{\partial N_{10}}\Delta N_{10} + \frac{\partial N_2}{\partial \Phi}\left(-\left(\frac{\partial P}{\partial \psi_2}\Delta\psi_2 + \frac{\partial P}{\partial N_{10}}\Delta N_{10} \right) * \frac{1}{\left(\frac{\partial P}{\partial \Phi} \right)} \right)$$

The variances for the number density are slightly cumbersome to show and are given by $\text{var}(N_1) = E[(\Delta N_1)^2]$ and $\text{var}(N_2) = E[(\Delta N_2)^2]$.

4.2.3 Example 3 Variance Equations

The equations for the variance in the number densities for Example 3 are more complicated than the variance equations for Example 2. The equations are also very awkward because of numerous terms; therefore, they are presented here in simplified form (readers can refer to the appendix for more details of the equations for Example 3). The equations presented for the variance in the number densities for Example 3 closely resemble the general variance equations shown in Chapter 3.

A change in the flux shape comes from the statistical uncertainty in the flux shape, and the uncertainty in the number densities. The equation for a change in the flux shape is $\Delta\psi = \Delta\psi_s + \Delta\psi_N = \Delta\psi_s + \frac{\partial\psi}{\partial\overline{N}}\Delta\overline{N}$. The variance in the flux shape is

$\mathrm{var}(\psi) = E\left[(\Delta\psi)^2\right] = \mathrm{var}(\psi_s) + \frac{\partial\psi}{\partial\overline{N}}^T Cov\left[\overline{N}, \overline{N}^T\right]\frac{\partial\psi}{\partial\overline{N}}$ where the covariances between energy groups are neglected, and the statistical uncertainty is taken to be independent of the flux shape uncertainty due to the number density uncertainties.

The effective cross sections are found using the equation $\sigma_a^1 = \frac{\sigma_{a1}^1\psi_1 + \sigma_{a2}^1\psi_2 + \sigma_{a3}^1\psi_3}{\psi_1 + \psi_2 + \psi_3}$, which is demonstrated for the effective absorption cross section of N_1. The following notation is used for the energy group cross section values σ_{jk}^i where j is the type of cross section for nuclide i in group k, and for the effective cross section values σ_j^i where j is the type of cross section for nuclide i. The change and the variance in the effective cross section is

$$\Delta\sigma_a^1 = \frac{\partial\sigma_a^1}{\partial\psi_1}\Delta\psi_1 + \frac{\partial\sigma_a^1}{\partial\psi_2}\Delta\psi_2 + \frac{\partial\sigma_a^1}{\partial\psi_3}\Delta\psi_3$$

$$\mathrm{var}\left(\sigma_a^1\right) = E\left[\left(\Delta\sigma_a^1\right)^2\right] = \left(\frac{\partial\sigma_a^1}{\partial\psi_1}\right)^2 * \mathrm{var}(\psi_1) + \left(\frac{\partial\sigma_a^1}{\partial\psi_2}\right)^2 * \mathrm{var}(\psi_2) + \left(\frac{\partial\sigma_a^1}{\partial\psi_3}\right)^2 * \mathrm{var}(\psi_3)$$

where covariances between groups are neglected and $\mathrm{var}(\psi_1)$ is the variance of the flux shape in the first energy group. A change in the flux comes from a change in the flux normalization equation (the power constraint) as follows:

$$P = 1.6\text{x}10^{-19}\,\Phi\sum_{ij} Q_j^i N_{i0}\sigma_j^i$$

$$\Rightarrow P = 1.6\text{x}10^{-19}\,\Phi\begin{bmatrix} Q_f^1 N_{10}\sigma_f^1 + Q_c^1 N_{10}\sigma_c^1 + Q_f^2 N_{20}\sigma_f^2 + Q_c^2 N_{20}\sigma_c^2 \\ + Q_f^3 N_{30}\sigma_f^3 + Q_c^3 N_{30}\sigma_c^3 + Q_c^4 N_{40}\sigma_c^4 \end{bmatrix}$$

$$\Delta P = \frac{\partial P}{\partial \Phi}\Delta\Phi + \frac{\partial P}{\partial N_{i0}}\Delta N_{i0} + \frac{\partial P}{\partial \sigma_j^i}\Delta\sigma_j^i$$

$$\Rightarrow \Delta P = \frac{\partial P}{\partial \Phi}\Delta\Phi + \frac{\partial P}{\partial N_{10}}\Delta N_{10} + \frac{\partial P}{\partial N_{20}}\Delta N_{20} + \frac{\partial P}{\partial N_{30}}\Delta N_{30} + \frac{\partial P}{\partial N_{40}}\Delta N_{40} + \frac{\partial P}{\partial \sigma_f^1}\Delta\sigma_f^1 +$$
$$\frac{\partial P}{\partial \sigma_c^1}\Delta\sigma_c^1 + \frac{\partial P}{\partial \sigma_f^2}\Delta\sigma_f^2 + \frac{\partial P}{\partial \sigma_c^2}\Delta\sigma_c^2 + \frac{\partial P}{\partial \sigma_f^3}\Delta\sigma_f^3 + \frac{\partial P}{\partial \sigma_c^3}\Delta\sigma_c^3 + \frac{\partial P}{\partial \sigma_c^4}\Delta\sigma_c^4$$

$$\text{constant power} \Rightarrow \text{no change in P} \Rightarrow \Delta P = 0$$

$$\Rightarrow \Delta\Phi = -\frac{1}{\dfrac{\partial P}{\partial \Phi}}\left(\begin{array}{l} \dfrac{\partial P}{\partial N_{10}}\Delta N_{10} + \dfrac{\partial P}{\partial N_{20}}\Delta N_{20} + \dfrac{\partial P}{\partial N_{30}}\Delta N_{30} + \dfrac{\partial P}{\partial N_{40}}\Delta N_{40} + \dfrac{\partial P}{\partial \sigma_f^1}\Delta\sigma_{1f} + \dfrac{\partial P}{\partial \sigma_c^1}\Delta\sigma_c^1 \\ + \dfrac{\partial P}{\partial \sigma_f^2}\Delta\sigma_f^2 + \dfrac{\partial P}{\partial \sigma_c^2}\Delta\sigma_c^2 + \dfrac{\partial P}{\partial \sigma_f^3}\Delta\sigma_f^3 + \dfrac{\partial P}{\partial \sigma_c^3}\Delta\sigma_c^3 + \dfrac{\partial P}{\partial \sigma_c^4}\Delta\sigma_c^4 \end{array}\right)$$

where the equation for the power is taken from the SCALE manual [15]. The notation in the above equation follows the form of X_j^i where j is the type of cross section for nuclide i, and N_{i0} is the number density of nuclide i for the previous time step. The variance in the flux normalization becomes:

$$\text{var}(\Phi) = E\left[(\Delta\Phi)^2\right] = \left[-\frac{1}{\dfrac{\partial P}{\partial \Phi}}\left(\begin{array}{l} \dfrac{\partial P}{\partial N_{10}}\Delta N_{10} + \dfrac{\partial P}{\partial N_{20}}\Delta N_{20} + \dfrac{\partial P}{\partial N_{30}}\Delta N_{30} + \dfrac{\partial P}{\partial N_{40}}\Delta N_{40} \\ + \dfrac{\partial P}{\partial \sigma_f^1}\Delta\sigma_f^1 + \dfrac{\partial P}{\partial \sigma_c^1}\Delta\sigma_c^1 + \dfrac{\partial P}{\partial \sigma_f^2}\Delta\sigma_f^2 \\ + \dfrac{\partial P}{\partial \sigma_c^2}\Delta\sigma_c^2 + \dfrac{\partial P}{\partial \sigma_f^3}\Delta\sigma_f^3 + \dfrac{\partial P}{\partial \sigma_c^3}\Delta\sigma_c^3 + \dfrac{\partial P}{\partial \sigma_c^4}\Delta\sigma_c^4 \end{array}\right)\right]^2$$

A change in the nuclide transmutation equations is:

$$\Delta N_1 = \frac{\partial N_1}{\partial N_{10}}\Delta N_{10} + \frac{\partial N_1}{\partial \Phi}\Delta\Phi + \frac{\partial N_1}{\partial \sigma_a^1}\Delta\sigma_a^1$$

$$\Delta N_2 = \frac{\partial N_2}{\partial N_{20}}\Delta N_{20} + \frac{\partial N_2}{\partial \Phi}\Delta\Phi + \frac{\partial N_1}{\partial \sigma_a^2}\Delta\sigma_a^2$$

$$\Delta N_3 = \frac{\partial N_3}{\partial N_{30}}\Delta N_{30} + \frac{\partial N_3}{\partial N_{20}}\Delta N_{20} + \frac{\partial N_3}{\partial \Phi}\Delta\Phi + \frac{\partial N_1}{\partial \sigma_a^3}\Delta\sigma_a^3 + \frac{\partial N_1}{\partial \sigma_c^2}\Delta\sigma_c^2 + \frac{\partial N_1}{\partial \sigma_a^2}\Delta\sigma_a^2$$

$$\Delta N_4 = \frac{\partial N_4}{\partial N_{40}}\Delta N_{40} + \frac{\partial N_4}{\partial N_{10}}\Delta N_{10} + \frac{\partial N_4}{\partial \Phi}\Delta\Phi + \frac{\partial N_1}{\partial \sigma_c^4}\Delta\sigma_c^4 + \frac{\partial N_1}{\partial \sigma_f^1}\Delta\sigma_f^1 + \frac{\partial N_1}{\partial \sigma_a^1}\Delta\sigma_a^1$$
$$+ \frac{\partial N_4}{\partial N_{30}}\Delta N_{30} + \frac{\partial N_4}{\partial N_{20}}\Delta N_{20} + \frac{\partial N_4}{\partial \sigma_f^3}\Delta\sigma_f^3 + \frac{\partial N_4}{\partial \sigma_a^3}\Delta\sigma_a^3 + \frac{\partial N_4}{\partial \sigma_c^2}\Delta\sigma_c^2 + \frac{\partial N_4}{\partial \sigma_a^2}\Delta\sigma_a^2$$

where $\Delta\Phi$ and $\Delta\sigma_j^i$ are defined by previous equations and must be substituted into the equations for a change in the number densities prior to solving for the variance in the number densities. The variance in the number densities is given with the following equations: $\text{var}(N_1) = E[(\Delta N_1)^2]$, $\text{var}(N_2) = E[(\Delta N_2)^2]$, $\text{var}(N_3) = E[(\Delta N_3)^2]$, and $\text{var}(N_4) = E[(\Delta N_4)^2]$.

4.2.4 Example 3 with Multiple Materials Variance Equations

The variance equations presented here are a continuation of the variance equations for Example 3, and show how multiple materials are incorporated into the equations. Most of the variance equations for Example 3 apply to multiple materials; however, there are a few changes that need to be made to some of the equations.

The equations for the flux shape stay the same, but the power of the system is now defined by multiple materials and is defined by the equation $P = \beta\sum_m \Phi_m \sum_{ij} Q_{ijm} N_{im} \sigma_{ijm}$,

where β equals 1.6×10^{-19} (constant conversion factor) and the summation over m is over the pin types (different materials) in the system.

The change in the flux normalization that comes from a change in the power constraint previously defined is:

$$\Delta P = \frac{\partial P}{\partial \Phi_m}\Delta\Phi_m + \frac{\partial P}{\partial N_{im}}\Delta N_{im} + \frac{\partial P}{\partial \sigma_{ijm}}\Delta\sigma_{ijm}$$

$$\text{constant power} \Rightarrow \text{no change in P} \Rightarrow \Delta P = 0$$

$$0 = \frac{\partial P}{\partial \Phi_m}\Delta\Phi_m + \frac{\partial P}{\partial N_{im}}\Delta N_{im} + \frac{\partial P}{\partial \sigma_{ijm}}\Delta\sigma_{ijm}$$

$$\Delta\Phi_m = -\left(\frac{\partial P}{\partial N_{im}}\Delta N_{im} + \frac{\partial P}{\partial \sigma_{ijm}}\Delta\sigma_{ijm}\right) * \frac{1}{\frac{\partial P}{\partial \Phi_m}}$$

The equations for the cross sections and the nuclide transmutation equations remain unchanged. The equations for a change in and variance of the nuclide transmutation equations are the same, except for the substitution of the change in the flux normalization (defined above). The other difference in the equations for Example 3 with multiple materials and Example 3 is the addition of covariance terms between the different materials (i.e., the covariances between material 1 and material 2).

The equations presented in this section show how the variance in the number densities is derived for each example problem. Chapter 5 and chapter 6 show the results and verification, respectively, of the research.

CHAPTER 5

RESULTS AND ANALYSIS

The results of this research are presented next along with an analysis of those results. Validation studies are demonstrated in the next chapter. Shown first are the results of the acceptability of using first order perturbation theory for calculating the variances in the number densities. This is done for each of the three example problems (Example 1, Example 2, and Example 3). Example 2 and Example 3 are then analyzed in depth. The number density can be found independently of the flux shape with Example 1; therefore, Example 1 is only used for investigating first order perturbation theory.

5.1 Acceptability of Using First Order Perturbation Theory

The effects of using first order perturbation theory in the equations for the variance in the number densities needed to be examined to determine if first order perturbation theory was acceptable for the application of calculating the standard deviation in the nuclide number densities. Example 1, Example 2, and Example 3 are used to investigate if this theory was appropriate for the derived equations used in the LUNGA method. To examine this effect, the change in nuclide number density was calculated by directly perturbing only the number density in the analytic equations by 2, 5, 7, 10 and 15 percent, and compared to the change in nuclide number density calculated from the equations used in the LUNGA method for Example 1 and Example 2. For Example 1 and Example 2, the equations examine the variance of the nuclide number densities in the nonlinear region with large time steps to fully test the accuracy of using a first order approximation.

The time regions used to investigate the use of first order perturbation theory in this research are shown in Figure 3 for Example 1, and Figure 4 and Figure 5 for Example 2. These regions were investigated because that is where the most nonlinear behavior of the nuclides occurs in Example 1 and Example 2. The same process is done with Example 3, except that the number density was perturbed by 0.5, 1, 5, and 10 percent for 12 time steps of 30 days per step.

The effects of using first order perturbation theory to calculate the variance and thus the standard deviation in the number densities is also investigated with Example 2 by directly perturbing the flux shape by 1 to 30 percent. The change in the flux shape and number densities calculated with direct perturbation of the flux shape is then compared to the change in the flux shape and number densities calculated using the LUNGA method.

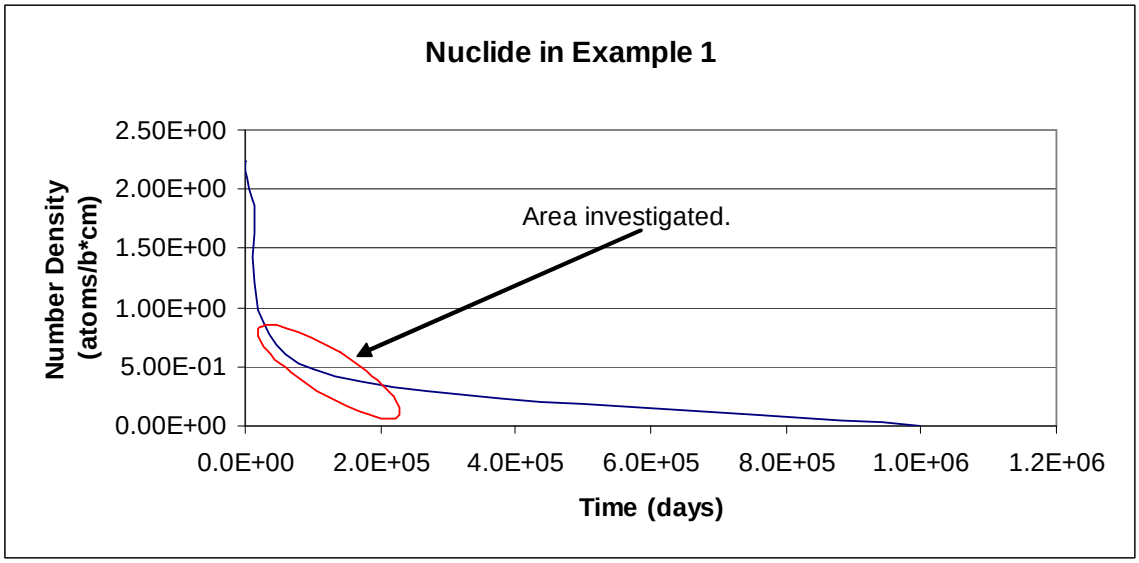

Figure 3. Plot of where the nuclide was examined in Example 1 (analytic solution).

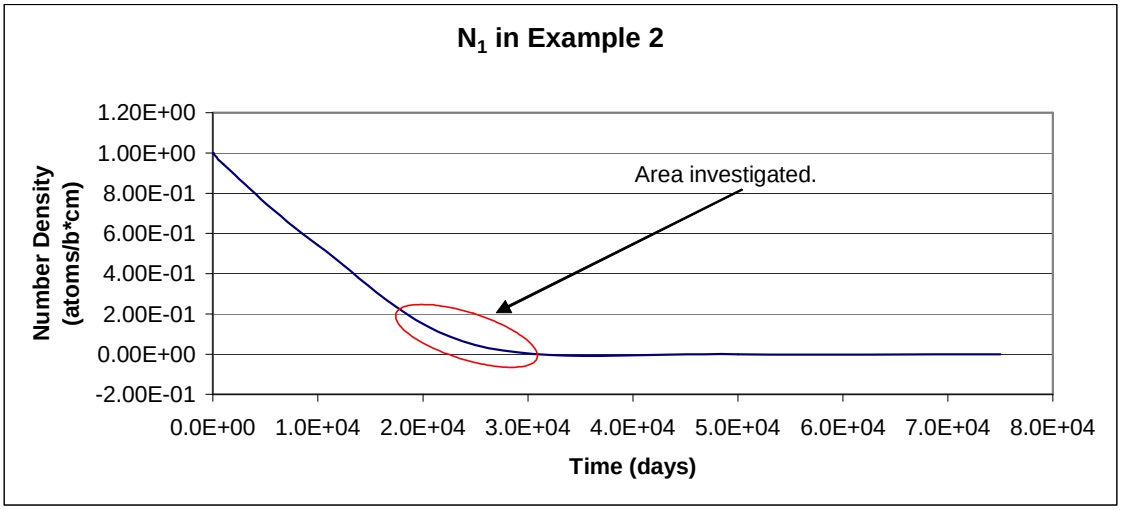

Figure 4. Plot of where N_1 was examined in Example 2 (analytic solution).

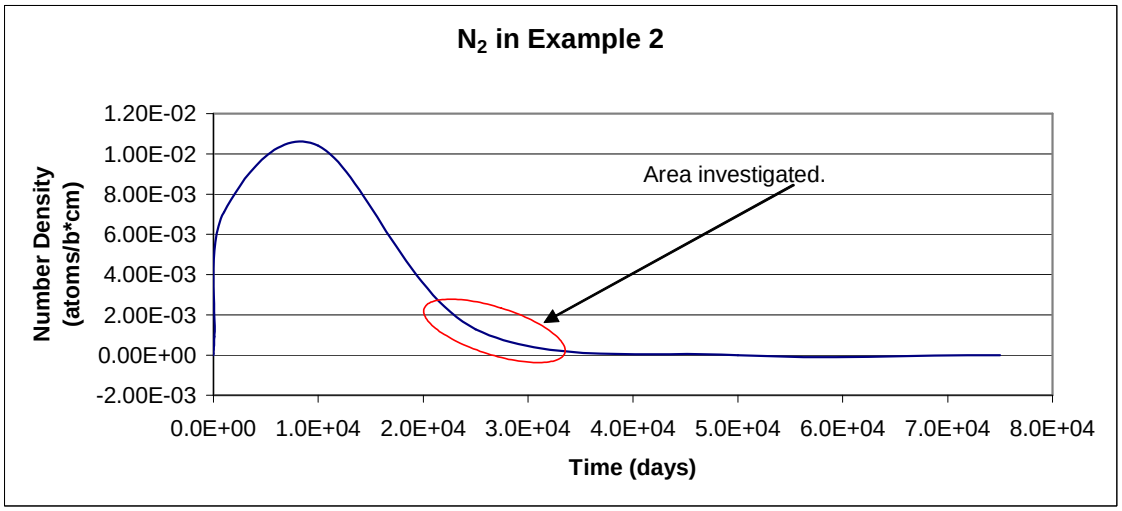

Figure 5. Plot of where N_2 was examined in Example 2 (analytic solution).

5.1.1 Perturbation of Number Density with Example 1

Table 3 specifies the parameters used in Example 1 and those parameters are constant during a time step. For simplification, the parameters are the same in each time step. This will not affect the method being used, as any value during a time step is taken as a constant during that time step, and parameters can only be updated after a time step. A comparison of changes in the number densities is given in Table 4. Table 5 shows the variances calculated for this example.

Table 3. Parameters for Example 1.

σ_f (cm^3)	1.00E-24
σ_a (cm^3)	2.00E-24
t (s)	2.16E+09
P (fission/s*cm^3)	2.00E+14
sd(ψ)	1.00E-05
ψ flux shape	1.00E+00

Table 4 shows that the derived equation predicts the change in nuclide number density very accurately, generally under a 5 percent difference, compared to directly perturbing the nuclide number density for a given time step and also after multiple time steps. Only in the last time step for a 7, 10 and 15 percent perturbation do the two methods differ by more than 5 percent. The calculations are preformed using large time steps of 2,500 days; however, the use of large time steps like these would probably not occur in a real simulated problem because better accuracy would be achieved with smaller time steps. Large time steps are used to test the bounds of a first order approximation and to examine the differences in the number densities where the curve was not very linear (see Figure 3). The use of large time steps might not be very

accurate, since the approximation is linear; however, Table 4 illustrates that the derived equation is very close to the actual change (direct perturbation) in the number density. Table 4 further illustrates the equation is fairly accurate up to at least a 15 percent perturbation in the number density. The equation and direct perturbation only differ by more than 10 percent on the last time step with a 15 percent perturbation in the number density. Finally, Table 4 shows the equation is under predicting the change in the number density compared to direct perturbation. This might not be a very desirable attribute, but the values are also very close to one another.

Table 4. Comparison of ΔN in Example 1.

	Time Step 1			Time Step 2		
Time/ Cumulative Time (days)	2500/2500			2500/5000		
N_0 (atoms/cm^3)	2.23E+24			1.51E+24		
	Change in number density=ΔN (atoms/cm^3)			Change in number density=ΔN (atoms/cm^3)		
Perturbation Amount (%)	Direct perturbation	LUNGA solution	Percent Difference	Direct perturbation	LUNGA solution	Percent Difference
2.0	4.21E+22	4.20E+22	-1.1E-01	2.70E+22	2.69E+22	-2.0E-01
5.0	1.05E+23	1.05E+23	-2.6E-01	6.76E+22	6.72E+22	-5.0E-01
7.0	1.48E+23	1.47E+23	-3.6E-01	9.48E+22	9.41E+22	-6.8E-01
10.0	2.11E+23	2.10E+23	-4.9E-01	1.36E+23	1.34E+23	-9.5E-01
15.0	3.17E+23	3.15E+23	-7.1E-01	2.05E+23	2.02E+23	-1.4E+00
	Time Step 3			Time Step 4		
Time/ Cumulative Time (days)	2500/7500			2500/10000		
N_0 (atoms/cm^3)	8.56E+23			3.12E+23		
	Change in number density=ΔN (atoms/cm^3)			Change in number density=ΔN (atoms/cm^3)		
Perturbation Amount (%)	Direct perturbation	LUNGA solution	Percent Difference	Direct perturbation	LUNGA solution	Percent Difference
2.0	1.26E+22	1.25E+22	-5.0E-01	1.51E+21	1.48E+21	-2.0E+00
5.0	3.18E+22	3.14E+22	-1.2E+00	3.89E+21	3.70E+21	-4.8E+00
7.0	4.47E+22	4.39E+22	-1.7E+00	5.55E+21	5.18E+21	-6.6E+00
10.0	6.42E+22	6.27E+22	-2.3E+00	8.14E+21	7.40E+21	-9.1E+00
15.0	9.74E+22	9.41E+22	-3.3E+00	1.28E+22	1.11E+22	-1.3E+01

Table 5 presents the variance and the standard deviation of the nuclide for this example. Note that the table for the variance and standard deviation of the nuclide only takes into account a change in the nuclide number density, which was investigated at this time to examine first order perturbation theory. Table 5 demonstrates that the relative uncertainty increases with each time step, and that the absolute uncertainty is increasing with time which was seen in other literature sources [19 and 21].

Table 5. Relative sd(N) for Example 1.

		Time Step 1	Time Step 2	Time Step 3	Time Step 4
N_0 (atoms/cm^3)		2.23E+24	1.51E+24	8.56E+23	3.12E+23
flux (n/cm^2*s)		8.96E+13	1.32E+14	2.34E+14	6.40E+14
N=N(t) (atoms/cm^3)		1.51E+24	8.56E+23	3.12E+23	1.96E+22
var(N) (atoms/cm^3)^2		1.59E+37	2.01E+37	1.21E+37	6.81E+35
sd(N) (atoms/cm^3)	absolute uncertainty	3.98E+18	4.49E+18	3.48E+18	8.25E+17
sd(N)/N(t)	relative uncertainty	2.63E-06	5.24E-06	1.11E-05	4.20E-05

5.1.2 Perturbation of Number Density with Example 2

Table 6 specifies the parameters used in Example 2 that are obtained from a report by Williams [26]. Like Example 1, the parameters for this example are constant through a time step and for simplification are the same in each time step. The comparison of changes in the number densities for a change in only the number density is given in Table 7 and Table 8. Table 9 and Table 10 present the variance in the number densities based only on a change in the number densities. Table 11 shows the comparison of changes in the flux shape and number densities for a change in only the flux shape.

Table 6. Parameters for Example 2.

σ_{ijk} nuclide i; cross section type j; in group k			
σ_{1r1} nuclide 1 (cm^2)	9.00E-24	X_1	1.00E+00
σ_{1a1} nuclide 1 (cm^2)	3.00E-24	X_2	0.00E+00
$\sigma_{1s,1-2}$ nuclide 1 (cm^2)	6.00E-24	γ	5.00E-01
σ_{1c2} nuclide 1 (cm^2)	1.00E-24	P (fission/s*cm^3)	2.00E+14
σ_{1a2} nuclide 1 (cm^2)	2.00E-24	Λ (s^{-1})	4.00E-09
σ_{1f2} nuclide 1 (cm^2)	1.00E-24	sd(ψ_1)	1.00E-05
σ_{2c2} nuclide 2 (cm^2)	1.00E-23	sd(ψ_2)	1.00E-05
$N1_0$ (atoms/cm^3)	1.00E+24	$N2_0$ (atoms/cm^3)	0.00E+00

Table 7 and Table 8 illustrate that the equations in the LUNGA method predict the change in nuclide number density very accurately compared to directly perturbing the nuclide number density for a given time step and also after multiple time steps. The only time the derived equations and the direct perturbation seem to vary greatly is in N_2 in the first time step, but the difference is only slightly larger than 5 percent with a 15 percent perturbation in the number densities in that time step. As with Example 1, the calculations are preformed using large time steps (2,500 days), and would probably not occur in a real simulated problem, but are used to examine the differences in the number densities where the curves were not very linear, as displayed in Figure 4 and Figure 5. Again the use of large time steps might not be very accurate since the equation is linear; however, Table 7 and Table 8 demonstrate that the equations used in the LUNGA method are very close to the actual change (direct perturbation) in the number density. This example also shows that the derived equations are accurate up to at least a 15 percent perturbation in the number density, which is considered good since the change in the number densities are much smaller than the amount of perturbation in the number densities. Finally, Table 7 and Table 8 reveal that the derived equations of the LUNGA method are under predicting the change in the number density compared to direct perturbation for N_1 and over predicting for N_2, which might not be a good trait; however, the values are very close to one another.

Table 7. Comparison of ΔN by direct perturbation of nuclides for time step 1 and time step 2 for Example 2.

	Time Step 1					
Time/Cummulative Time (days)	20000/20000					
$N_1(0)$ (atoms/cm^3)	1.000E+24					
$N_2(0)$ (atoms/cm^3)	0.000E+00					
	Change in number density=ΔN_1 (atoms/cm^3)			Change in number density=ΔN_2 (atoms/cm^3)		
Perturbation Amount (%)	Direct perturbation in $N_1(0)$	LUNGA solution	Percent Difference	Direct perturbation in $N_2(0)$	LUNGA solution	Percent Difference
2.0	1.45E+22	1.44E+22	-5.2E-01	1.69E+20	1.70E+20	6.6E-01
5.0	3.66E+22	3.61E+22	-1.3E+00	4.18E+20	4.25E+20	1.7E+00
7.0	5.14E+22	5.06E+22	-1.7E+00	5.82E+20	5.96E+20	2.3E+00
10.0	7.40E+22	7.22E+22	-2.4E+00	8.23E+20	8.51E+20	3.4E+00
15.0	1.12E+23	1.08E+23	-3.5E+00	1.21E+21	1.28E+21	5.2E+00
	Time Step 2					
Time/Cummulative Time (days)	2500/22500					
$N_1(0)$ (atoms/cm^3)	3.546E+23					
$N_2(0)$ (atoms/cm^3)	6.566E+21					
	Change in number density=ΔN_1 (atoms/cm^3)			Change in number density=ΔN_2 (atoms/cm^3)		
Perturbation Amount (%)	Direct perturbation in $N_1(0)$	LUNGA solution	Percent Difference	Direct perturbation in $N_2(0)$	LUNGA solution	Percent Difference
2.0	6.71E+21	6.70E+21	-1.0E-01	1.33E+20	1.33E+20	7.2E-01
5.0	1.68E+22	1.67E+22	-2.5E-01	3.28E+20	3.34E+20	1.8E+00
7.0	2.35E+22	2.34E+22	-3.4E-01	4.56E+20	4.67E+20	2.5E+00
10.0	3.37E+22	3.35E+22	-4.7E-01	6.45E+20	6.67E+20	3.5E+00
15.0	5.06E+22	5.02E+22	-6.8E-01	9.51E+20	1.00E+21	5.3E+00

Table 8. Comparison of ΔN by direct perturbation of nuclides for time step 3 and time step 4 for Example 2.

	Time Step 3					
Time/Cummulative Time (days)	2500/25000					
$N_1(0)$ (atoms/cm^3)	2.433E+23					
$N_2(0)$ (atoms/cm^3)	7.929E+21					
	Change in number density=ΔN_1 (atoms/cm^3)			Change in number density=ΔN_2 (atoms/cm^3)		
Perturbation Amount (%)	Direct perturbation in $N_1(0)$	LUNGA solution	Percent Difference	Direct perturbation in $N_2(0)$	LUNGA solution	Percent Difference
2.0	4.34E+21	4.33E+21	-2.0E-01	1.32E+20	1.32E+20	4.3E-01
5.0	1.09E+22	1.08E+22	-4.8E-01	3.27E+20	3.31E+20	1.1E+00
7.0	1.53E+22	1.52E+22	-6.6E-01	4.56E+20	4.63E+20	1.5E+00
10.0	2.19E+22	2.17E+22	-9.3E-01	6.47E+20	6.61E+20	2.2E+00
15.0	3.29E+22	3.25E+22	-1.3E+00	9.61E+20	9.92E+20	3.2E+00
	Time Step 4					
Time/Cummulative Time (days)	2500/27500					
$N_1(0)$ (atoms/cm^3)	1.387E+23					
$N_2(0)$ (atoms/cm^3)	5.751E+21					
	Change in number density=ΔN_1 (atoms/cm^3)			Change in number density=ΔN_2 (atoms/cm^3)		
Perturbation Amount (%)	Direct perturbation in $N_1(0)$	LUNGA solution	Percent Difference	Direct perturbation in $N_2(0)$	LUNGA solution	Percent Difference
2.0	2.05E+21	2.04E+21	-4.9E-01	8.97E+19	8.97E+19	-3.7E-03
5.0	5.17E+21	5.11E+21	-1.2E+00	2.24E+20	2.24E+20	1.4E-02
7.0	7.27E+21	7.15E+21	-1.6E+00	3.14E+20	3.14E+20	4.0E-02
10.0	1.05E+22	1.02E+22	-2.3E+00	4.48E+20	4.49E+20	9.9E-02
15.0	1.58E+22	1.53E+22	-3.3E+00	6.71E+20	6.73E+20	2.4E-01

The behavior of N_2 is interesting in this example. The derived equations are over predicting the change in number density for N_2 compared to direct perturbation and the equation seems to better predict the change in number density for N_2 as more time steps pass. Coincidentally, this is indicating that the derived equations in the LUNGA method can more accurately predict a change in the number density as the calculation progress in time (with more passing time steps). Examining at the trend of N_2 in time, it looks like

the derived equations could start under predicting the number density after some number of time steps, but more steps would be needed to see if this is the case. This is interesting because then the equations would under predict the number densities for both N_1 and N_2, which is beneficial as both number density values might then be under predicted. However, it would not be favorable to have N_2 being over predicted and then start being under predicted as it would be difficult to know if the exact value is more or less than the value calculated using the derived equations of the LUNGA method.

Table 9 shows the variance and the standard deviation in the number densities for Example 2. Note that the variance and standard deviation in the number densities in the table only take into account a change in the nuclide number density, which is used at this time to investigate the affects of first order perturbation theory.

Table 9. Relative sd(N) with 2,500-day time steps for Example 2.

		Time Step 1	Time Step 2	Time Step 3	Time Step 4
Time/Cummulative Time (days)		20000/20000	2500/22500	2500/25000	2500/27500
$N_1(0)$ (atoms/cm^3)	beginning of time step	1.00E+24	3.55E+23	2.43E+23	1.39E+23
$N_2(0)$ (atoms/cm^3)		0.00E+00	6.57E+21	7.93E+21	5.75E+21
Φ (n/cm^2*s)	flux	2.00E+14	5.64E+14	8.22E+14	1.44E+15
$N_1=N_1(t)$ (atoms/cm^3)	end of time step	3.55E+23	2.43E+23	1.39E+23	5.11E+22
$N_2=N_2(t)$ (atoms/cm^3)		6.57E+21	7.93E+21	5.75E+21	2.64E+21
var(N_1) (atoms/cm^3)^2	variance	1.50E+37	1.43E+37	1.20E+37	6.75E+36
sd(N_1) (atoms/cm^3)	absolute uncertainty	3.88E+18	3.78E+18	3.46E+18	2.60E+18
sd(N_1)/$N_1(t)$	relative uncertainty	1.09E-05	1.55E-05	2.49E-05	5.08E-05
var(N_2) (atoms/cm^3)^2	variance	4.11E+33	3.71E+33	1.12E+34	3.57E+34
sd(N_2) (atoms/cm^3)	absolute uncertainty	6.41E+16	6.09E+16	1.06E+17	1.89E+17
sd(N_2)/$N_2(t)$	relative uncertainty	9.76E-06	7.68E-06	1.84E-05	7.15E-05

Table 9 shows that the absolute error in the number density for each nuclide decreases with each time step, which is opposite of what was seen in the previous example and other references [19 and 21]. However, the table ranges from 20,000 to 27,500 days, which is very far in time during the calculation. Table 10 gives the variance and standard deviation in the number densities with time steps of 1,200 days and the table shows that the absolute error in the number density for N_1 increases with time up to time step 14, where it then starts to decrease with time. In Table 10, the absolute uncertainty of N_2 continues to increase with time even after time step 14. Table 9 and Table 10 show that the relative uncertainty in the number densities of both nuclides increases with time, which was found in the previous example.

Table 10. Relative sd(N) with 1,200-day time steps for Example 2.

Time step size of 1200 days per time step									
		Time Step 1	Time Step 2	Time Step 3	Time Step 4	Time Step 5	Time Step 6	Time Step 7	Time Step 8
$N1_0$ (atoms/cm^3)	beginning of time step	1.00E+24	9.40E+23	8.79E+23	8.17E+23	7.56E+23	6.94E+23	6.33E+23	5.72E+23
$N2_0$ (atoms/cm^3)		0.00E+00	7.46E+21	1.13E+22	1.32E+22	1.40E+22	1.42E+22	1.40E+22	1.36E+22
Φ (n/cm^2*s)	flux	2.00E+14	2.13E+14	2.28E+14	2.45E+14	2.65E+14	2.88E+14	3.16E+14	3.50E+14
$N_1=N_1(t)$ (atoms/cm^3)	end of time step	9.40E+23	8.79E+23	8.17E+23	7.56E+23	6.94E+23	6.33E+23	5.72E+23	5.11E+23
$N_2=N_2(t)$ (atoms/cm^3)		7.46E+21	1.13E+22	1.32E+22	1.40E+22	1.42E+22	1.40E+22	1.36E+22	1.30E+22
var(N_1) (atoms/cm^3)^2	variance	3.80E+35	7.57E+35	1.13E+36	1.50E+36	1.86E+36	2.21E+36	2.55E+36	2.87E+36
sd(N_1) (atoms/cm^3)	absolute uncertainty	6.16E+17	8.70E+17	1.06E+18	1.22E+18	1.36E+18	1.49E+18	1.60E+18	1.69E+18
sd(N_1)/N_1(t)	relative uncertainty	6.56E-07	9.90E-07	1.30E-06	1.62E-06	1.96E-06	2.35E-06	2.79E-06	3.32E-06
var(N_2) (atoms/cm^3)^2	variance	7.15E+30	1.10E+31	1.64E+31	2.53E+31	3.87E+31	5.82E+31	8.66E+31	1.29E+32
sd(N_2) (atoms/cm^3)	absolute uncertainty	2.67E+15	3.32E+15	4.05E+15	5.03E+15	6.22E+15	7.63E+15	9.31E+15	1.13E+16
sd(N_2)/N_2(t)	relative uncertainty	3.58E-07	2.92E-07	3.06E-07	3.58E-07	4.38E-07	5.45E-07	6.85E-07	8.72E-07
		Time Step 9	Time Step 10	Time Step 11	Time Step 12	Time Step 13	Time Step 14	Time Step 15	Time Step 16
$N1_0$ (atoms/cm^3)	beginning of time step	5.11E+23	4.50E+23	3.89E+23	3.29E+23	2.70E+23	2.11E+23	1.54E+23	1.00E+23
$N2_0$ (atoms/cm^3)		1.30E+22	1.23E+22	1.15E+22	1.05E+22	9.44E+21	8.16E+21	6.65E+21	4.87E+21
Φ (n/cm^2*s)	flux	3.92E+14	4.45E+14	5.14E+14	6.08E+14	7.42E+14	9.47E+14	1.30E+15	2.00E+15
$N_1=N_1(t)$ (atoms/cm^3)	end of time step	4.50E+23	3.89E+23	3.29E+23	2.70E+23	2.11E+23	1.54E+23	1.00E+23	5.12E+22
$N_2=N_2(t)$ (atoms/cm^3)		1.23E+22	1.15E+22	1.05E+22	9.44E+21	8.16E+21	6.65E+21	4.87E+21	2.85E+21
var(N_1) (atoms/cm^3)^2	variance	3.17E+36	3.44E+36	3.67E+36	3.84E+36	3.92E+36	3.85E+36	3.52E+36	2.69E+36
sd(N_1) (atoms/cm^3)	absolute uncertainty	1.78E+18	1.85E+18	1.92E+18	1.96E+18	1.98E+18	1.96E+18	1.88E+18	1.64E+18
sd(N_1)/N_1(t)	relative uncertainty	3.96E-06	4.77E-06	5.82E-06	7.27E-06	9.38E-06	1.27E-05	1.87E-05	3.20E-05
var(N_2) (atoms/cm^3)^2	variance	1.92E+32	2.91E+32	4.50E+32	7.20E+32	1.20E+33	2.12E+33	4.03E+33	8.57E+33
sd(N_2) (atoms/cm^3)	absolute uncertainty	1.39E+16	1.70E+16	2.12E+16	2.68E+16	3.47E+16	4.60E+16	6.35E+16	9.26E+16
sd(N_2)/N_2(t)	relative uncertainty	1.13E-06	1.48E-06	2.01E-06	2.84E-06	4.25E-06	6.93E-06	1.30E-05	3.25E-05

5.1.3 Perturbation of Statistical Component in the Flux Shape with Example 2

A change in the number densities and the flux shape in Example 2 are examined due to perturbations in the statistical component of the flux shape. Table 11 exhibits the change in the number densities and the flux shape for different perturbations in the statistical component of the flux shape for one time step. Figure 6 to Figure 8 show different perturbations in the statistical component of the flux shape for multiple time steps of varying sizes. Figure 9 to Figure 11 present perturbations in the statistical component of the flux shape for time steps of 1,000 days.

Table 11 shows the change in the flux shape and the change in the nuclide number densities due to a change in only the flux shape for a single time step of two days. Table 11 reveals that the equations used in the LUNGA method to calculate the flux shape and nuclide number densities, predict the change in the flux shape and change in the nuclide number densities very accurately compared to directly perturbing the flux shape. Table 11 also shows that a 30 percent perturbation in the flux shape yields only a 10 percent difference between the equations used in the LUNGA method and the direct perturbation results. Table 11 further demonstrates that the equations used in the LUNGA method are over predicting the change in both the number densities and the flux shape. Also, Table 11 indicates that the percent difference for N_1, N_2, and the ψ_N term are approximately the same and increase about the same amount for each perturbation. The effects of multiple time steps are described next.

Table 11. Comparison of $\Delta\psi$ and ΔN for perturbation in the ψ_S component of the flux shape for Example 2.

Flux Perturbation Comparison									
The change in the number density and the flux shape due to a perturbation in the statistical component of the flux shape.									
	Equations of LUNGA method			Direct Perturbation			Percent Difference (%)		
Perturbation Amount (%)	ΔN_1	ΔN_2	$\Delta\Psi$	ΔN_1	ΔN_2	$\Delta\Psi$	ΔN_1	ΔN_2	$\Delta\Psi$
1.00	2.30E-07	1.99E-12	2.98E-11	2.30E-07	1.98E-12	2.97E-11	-3.3E-01	-3.3E-01	-3.7E-01
1.50	3.46E-07	2.98E-12	4.48E-11	3.44E-07	2.97E-12	4.45E-11	-5.0E-01	-5.0E-01	-5.4E-01
1.75	4.03E-07	3.48E-12	5.22E-11	4.01E-07	3.46E-12	5.19E-11	-5.8E-01	-5.8E-01	-6.2E-01
2.00	4.61E-07	3.98E-12	5.97E-11	4.58E-07	3.95E-12	5.93E-11	-6.7E-01	-6.7E-01	-7.0E-01
3.00	6.91E-07	5.97E-12	8.95E-11	6.84E-07	5.91E-12	8.86E-11	-1.0E+00	-1.0E+00	-1.0E+00
5.00	1.15E-06	9.95E-12	1.49E-10	1.13E-06	9.79E-12	1.47E-10	-1.7E+00	-1.7E+00	-1.7E+00
10.00	2.30E-06	1.99E-11	2.98E-10	2.23E-06	1.93E-11	2.89E-10	-3.3E+00	-3.3E+00	-3.4E+00
15.00	3.46E-06	2.98E-11	4.48E-10	3.29E-06	2.84E-11	4.26E-10	-5.0E+00	-5.0E+00	-5.0E+00
30.00	6.91E-06	5.97E-11	8.95E-10	6.28E-06	5.43E-11	8.14E-10	-1.0E+01	-1.0E+01	-1.0E+01

Figure 6 to Figure 8 display the change in the number densities and the ψ_N term due to perturbations of different sizes in the statistical component of the flux and multiple time steps. The perturbation of the statistical component of the flux is the same for each time step and includes perturbations of 1, 5, 10, and 25 percent in the statistical component of the flux. The time steps include: 100-days for each of the first 5 steps, 250-days for the next 2 steps, and 1,000-days for the last step.

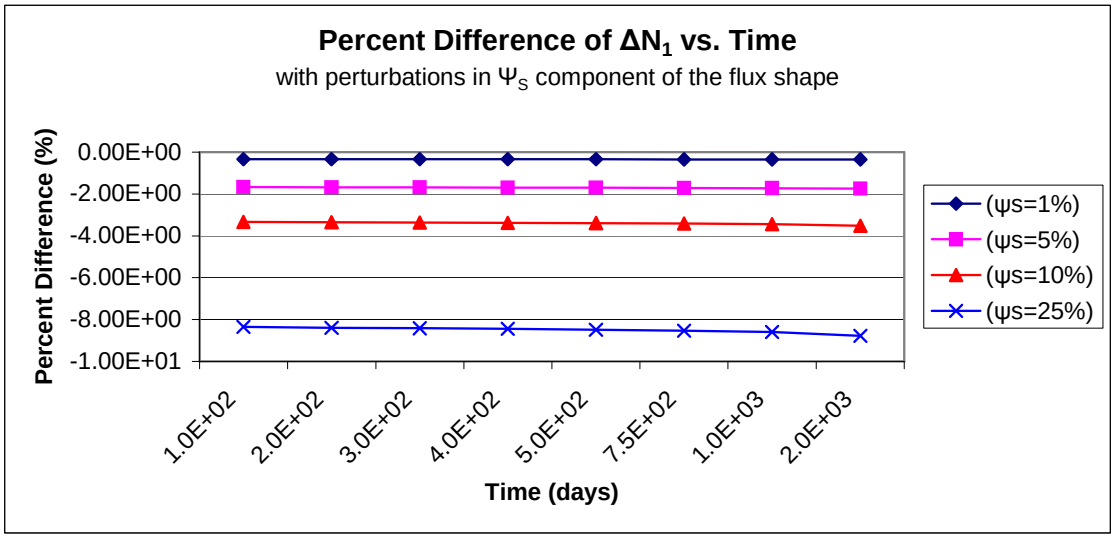

Figure 6. Percent difference of ΔN_1 for perturbation of the ψ_S term for Example 2.

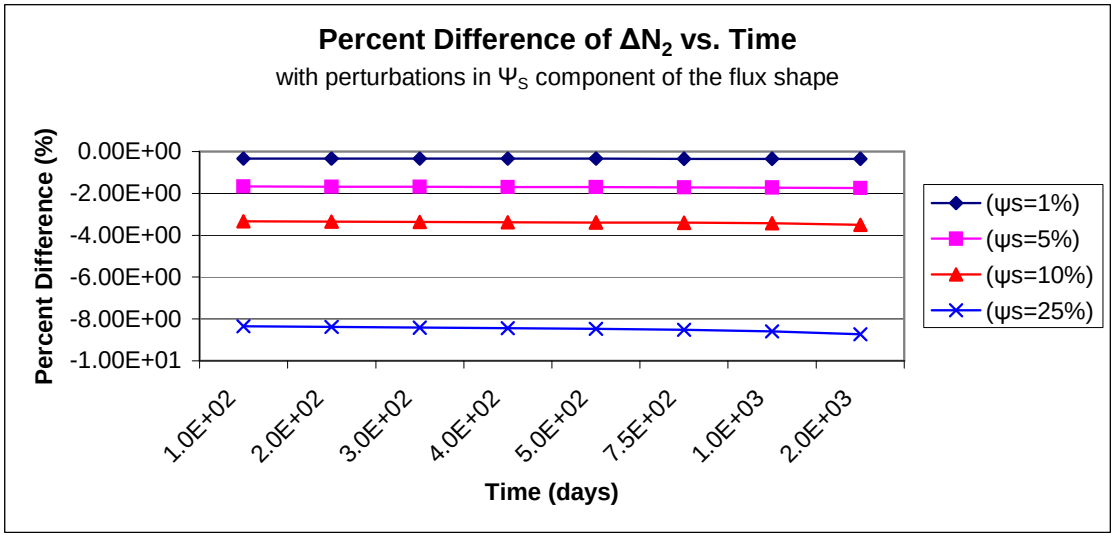

Figure 7. Percent difference of ΔN_2 for perturbation of the ψ_S term for Example 2.

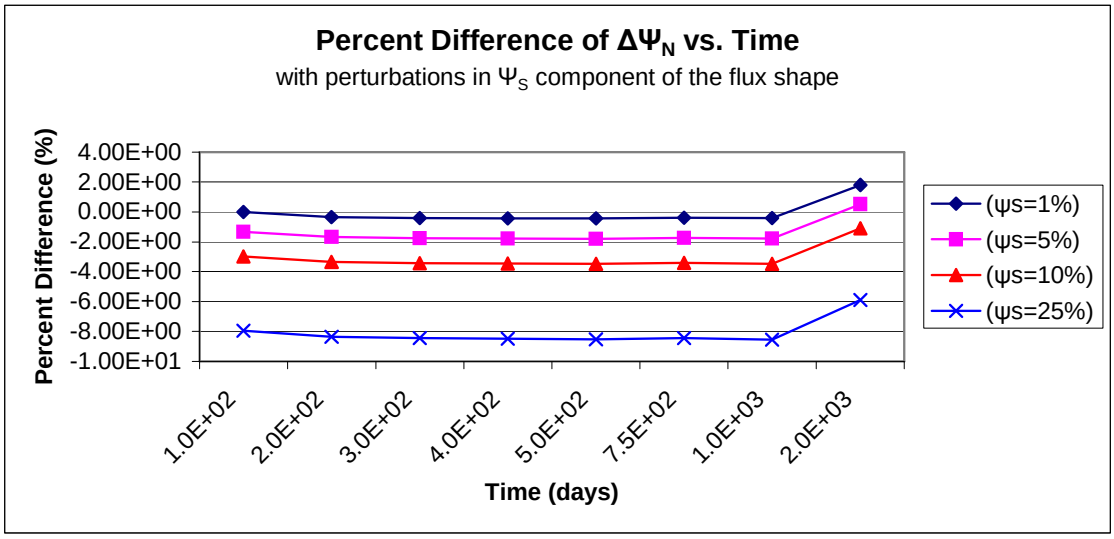

Figure 8. Percent difference of $\Delta\psi_N$ for perturbation of the ψ_S term for Example 2.

The negative numbers in Figure 6 to Figure 8 indicate the uncertainties calculated by the equations in the LUNGA method are greater than the uncertainties calculated by direct perturbation. As expected, Figure 6 to Figure 8 demonstrate that with increasing uncertainty in the ψ_S component of the flux shape the percent difference between the equations in the LUNGA method and direct perturbation increases, and also show that a change in the nuclides and the flux shape stays almost constant with time for each perturbation of the statistical component of the flux shape. Also in Figure 6 to Figure 8, the trend of the differences between a change in the nuclides and the flux shape is the same regardless of the amount of the perturbation in the statistical component of the flux shape. With a time step of 1,000 days, something different happens to the curve for a change in the flux shape due to a perturbation of the statistical component of the flux shape; the curve suddenly increases in the other direction, and the approximation starts to under predict a change in the flux shape compared to direct perturbation. The behavior with longer time steps is examined at more closely in Figure 9 to Figure 11.

Figure 9 to Figure 11 show the change in the number densities and the ψ_N term due to perturbations in the statistical component of the flux (1, 5, 10 and 25 percent) for multiple time steps (1,000 days per step) to further investigate the behavior that is seen in Figure 8. Again the perturbation of the statistical component of the flux is the same for each time step. Figure 9 and Figure 10 illustrate that a perturbation of the statistical component of the flux shape with large time steps does not impact a change in the number densities. This means a perturbation of the statistical component of the flux shape does not have much of an affect on a change in the nuclides.

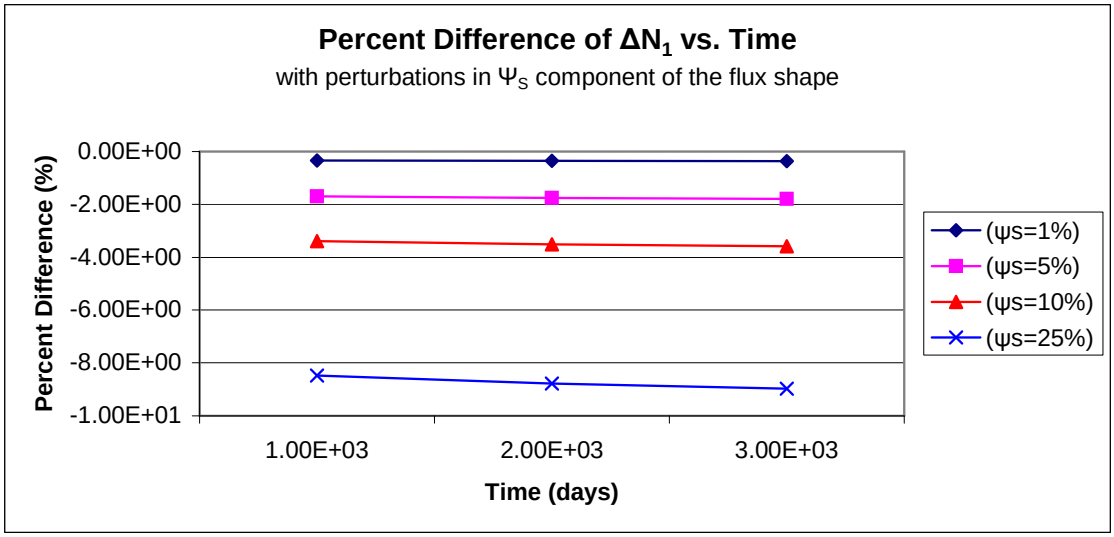

Figure 9. Percent difference of ΔN_1 for perturbation of the ψ_S component of the flux shape with 1,000 day time steps for Example 2.

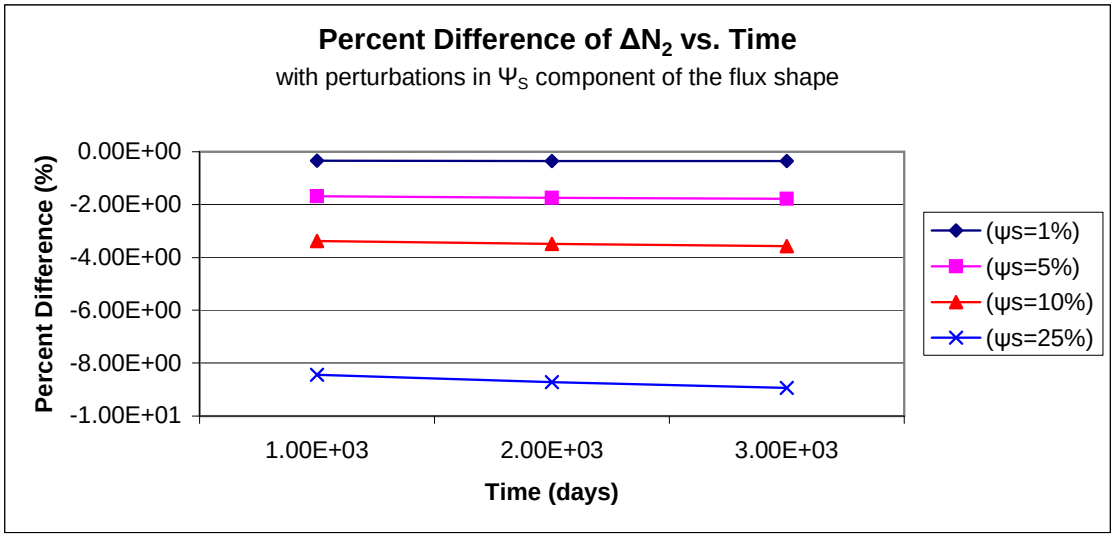

Figure 10. Percent difference of ΔN_2 for perturbation of ψ_S component of the flux shape with 1,000 days time steps for Example 2.

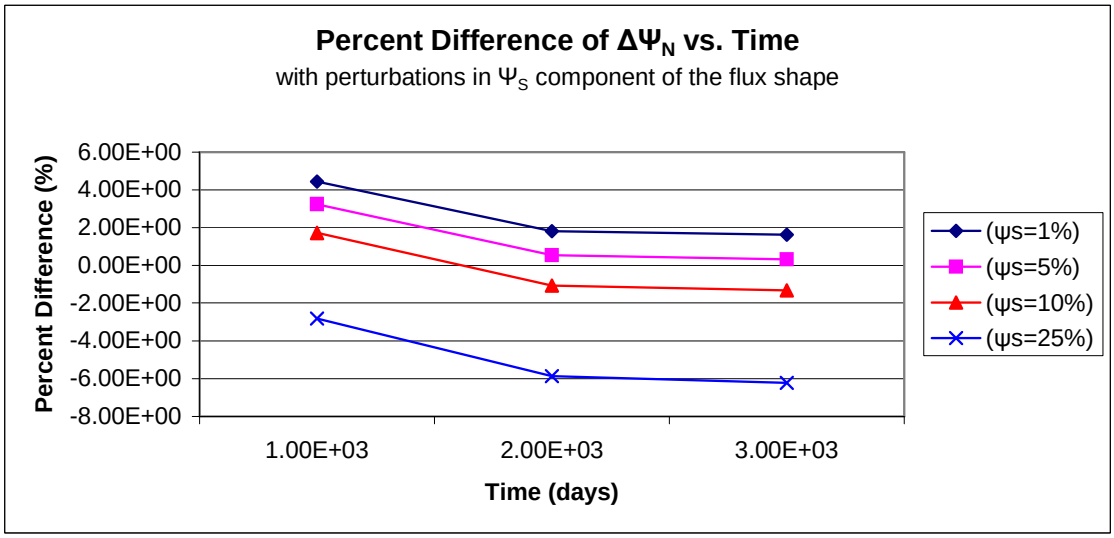

Figure 11. Percent difference of $\Delta\psi_N$ for perturbation of ψ_S component of the flux shape with 1,000 days time steps for Example 2.

A perturbation of the statistical component of the flux shape with large time steps does have a large impact on a change in the flux shape as seen in Figure 11. With a perturbation of 1 or 5 percent, the approximation is calculating uncertainties less than direct perturbation. With a perturbation of 10 or 25 percent, the approximation is calculating uncertainties greater than direct perturbation. Figure 11 reveals that with large time steps the equations in the LUNGA method get worse in time compared to direct perturbation; that means the difference between the LUNGA method and the direct perturbation becomes larger with time, and can be seen best with the curve of a 25 percent perturbation in the statistical component of the flux shape. All of the curves in Figure 11 show signs of this behavior, but additional time steps would be needed to confirm this behavior for the different perturbations in the statistical component of the flux shape. The Analysis of Example 2 section presents a general analysis to find the variance and standard deviation, which takes into account changes in flux shape, flux normalization, and nuclide number density.

5.1.4 Perturbation with Example 3

Table 12 specifies an example of the initial parameters used in Example 3. Like Example 1 and Example 2, the parameters for this example are constant through a time step; however, unlike Example 1 and Example 2 the parameters in Example 3 are updated after every time step.

Table 12. Parameters for Example 3.

σ_{ijk} - nuclide i cross section type j in group k; γ_{ik} - nuclide i in group k							
σ_{1a1} (cm^2)	1.27589E-24	σ_{2a1} (cm^2)	4.43E-25	σ_{3a1} (cm^2)	1.86475E-24	σ_{4a1} (cm^2)	1.28E-25
σ_{1a2} (cm^2)	9.09803E-24	σ_{2a2} (cm^2)	3.94E-25	σ_{3a2} (cm^2)	1.46996E-23	σ_{4a2} (cm^2)	1.80E-22
σ_{1a3} (cm^2)	3.99381E-22	σ_{2a3} (cm^2)	2.06E-24	σ_{3a3} (cm^2)	1.13315E-21	σ_{4a3} (cm^2)	4.67E-21
σ_{1c1} (cm^2)	5.79903E-26	σ_{2c1} (cm^2)	5.43E-26	σ_{3c1} (cm^2)	1.05721E-26	σ_{4c1} (cm^2)	1.28E-25
σ_{1c2} (cm^2)	2.79283E-24	σ_{2c2} (cm^2)	3.93E-25	σ_{3c2} (cm^2)	5.39522E-24	σ_{4c2} (cm^2)	1.80E-22
σ_{1c3} (cm^2)	5.84617E-23	σ_{2c3} (cm^2)	2.06E-24	σ_{3c3} (cm^2)	3.58844E-22	σ_{4c3} (cm^2)	4.67E-21
σ_{1f1} (cm^2)	1.2179E-24	σ_{2f1} (cm^2)	3.89E-25	σ_{3f1} (cm^2)	1.85418E-24		
σ_{1f2} (cm^2)	6.3052E-24	σ_{2f2} (cm^2)	7.22E-28	σ_{3f2} (cm^2)	9.30437E-24		
σ_{1f3} (cm^2)	3.40919E-22	σ_{2f3} (cm^2)	8.88E-30	σ_{3f3} (cm^2)	7.74307E-22		
σ_{1s12} (cm^2)	1.1276E-24	σ_{2s12} (cm^2)	1.26E-24	σ_{3s12} (cm^2)	7.2388E-25	σ_{4s12} (cm^2)	1.22E-24
σ_{1s13} (cm^2)	5.7502E-36	σ_{2s13} (cm^2)	9.58E-38	σ_{3s13} (cm^2)	2.16E-36	σ_{4s13} (cm^2)	2.94E-32
σ_{1s23} (cm^2)	6.2071E-27	σ_{2s23} (cm^2)	4.17E-27	σ_{3s23} (cm^2)	5.002E-27	σ_{4s23} (cm^2)	8.45E-25
ν_{11} (n/fission)	2.73368	ν_{21} (n/fission)	2.83086	ν_{31} (n/fission)	3.25224		
ν_{12} (n/fission)	2.43776	ν_{22} (n/fission)	2.53597	ν_{32} (n/fission)	2.87545		
ν_{13} (n/fission)	2.4367	ν_{23} (n/fission)	2.49209	ν_{33} (n/fission)	2.87247		
Λ_3 (s^{-1})	9.12E-13	Q1f (MeV)	194.02				
Λ_4 (s^{-1})	4.63E-09	Q1c (MeV)	6.545				
Λ_5 (s^{-1})	4.81E-04	Q2f (MeV)	198.12				
Λ_7 (s^{-1})	3.34E-06	Q2c (MeV)	4.804				
γ_{4from1}	2.63E-08	Q3f (MeV)	200.05				
γ_{4from2}	2.11E-09	Q3c (MeV)	6.533				
γ_{4from3}	1.93E-06	Q4c (MeV)	6.49				

For direct perturbation in Example 3, the changes in the number densities are examined two different ways. One way is by directly perturbing the governing equations for Example 3, and the other way is by directly perturbing the number densities in SCALE. The comparison for the changes in the number densities between using the

LUNGA method and direct perturbation is presented in Table 13, and the comparison for the changes in the number densities between the equations in the LUNGA method and SCALE is shown in Figure 12 to Figure 15.

Table 13. Percent difference of the relative ΔN for direct perturbation and the LUNGA method for Example 3.

Percent difference of relative change in number density between direct perturbation and derived equations in the LUNGA method							
		Time (days)					
Nuclide	Perturbation (%)	30	60	90	120	150	180
	0.5	6.5E-05	6.4E-05	6.4E-05	6.4E-05	6.4E-05	6.3E-05
	1	1.3E-04	1.3E-04	1.3E-04	1.3E-04	1.3E-04	1.3E-04
	5	6.2E-04	6.2E-04	6.1E-04	6.1E-04	6.1E-04	6.1E-04
N_1	10	1.2E-03	1.2E-03	1.2E-03	1.2E-03	1.2E-03	1.2E-03
	0.5	2.5E-07	2.4E-07	2.4E-07	2.4E-07	2.4E-07	2.4E-07
	1	4.9E-07	4.9E-07	4.8E-07	4.8E-07	4.8E-07	4.8E-07
	5	2.4E-06	2.3E-06	2.3E-06	2.3E-06	2.3E-06	2.3E-06
N_2	10	4.5E-06	4.5E-06	4.5E-06	4.4E-06	4.4E-06	4.4E-06
	0.5	-5.0E-01	-2.5E-03	-1.2E-03	-8.1E-04	-6.1E-04	-4.8E-04
	1	-1.0E+00	-4.9E-03	-2.4E-03	-1.6E-03	-1.2E-03	-9.6E-04
	5	-5.0E+00	-2.4E-02	-1.2E-02	-7.8E-03	-5.8E-03	-4.6E-03
N_3	10	-1.0E+01	-4.5E-02	-2.2E-02	-1.5E-02	-1.1E-02	-8.8E-03
	0.5	-4.5E-01	-3.1E-02	-1.3E-02	-7.6E-03	-4.8E-03	-3.3E-03
	1	-9.0E-01	-6.2E-02	-2.7E-02	-1.5E-02	-9.6E-03	-6.6E-03
	5	-4.5E+00	-3.0E-01	-1.3E-01	-7.3E-02	-4.6E-02	-3.2E-02
N_4	10	-9.0E+00	-5.7E-01	-2.5E-01	-1.4E-01	-8.9E-02	-6.1E-02
		Time (days)					
Nuclide	Perturbation (%)	210	240	270	300	330	360
	0.5	6.3E-05	6.3E-05	6.2E-05	6.2E-05	6.2E-05	6.2E-05
	1	1.3E-04	1.2E-04	1.2E-04	1.2E-04	1.2E-04	1.2E-04
	5	6.0E-04	6.0E-04	6.0E-04	5.9E-04	5.9E-04	5.9E-04
N_1	10	1.2E-03	1.1E-03	1.1E-03	1.1E-03	1.1E-03	1.1E-03
	0.5	2.4E-07	2.4E-07	2.4E-07	2.4E-07	2.3E-07	2.3E-07
	1	4.8E-07	4.7E-07	4.7E-07	4.7E-07	4.7E-07	4.7E-07
	5	2.3E-06	2.3E-06	2.3E-06	2.3E-06	2.2E-06	2.2E-06
N_2	10	4.4E-06	4.4E-06	4.3E-06	4.3E-06	4.3E-06	4.3E-06
	0.5	-4.0E-04	-3.4E-04	-2.9E-04	-2.6E-04	-2.3E-04	-2.1E-04
	1	-7.9E-04	-6.7E-04	-5.8E-04	-5.2E-04	-4.6E-04	-4.2E-04
	5	-3.8E-03	-3.2E-03	-2.8E-03	-2.5E-03	-2.2E-03	-2.0E-03
N_3	10	-7.3E-03	-6.2E-03	-5.4E-03	-4.7E-03	-4.2E-03	-3.8E-03
	0.5	-2.4E-03	-1.8E-03	-1.5E-03	-1.2E-03	-1.1E-03	-9.6E-04
	1	-4.8E-03	-3.7E-03	-2.9E-03	-2.5E-03	-2.1E-03	-1.9E-03
	5	-2.3E-02	-1.8E-02	-1.4E-02	-1.2E-02	-1.0E-02	-9.2E-03
N_4	10	-4.4E-02	-3.4E-02	-2.7E-02	-2.3E-02	-2.0E-02	-1.8E-02

Table 13 indicates that the equations used in the LUNGA method predict a change in the number densities very well compared with the direct perturbation of the number densities in the LUNGA equations. Generally the differences are very small, with the differences much less than 1 percent. The only place where the percent differences are not consistent with the other values in the table is in the first time step (from t=0 to t=30d) where the equations and the perturbations in N_3 and N_4 vary up to 10 percent; however, the equations are over estimating the change in the number densities, therefore the true uncertainty is smaller than what the equations are predicting. After investigation, this happens because of the number density going from a concentration of zero to a given concentration in a non-linear manner. Since the LUNGA equations are based on a linear method, it is reasonable that the equations might not work correctly in a non-linear region.

Next, Figure 12 to Figure 15 illustrate the percent difference between the LUNGA equations and SCALE. In the figures a negative number means that the equations are over predicting changes in the number densities compared to the direct perturbation in SCALE.

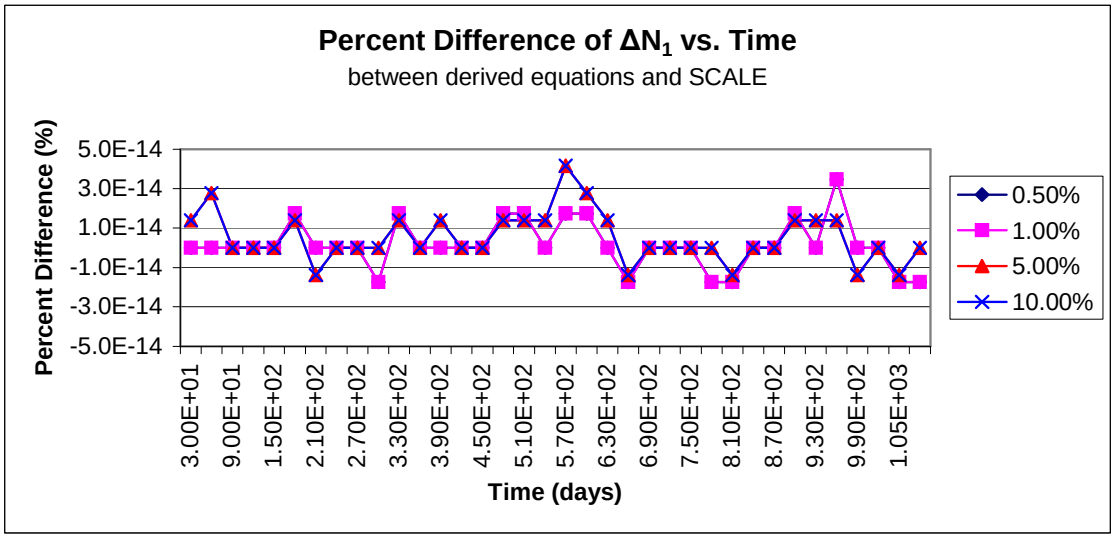

Figure 12. Percent difference of relative ΔN_1 between LUNGA method and direct perturbation in SCALE for Example 3.

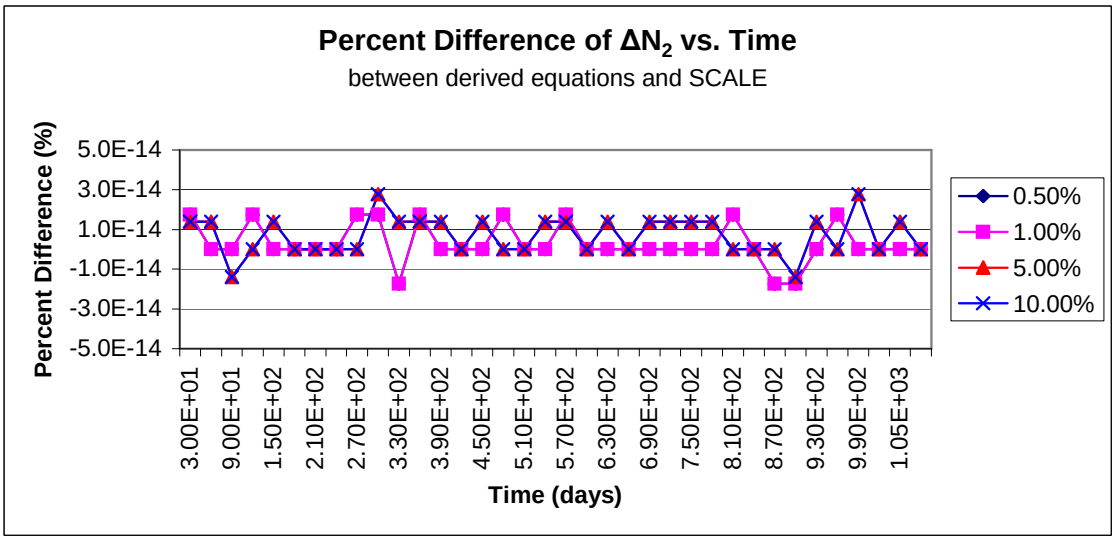

Figure 13. Percent difference of relative ΔN_2 between LUNGA method and direct perturbation in SCALE for Example 3.

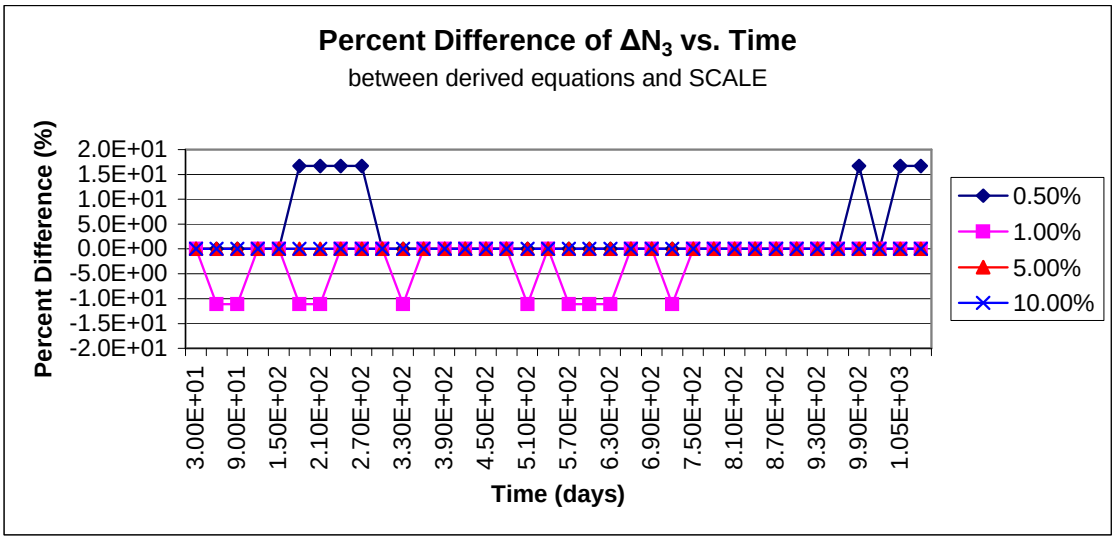

Figure 14. Percent difference of relative ΔN_3 between LUNGA method and direct perturbation in SCALE for Example 3.

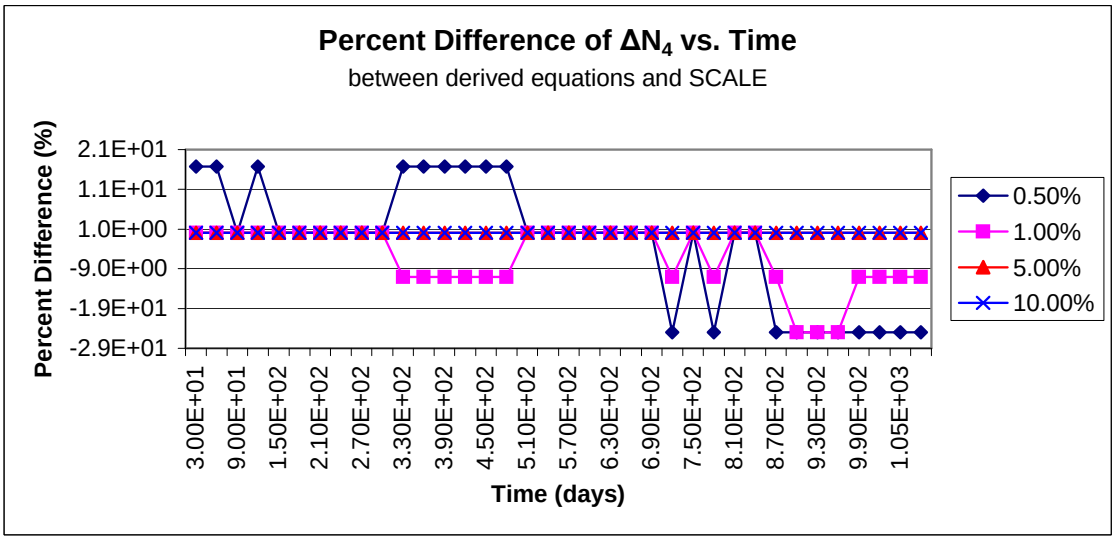

Figure 15. Percent difference of relative ΔN_4 between LUNGA method and direct perturbation in SCALE for Example 3.

Figure 12 to Figure 15 display the changes in the number densities between the equations in the LUNGA method and direct perturbation in SCALE. Figure 12 shows that the LUNGA equations predict a change in N_1 (^{235}U) very well compared to the direct perturbation in SCALE. Generally the difference between the two methods is much less than 1 percent (essentially zero). Figure 13 exhibits that the equations also predict a change in N_2 (^{238}U) very well compared to SCALE and generally the percent difference is less than 1 percent between the two methods (again basically zero). Figure 14 and Figure 15 indicate that the equations used in the LUNGA method are very capable of predicting a change in N_3 (^{239}pu) and N_4 (^{155}Eu) compared to SCALE. Generally the percent difference between the two methods is less than 1 percent for both N_3 and N_4. Interestingly, N_3 and N_4 appear to behave better with a larger perturbation in the number density as depicted with the 5 and 10 percent perturbation curves in Figure 14 and Figure 15. Ironically, the bigger differences between the two methods come with the smaller perturbations of 0.5 and 1 percent, where the percent difference between the two methods can be up to 16 percent for N_3 and 25 percent for N_4.

Some of the differences are a little bigger than what is expected, but there are a few reasons that can explain the differences. The first reason is because TRITON uses a predictor/corrector process that depletes the mixture to the midpoint of the cycle then does another transport calculation with these number densities to calculate the flux and to weight the cross sections, which are then used in the final depletion calculation. This difference yields slightly different flux shapes and one-group cross sections from the LUNGA equations, which has an impact on the output number densities. The other reason is rounding errors in both MathCad and SCALE. Eliminating the effects of the

differences in fluxes and cross sections, and the rounding errors should make the equations match much closer to the direct perturbation in SCALE, which is what happens between the equations and the direct perturbation in the equations, as seen in Table 13.

5.2 Analysis of Example 2

In this section, Example 2 is analyzed further and the equations for the standard deviation in the number densities take into account a change in the flux shape, flux normalization, and number densities. A few different variations of Example 2 are investigated to study the effect on the variance in the number densities including different values of the statistical component in the flux shape (ψ_S values) and different size time steps.

MathCad is used to solve for the flux shape in Example 2. The eigenvectors output by MathCad are normalized, and the flux shape of energy group 2 (ψ_2) is taken as 1. The variance for the flux shape of energy group 2 due to a change in the number densities (the ψ_{N2} term) and the percent difference between the LUNGA and exact methods is then equal to zero. This would not happen in a real system, but is not seen as a problem since the flux shape is a ratio between energy group 1 and energy group 2 in Example 2.

One variation of Example 2 investigated is different ψ_S values in the flux shape. The analysis is done with 250-day time steps, and no uncertainty in the initial number densities. The different ψ_S values in the flux shape used in the analysis are 5 and 25 percent. As expected the larger the variance in the statistical component of the flux shape becomes, the more uncertainty it introduces into the number densities and therefore the larger the standard deviation in the number densities become, which is shown in Figure

16 for N_1 and N_2. Figure 16 shows that the LUNGA method agrees very well with the exact method. Figure 17 presents the difference between the LUNGA and exact methods for the standard deviation of the number densities and shows that the two methods calculate very similar results. The percent difference between the standard deviation of the number densities between the LUNGA and exact methods increases with increasing variance of the statistical component in the flux shape. That is logical because larger values in the variance of the statistical component in the flux shape introduce more uncertainty into the calculation.

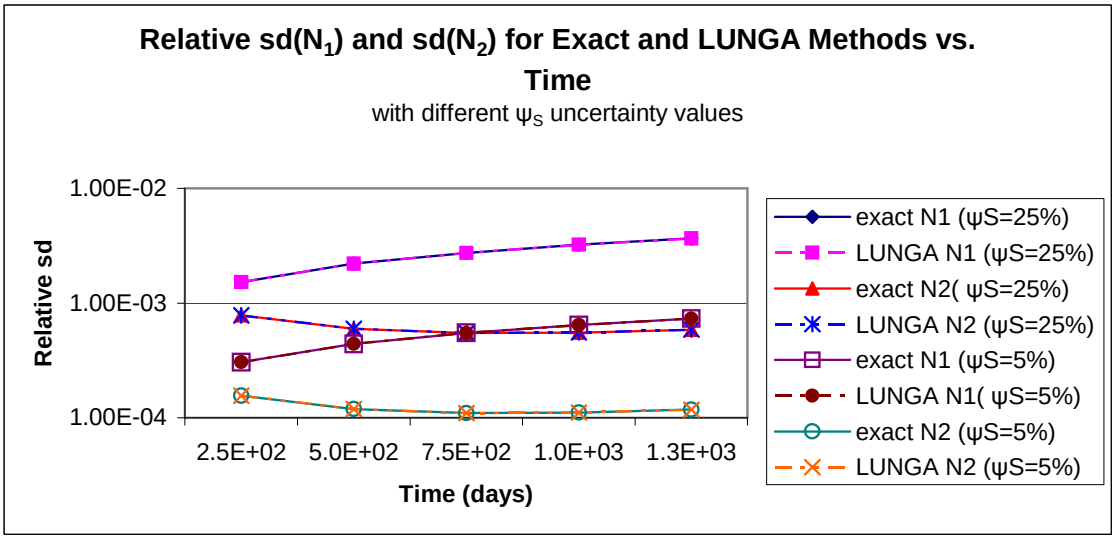

Figure 16. Relative sd(N_1) and sd(N_2) with different magnitudes of ψ_S uncertainty for Example 2.

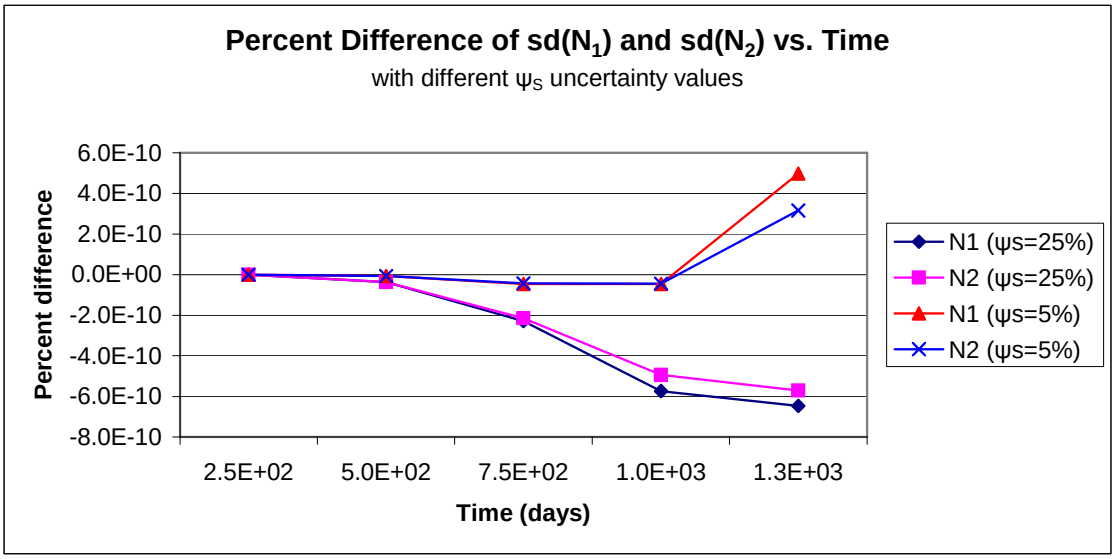

Figure 17. Percent difference of relative sd(N_1) and sd(N_2) with varying magnitudes of ψ_S uncertainty for Example 2.

The relative standard deviation of the ψ_N term for energy group 1 (ψ_{N1}) for the exact and LUNGA methods is shown in Figure 18, which shows that the two methods agree very well and that the standard deviation of ψ_{N1} increases as the statistical uncertainty increases. The difference of ψ_{N1} between the LUNGA and exact methods also increases with increasing values of the variance of the statistical component in the flux shape. This means the greater the statistical uncertainty in a calculation the less accurate the approximation becomes, as can be seen in Figure 19. Therefore, in a calculation, the statistical uncertainty should be kept as small as the calculation allows.

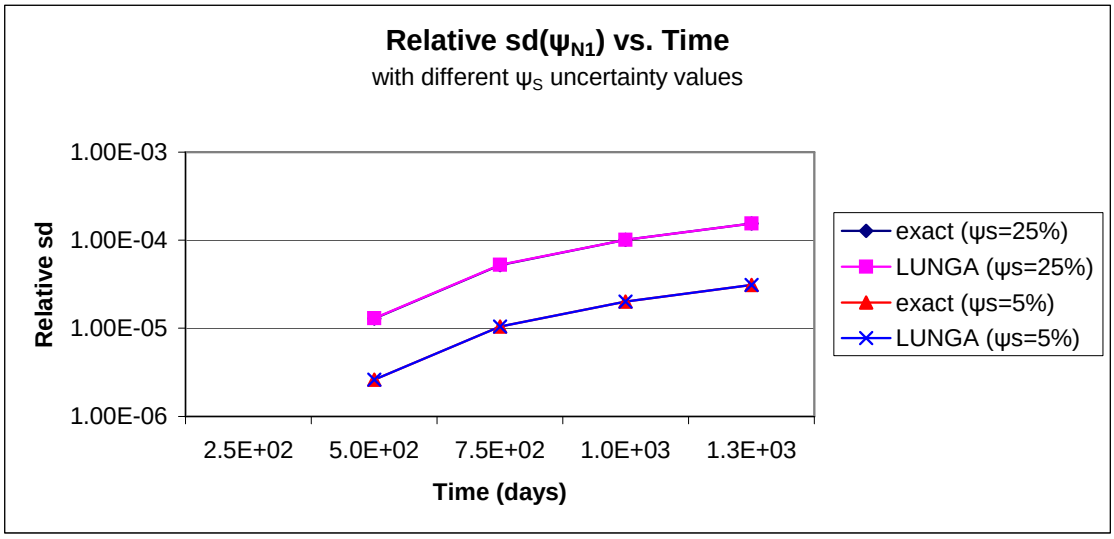

Figure 18. Relative sd(ψ_{N1}) with varying magnitudes of ψ_S uncertainty for Example 2.

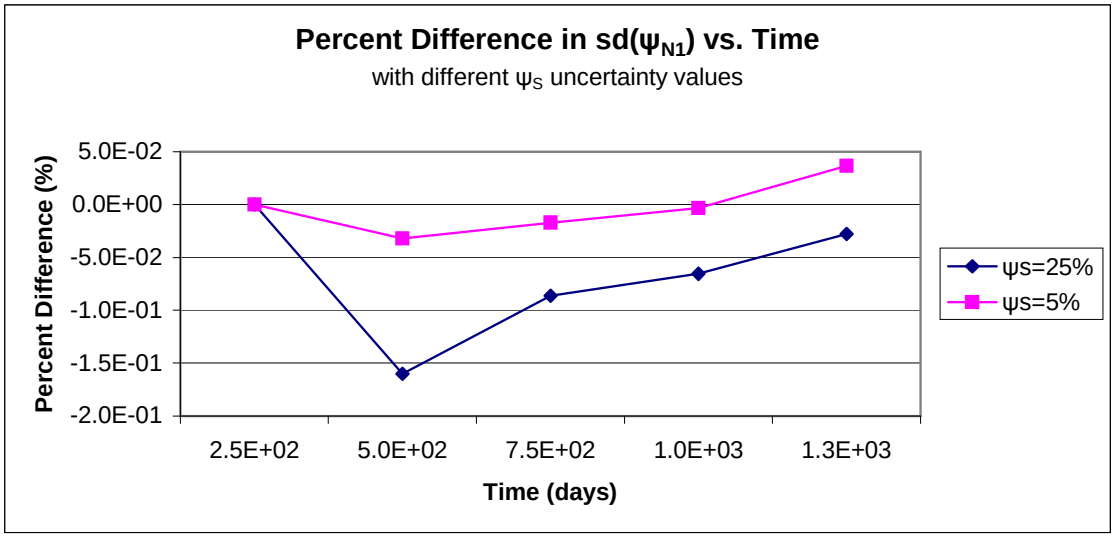

Figure 19. Percent difference of sd(ψ_{N1}) with varying magnitudes of ψ_S uncertainty for Example 2.

Another variation of Example 2 investigated is long time steps. The analysis is done with 250-day time steps with 0.11 percent uncertainty in ψ_{s1} and 1.10 percent uncertainty in ψ_{s2} and no uncertainty in the initial number densities. Figure 20 to Figure 23 present the results of the 250-day time step variant. Figure 20 shows that the LUNGA method agrees very well with the exact method in calculating the standard deviation of the number densities. Figure 21 reveals the differences between the two methods are essential equal to zero. Figure 22 illustrates that the two methods also agree very well in calculating the standard deviation of the ψ_{N1} term, and Figure 23 shows that the differences between the two methods are much less than 1 percent. Figure 20 to Figure 23 indicate that the LUNGA method is capable of calculating the standard deviations in the number densities and the ψ_N term with a large time step.

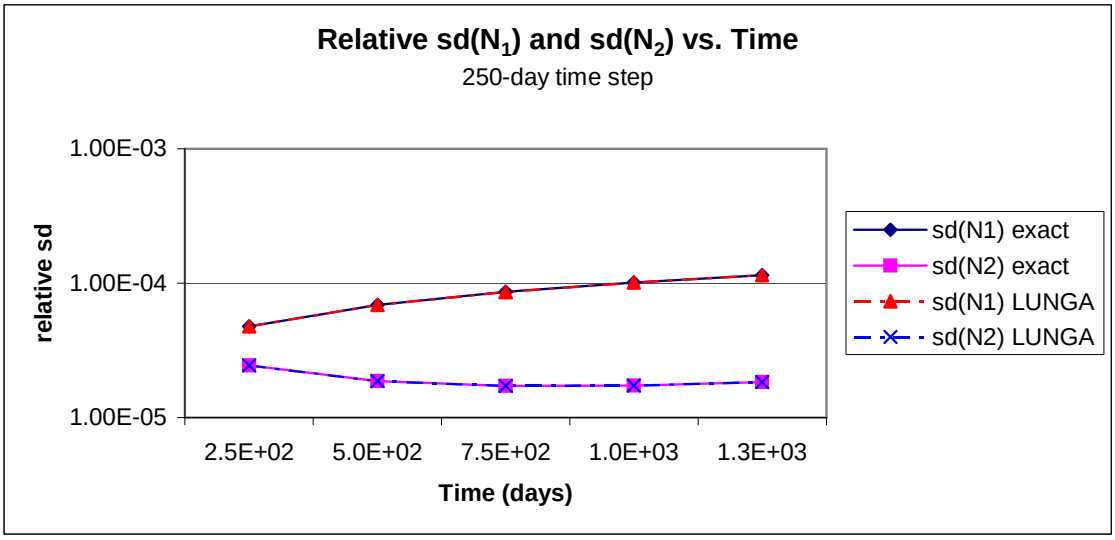

Figure 20. Relative sd(N_1) and sd(N_2) with 250-day time steps for Example 2.

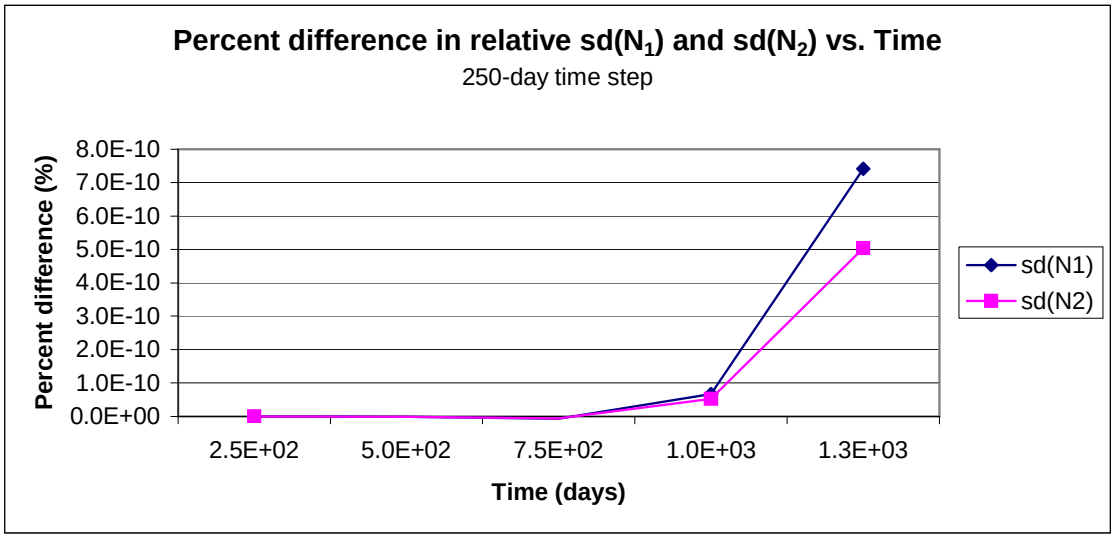

Figure 21. Percent difference of relative sd(N_1) and sd(N_2) with 250-day time steps for Example 2.

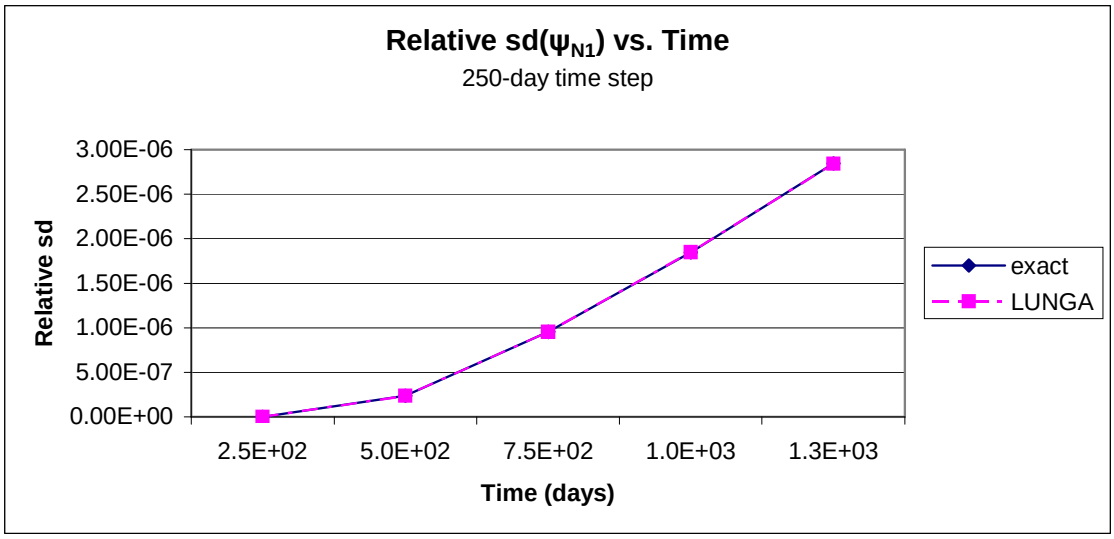

Figure 22. Relative sd(ψ_{N1}) with 250-day time steps for Example 2.

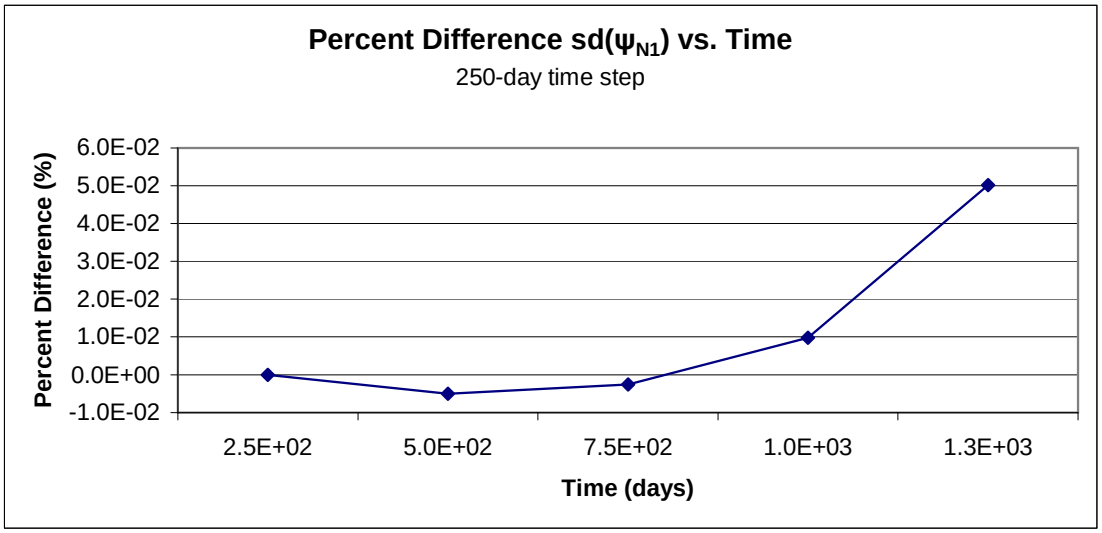

Figure 23. Percent difference of sd(ψ_{N1}) with 250-day time steps for Example 2.

Figure 20 to Figure 23 demonstrate that the exact and LUNGA methods agree well with large time steps; therefore, it is expected that the exact and LUNGA methods would agree very well with short time steps. The last variation of Example 2 investigated is with small time steps. This analysis is done with 2-day time steps with 0.11 percent uncertainty in ψ_{s1} and 1.10 percent uncertainty in ψ_{s2} and no uncertainty in the initial number densities like the 250-day variant. Small time steps are used to investigate the behavior of the standard deviations with multiple time steps and a more realistic size time step that might be used in a calculation. Figure 24 to Figure 27 show the results of the 2-day time step variant.

Figure 24 reveals that the LUNGA method agrees very well with the exact method in calculating the standard deviation of the number densities. The differences between the two methods are basically zero as seen in Figure 25. Figure 26 shows that the two methods also agree very well in calculating the standard deviation of the ψ_{N1} term. The percent difference in the standard deviation of the ψ_{N1} term hovers around zero (much

less than 1 percent) as seen in Figure 27. As expected, smaller time steps should and do produce smaller standard deviations in both the number densities and the ψ_N term.

Some interesting observations come from the percent differences between the exact and LUNGA methods for both the standard deviations in the number densities and in the ψ_N term, as seen in Figure 25 and Figure 27. Figure 25 illustrates for a small time step that the percent difference of the standard deviation for N_1 and N_2 shows at times the LUNGA method is over and under predicting the standard deviation of the number densities compared to the exact method, which is not seen with the larger time steps. What is also interesting is that the over and under predicting of the standard deviation of the number densities bounce around the value of zero for both nuclides (see Figure 25). Figure 27 shows that the percent difference between the exact and LUNGA methods for calculating the standard deviation of the ψ_{N1} term is very small and fluctuates around a value of zero, which is not really seen with the larger time steps.

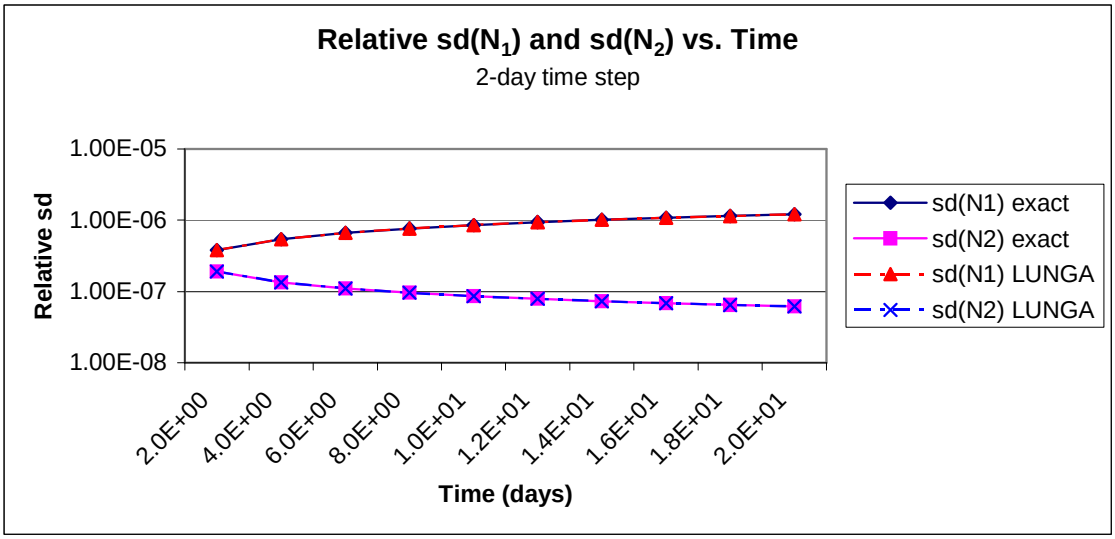

Figure 24. Relative sd(N_1) and sd(N_2) with 2-day time steps for Example 2.

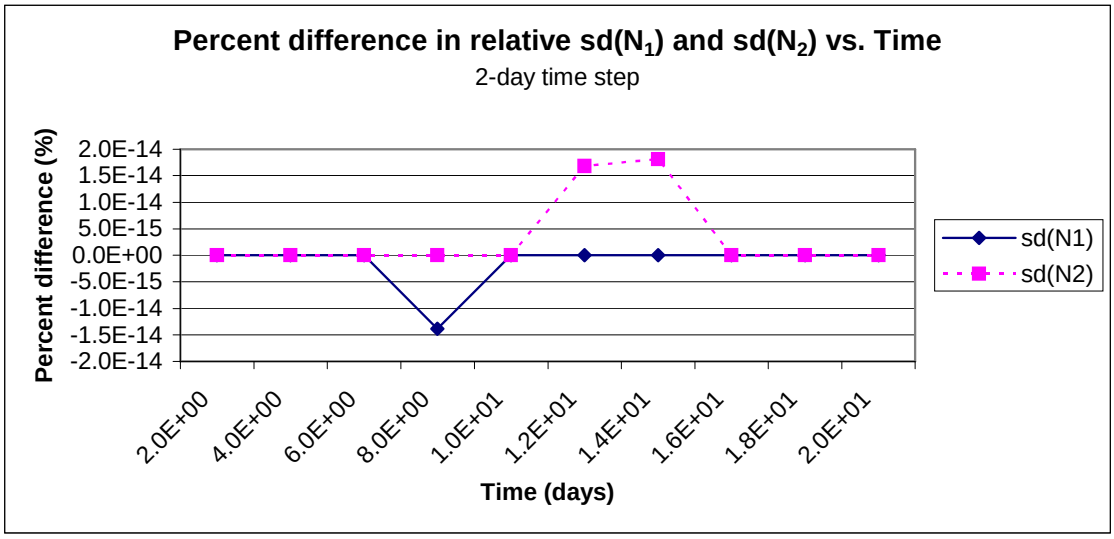

Figure 25. Percent difference of relative sd(N_1) and sd(N_2) with 2-day time steps for Example 2.

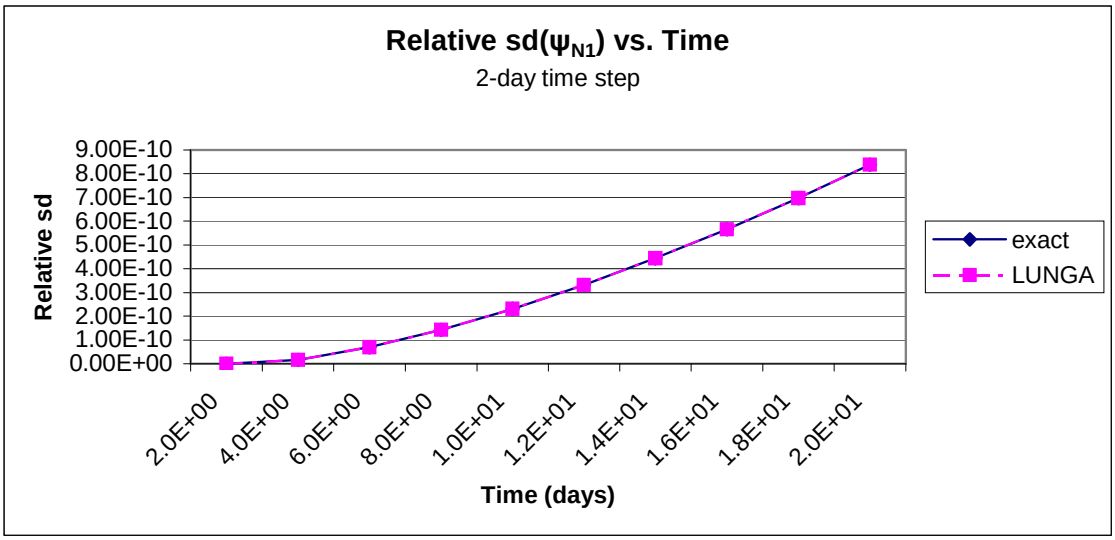

Figure 26. Relative sd(ψ_{N1}) with 2-day time steps for Example 2.

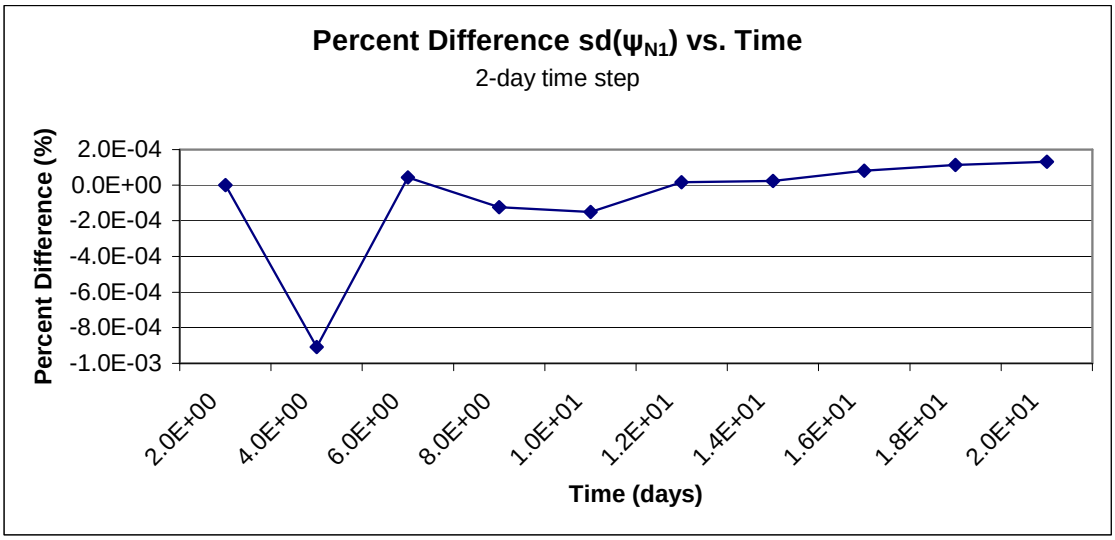

Figure 27. Percent difference of relative sd(ψ_{N1}) with 2-day time steps for Example 2.

As expected a smaller time step produces a smaller standard deviation in the number densities (Figure 20 and Figure 24) and a smaller standard deviation in the ψ_{N1} term (Figure 22 and Figure 26). The analysis demonstrates that larger (longer) time steps can be used without sacrificing much accuracy. This means that smaller (shorter) time steps could be used to calculate the standard deviation in the number densities when the system requires small time steps or greater refinement, and larger time steps could be used when nothing of interest is happening in the system or a quick calculation is desired.

5.3 Analysis of Example 3

In this section, Example 3 (the benchmark problem) is analyzed in depth. The example can be solved semi-analytically, meaning everything is solved analytically with the aid of computer software (MathCad) to calculate the flux shape. The example can also be solved with KENO and the results can then be compared to those from the analytic solution.

A few different variations are studied to investigate the differences between the exact and LUNGA methods, and the behavior of the system of nuclides in this example. The different variations include: the analytic solution and the KENO solution with different ψ_S values, different power levels, different normalization of the cross sections, and fast and thermal neutron spectrums (i.e. fast and thermal reactor systems).

Example 3 is investigated with a fast neutron spectrum with total normalization of the cross sections (cross sections are normalized using all energy groups). Figure 28 presents the relative standard deviation of the number densities for the exact and LUNGA methods. Figure 30 displays the relative standard deviation of the ψ_N term for the exact and LUNGA methods. Figure 29 and Figure 31 show the percent difference between the exact and LUNGA methods for standard deviation of the number densities and standard deviation of the ψ_N term respectively. Figure 28 indicates that the LUNGA method agrees very well with the exact method in calculating the standard deviation of the nuclide number densities. Figure 29 reveals that the LUNGA method differs from the exact method by much less than 1 percent. Figure 30 and Figure 31 show that the LUNGA and exact methods for calculating the standard deviation of the ψ_N term are considerable different. At times the trends appear to follow one another and at times they do not as seen in Figure 30. However, the figure does indicate that at times the two methods can agree to some degree as seen with the standard deviation of the ψ_{N3} term curve in Figure 30.

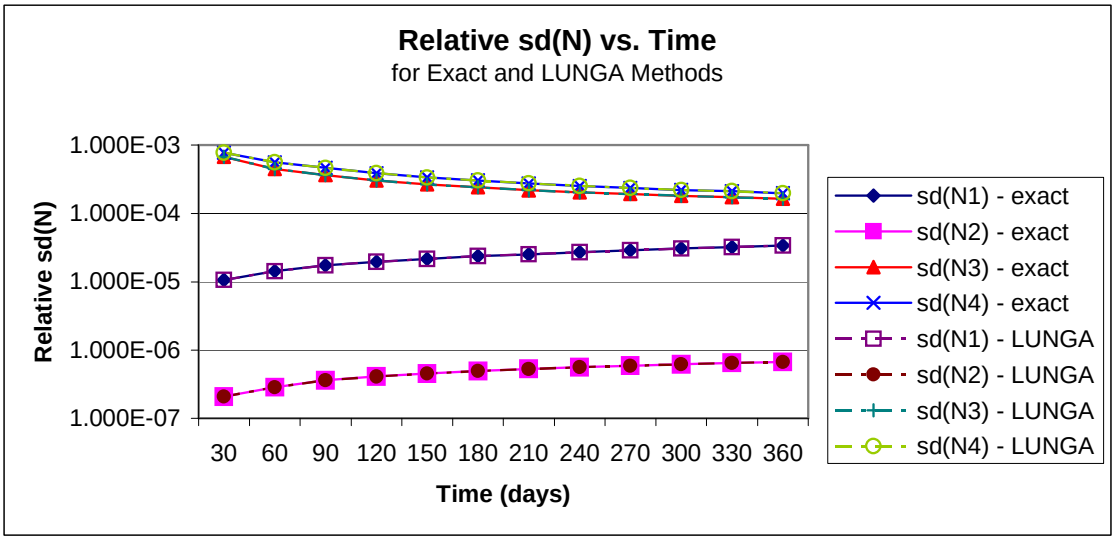

Figure 28. Relative sd(N) with total normalization of cross sections for Example 3.

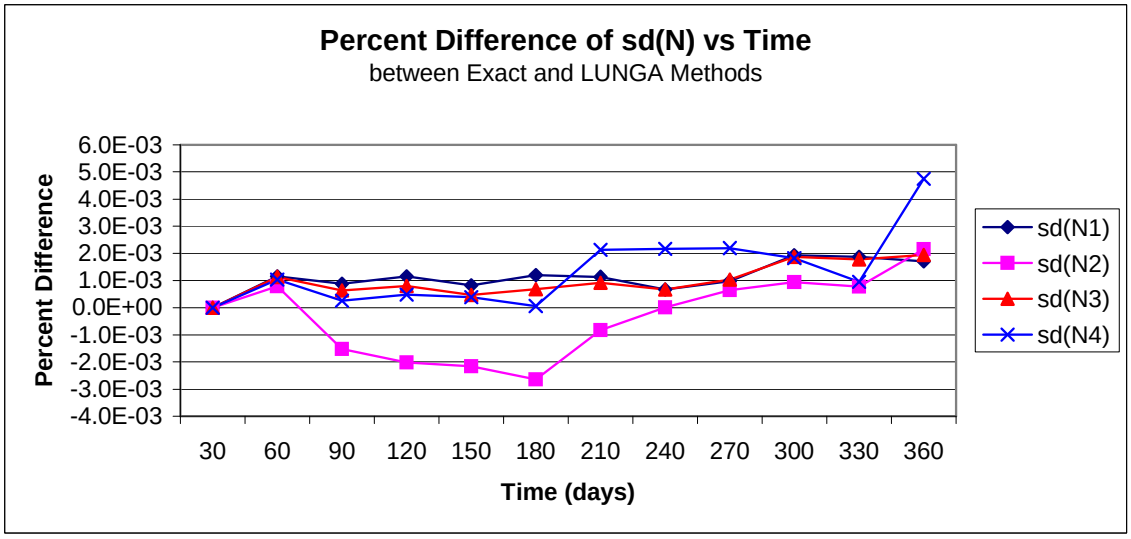

Figure 29. Percent difference of sd(N) with total normalization of cross sections for Example 3.

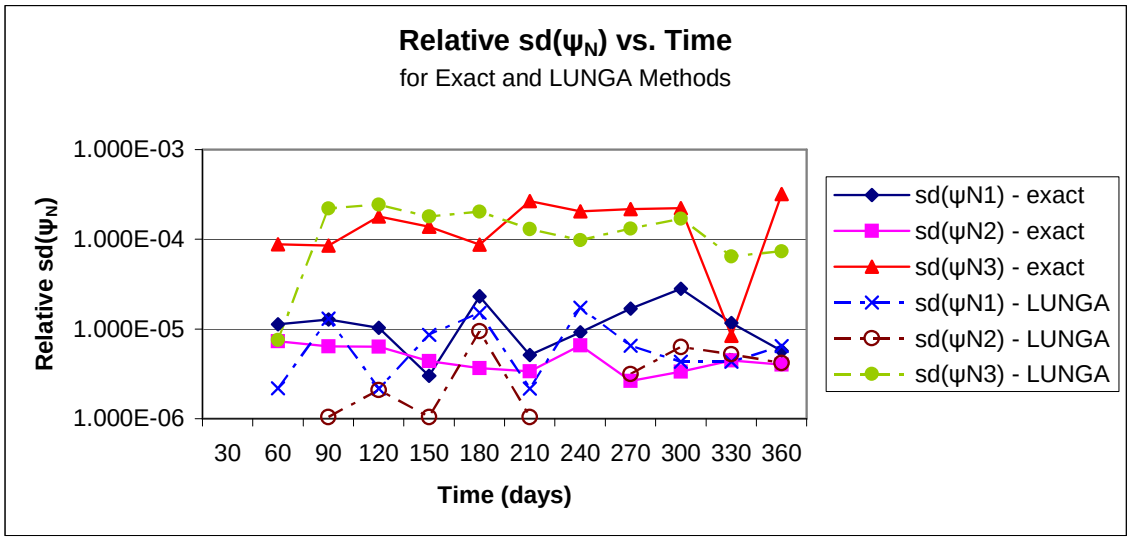

Figure 30. Relative sd(ψ_N) with total normalization of cross sections for Example 3.

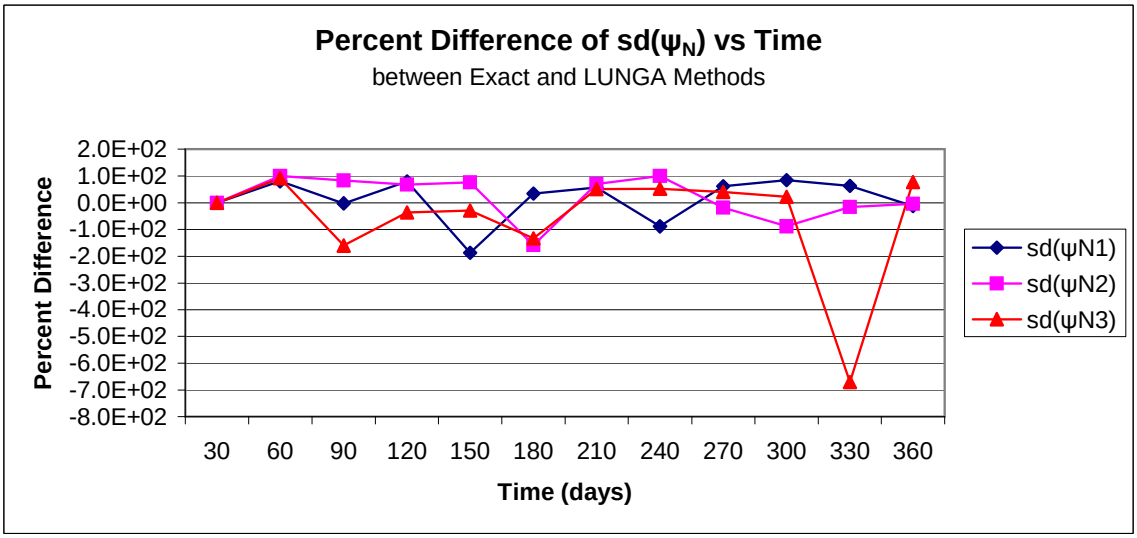

Figure 31. Percent difference of sd(ψ_N) with total normalization of cross sections for Example 3.

Example 3 is also investigated with a fast neutron spectrum with total normalization of the cross sections solved analytically. Here MathCad is used to solve for the flux shape of the system. Figure 32 presents the relative standard deviation of the number densities for the exact and LUNGA methods and shows that the two methods agree very well with one another. Figure 33 depicts the percent difference between the exact and LUNGA methods. Figure 33 illustrates that the LUNGA method agrees well with the exact method with under a 1 percent difference between the two methods. However, Figure 33 also shows that the percent difference is growing in time, but that the LUNGA method is over predicting the standard deviation in the number densities compared to the exact method. Figure 34 displays the relative standard deviation of the ψ_N term and shows that the exact and LUNGA methods exhibit the same trends even though the percent difference between the two methods is large as seen in Figure 35. In Figure 35 the difference in the ψ_{N2} term is equal to zero; however, this is because of how MathCad solves the system for the flux shape and not because the difference is actually equal to zero.

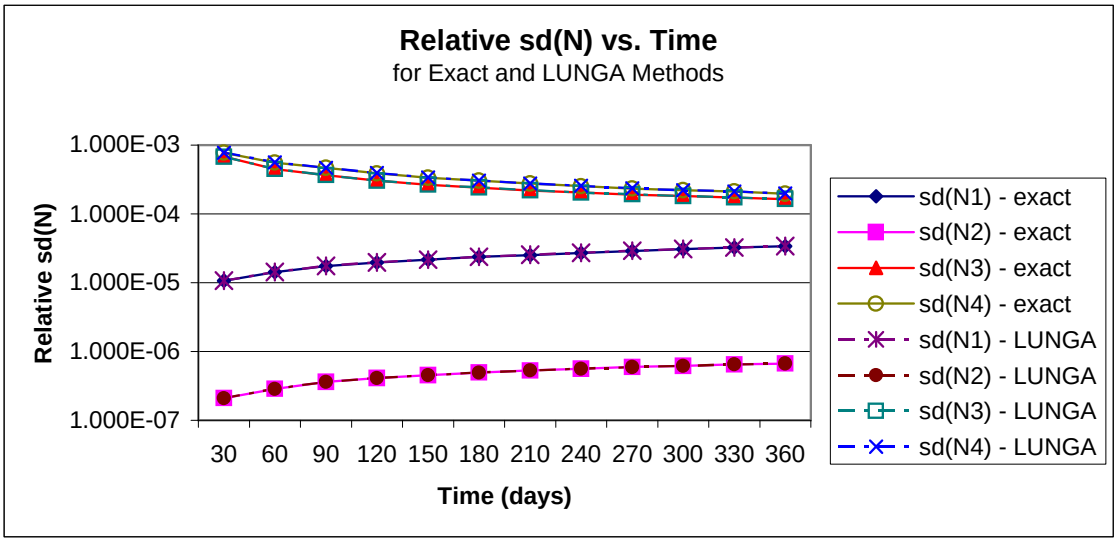

Figure 32. Relative sd(N) with total normalization of cross sections for Example 3 solved analytically.

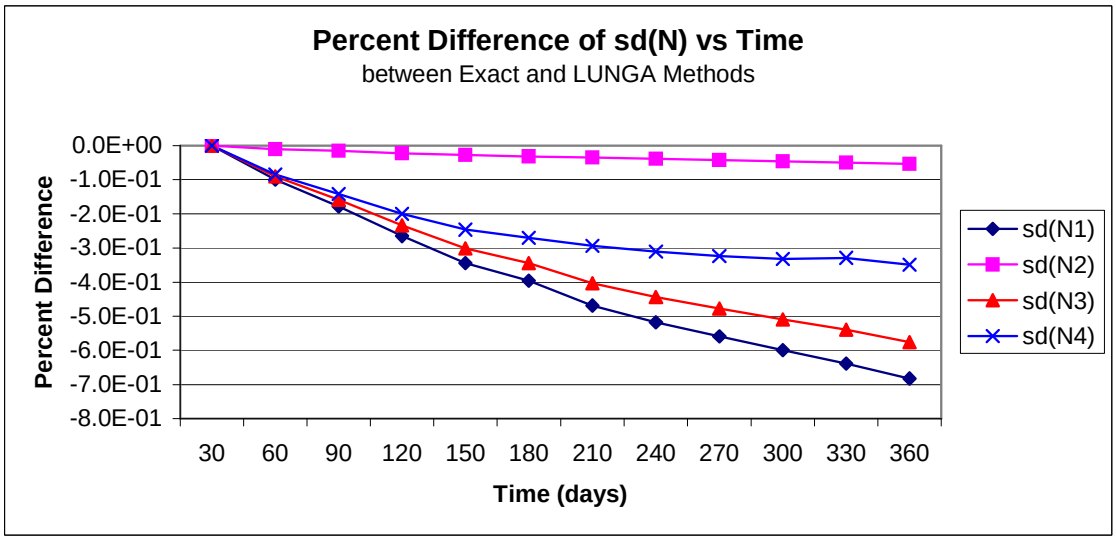

Figure 33. Percent difference of relative sd(N) with total normalization of cross sections for Example 3 solved analytically.

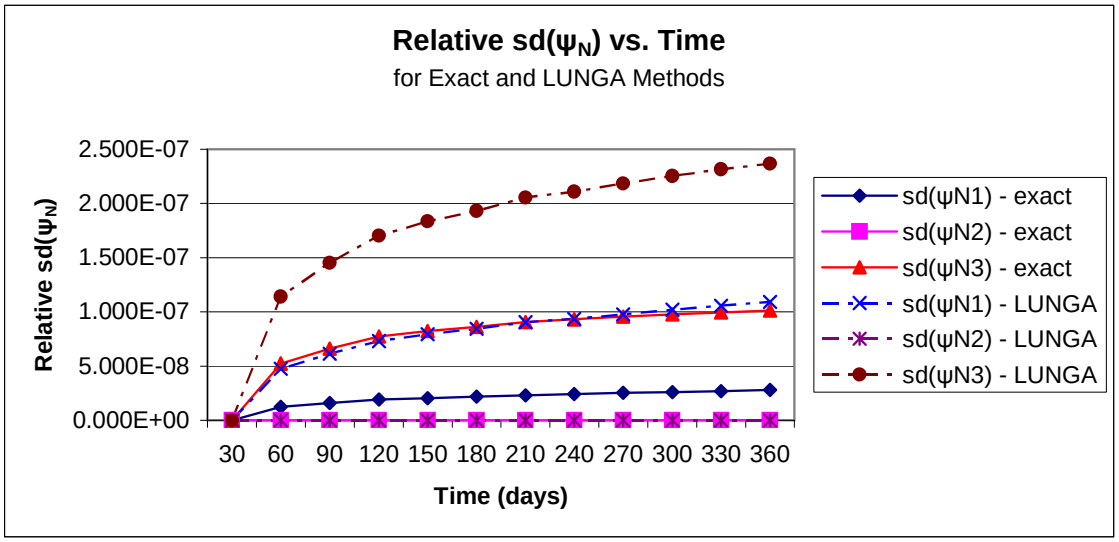

Figure 34. Relative sd(ψ_N) with total normalization of cross sections for Example 3 solved analytically.

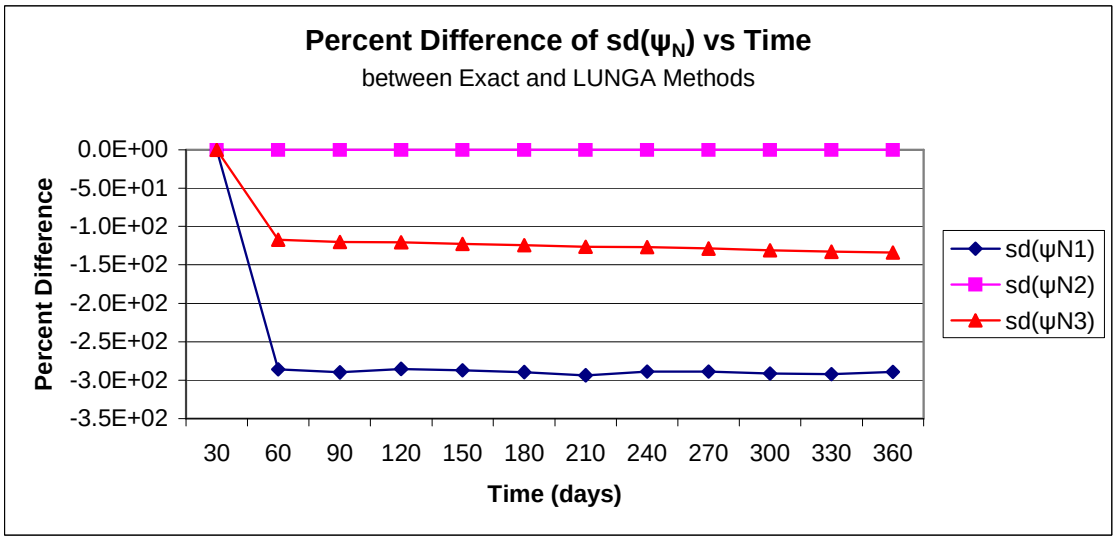

Figure 35. Percent difference of relative sd(ψN) with total normalization of cross sections for Example 3 solved analytically.

Solving Example 3 analytically allows for the comparison and initial check of the standard deviations of the nuclide number densities to those calculated with the Monte Carlo calculations. Figure 36 and Figure 37 show the percent difference between the Monte Carlo and analytic solutions for the exact and LUNGA methods for Example 3. As seen in the figures, the Monte Carlo calculated standard deviations of the nuclide number densities agreed very well with those calculated analytically for both the exact and LUNGA methods, with less than a 1 percent difference for both methods.

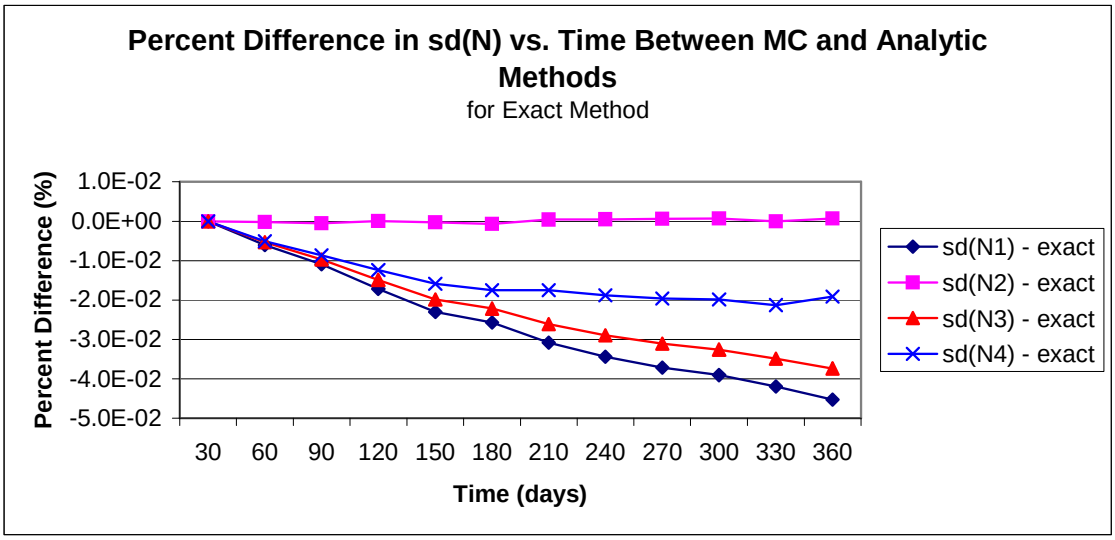

Figure 36. Percent difference between the MC and analytic solutions with the exact method for Example 3.

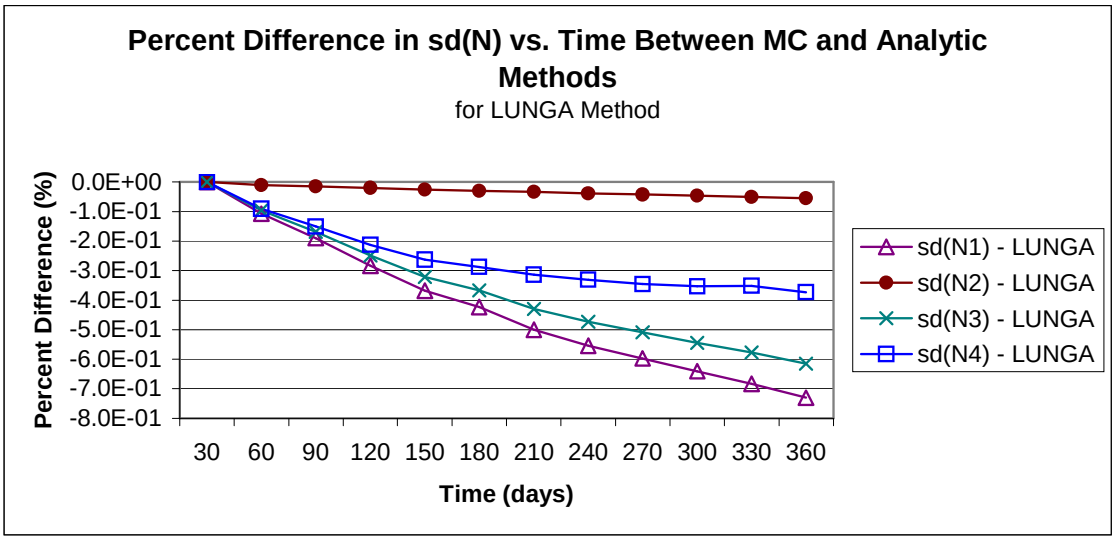

Figure 37. Percent difference between the MC and analytic solutions with the LUNGA method for Example 3.

Example 3 is examined with a fast neutron spectrum with thermal normalization of the cross sections (cross sections are normalized using the only thermal energy groups). Figure 38 displays the relative standard deviation of the number densities and Figure 39 shows the percent difference in the relative standard deviation of the number densities for the exact and LUNGA methods. Figure 40 presents the relative standard deviation of the ψ_N term and Figure 41 shows the percent difference in the relative standard deviation of the ψ_N term for the exact and LUNGA methods. As with the previous investigation of Example 3, Figure 38 and Figure 39 reveal that the LUNGA method agrees very well with the exact method in calculating the standard deviations in the nuclide number densities. Figure 40 and Figure 41 illustrate that the LUNGA method does not calculate the standard deviation of the ψ_N term very well, as seen in the previous investigation of Example 3.

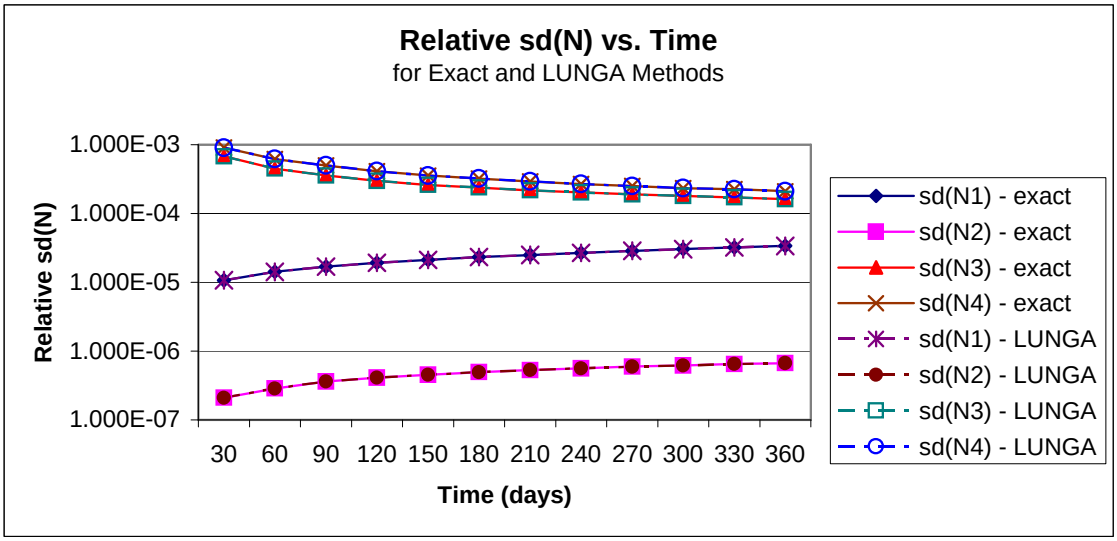

Figure 38. Relative sd(N) with thermal cross section normalization for Example 3.

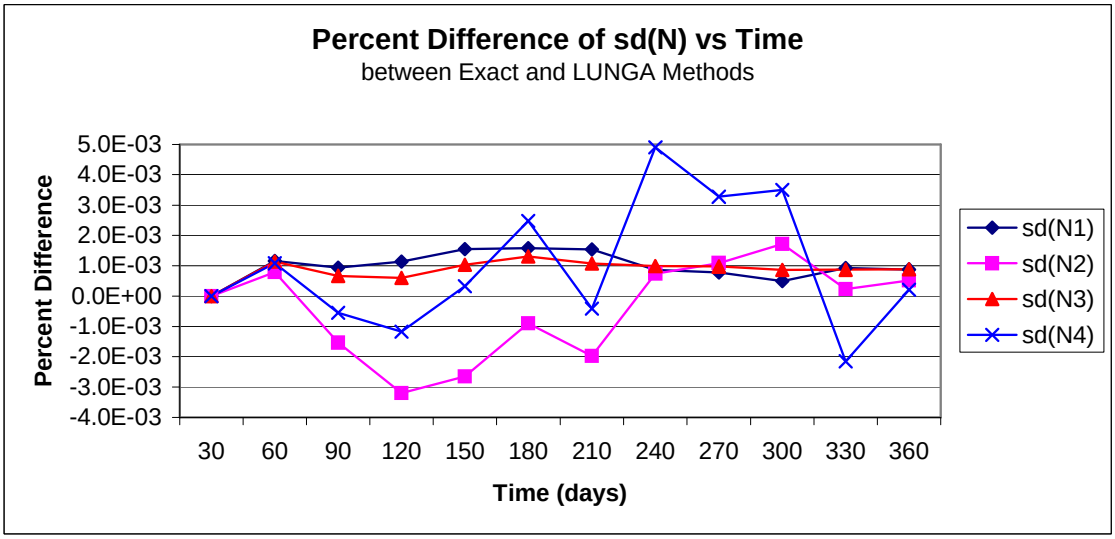

Figure 39. Percent difference of relative sd(N) with thermal cross section normalization for Example 3.

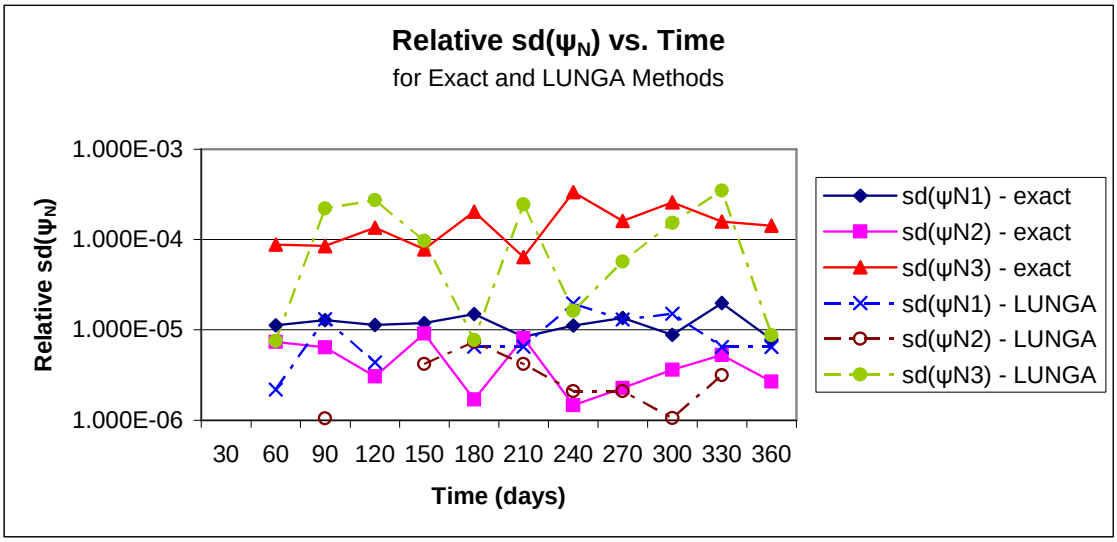

Figure 40. Relative sd(ψ_N) with thermal cross section normalization for Example 3.

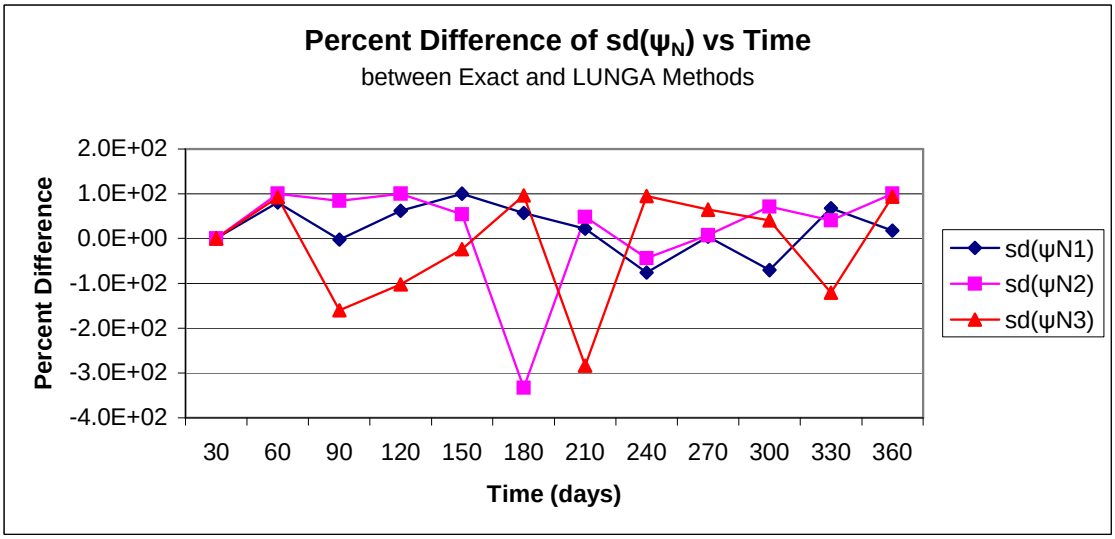

Figure 41. Percent difference of relative sd(ψ_N) with thermal cross section normalization for Example 3.

Example 3 is also examined with a fast neutron spectrum, thermal normalization of the cross sections, and extended equations. The extended equations include ^{239}U and ^{239}Np, which are introduced to more closely model what happens in SCALE. Since ^{239}U and ^{239}Np decay quickly in comparison to the time step, they are taken to have no uncertainty associated with them. Figure 42 presents the relative standard deviation of the number densities and Figure 43 expresses the percent difference for the relative standard deviation of the number densities for the exact and LUNGA methods. Figure 44 displays the relative standard deviation of the ψ_N term and Figure 45 shows the percent difference in the relative standard deviation of the ψ_N term for the exact and LUNGA methods. As seen with other iterations of Example 3, Figure 42 and Figure 43 illustrate that the LUNGA method agrees very well with the exact method in calculating the standard deviations in the nuclide number densities, but does not agree in calculating the standard deviation of the ψ_N term which can be seen in Figure 44 and Figure 45. The variation was anticipated to resemble the previous variation, which it did as seen in Figure 38 to Figure 41 and Figure 42 to Figure 45. Including ^{239}U and ^{239}Np was not expected to and did not change the results of the standard deviation of the number densities or standard deviation of the ψ_N term, but made the calculated number densities match more closely to those calculated by SCALE during the verification stage of the research.

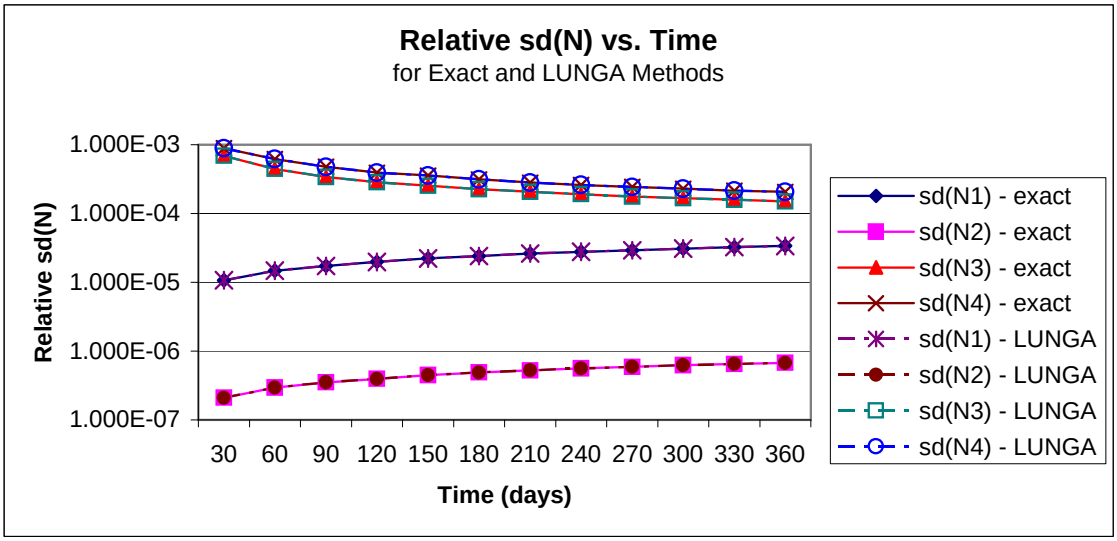

Figure 42. Relative sd(N) with extended equations for Example 3.

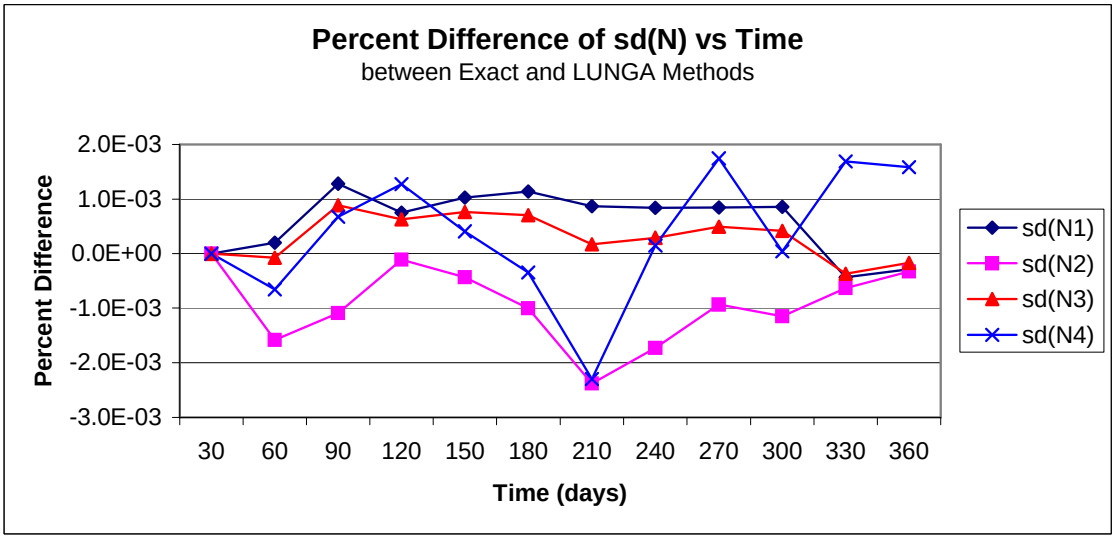

Figure 43. Percent difference of relative sd(N) with extended equations for Example 3.

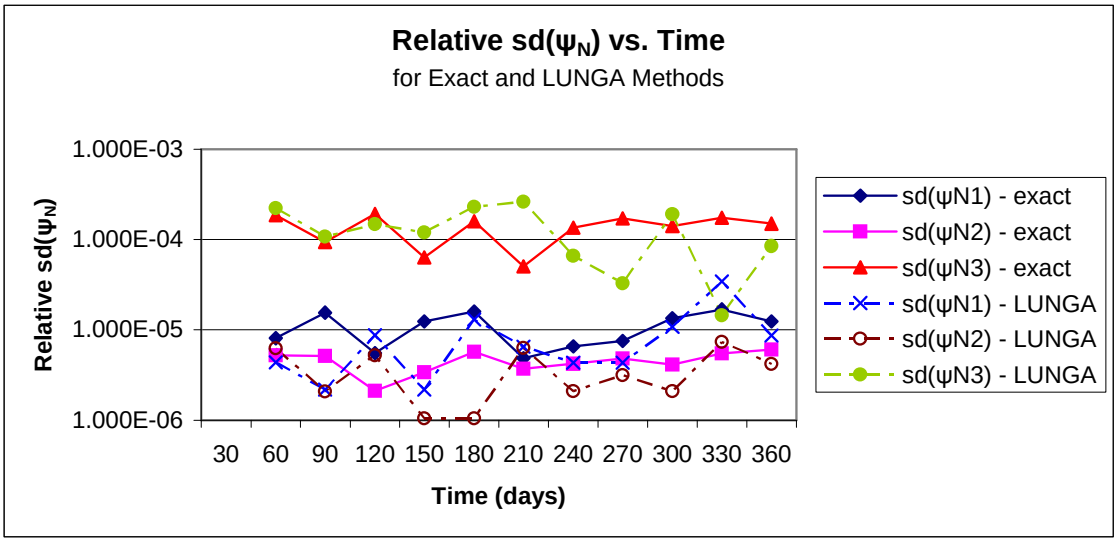

Figure 44. Relative sd(ψ_N) with extended equations for Example 3.

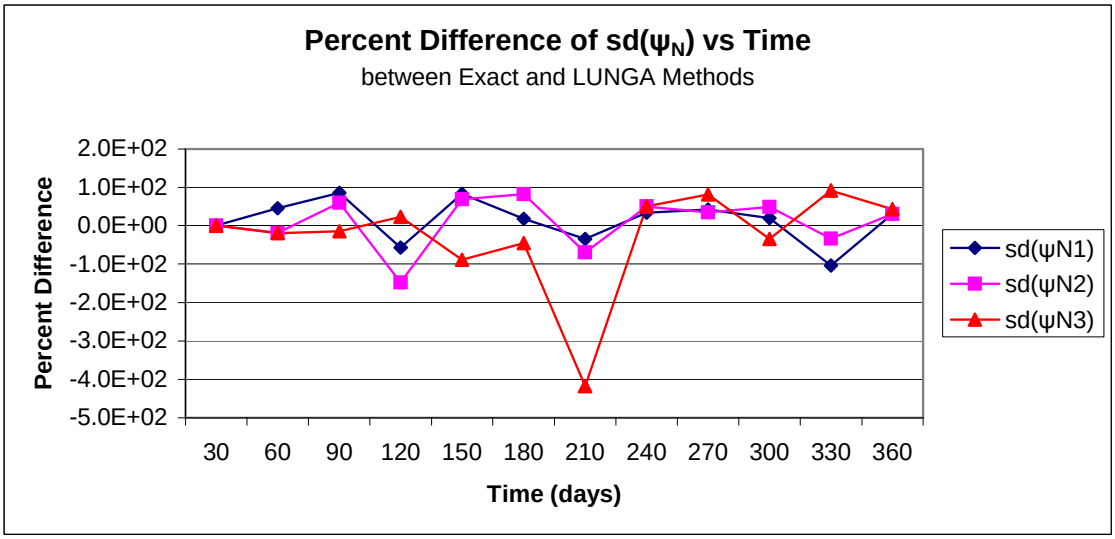

Figure 45. Percent difference of relative sd(ψ_N) with extended equations for Example 3.

Example 3 is investigated with a thermal neutron spectrum, thermal normalization of the cross sections, and the extended equations. Figure 46 shows the relative standard deviation in the number densities and Figure 47 presents the percent difference in the relative standard deviation in the number densities for the exact and LUNGA methods. Figure 48 displays the relative standard deviation in the ψ_N term and Figure 49 depicts the percent difference in the relative standard deviation in the ψ_N term for the exact and LUNGA methods. As seen in the other variations of Example 3, Figure 46 and Figure 47 illustrate that the LUNGA method agrees very well with the exact method in calculating the standard deviations in the nuclide number densities, but does not agree well when calculating the standard deviation of the ψ_N term as seen in Figure 48 and Figure 49.

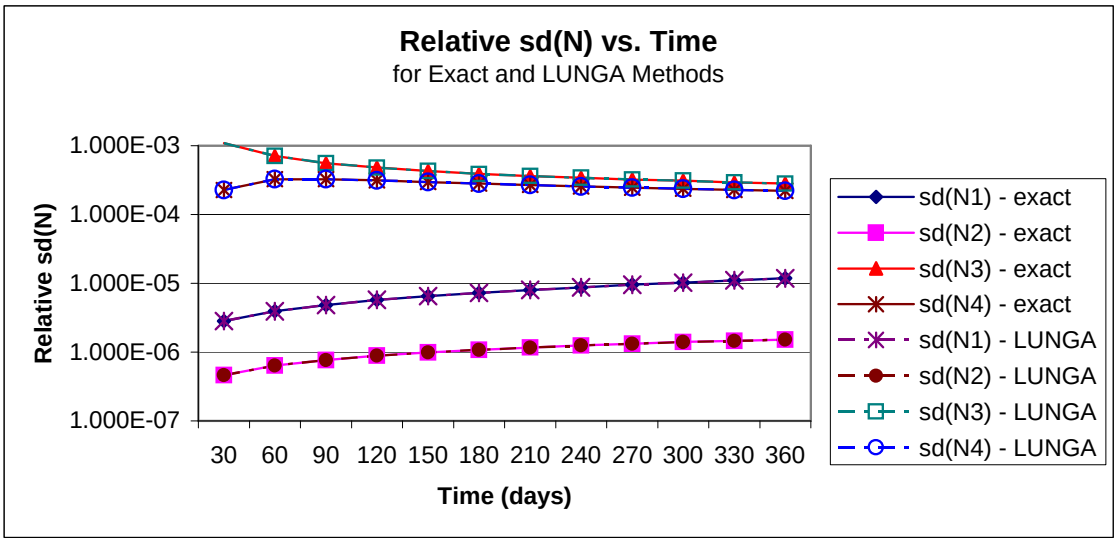

Figure 46. Relative sd(N) with thermal neutron spectrum and thermal cross section normalization for Example 3.

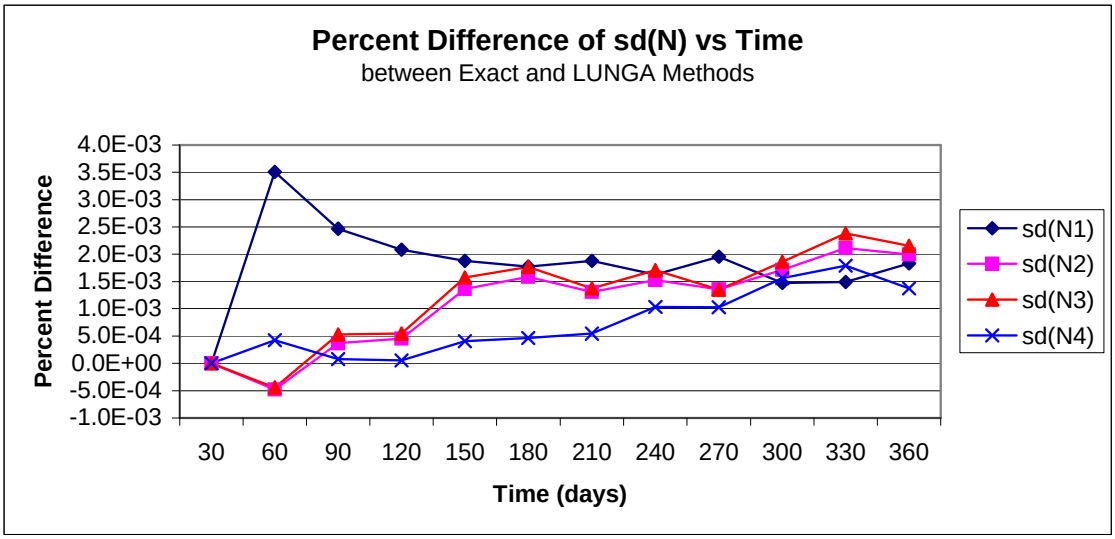

Figure 47. Percent difference of relative sd(N) with thermal neutron spectrum and thermal cross section normalization for Example 3.

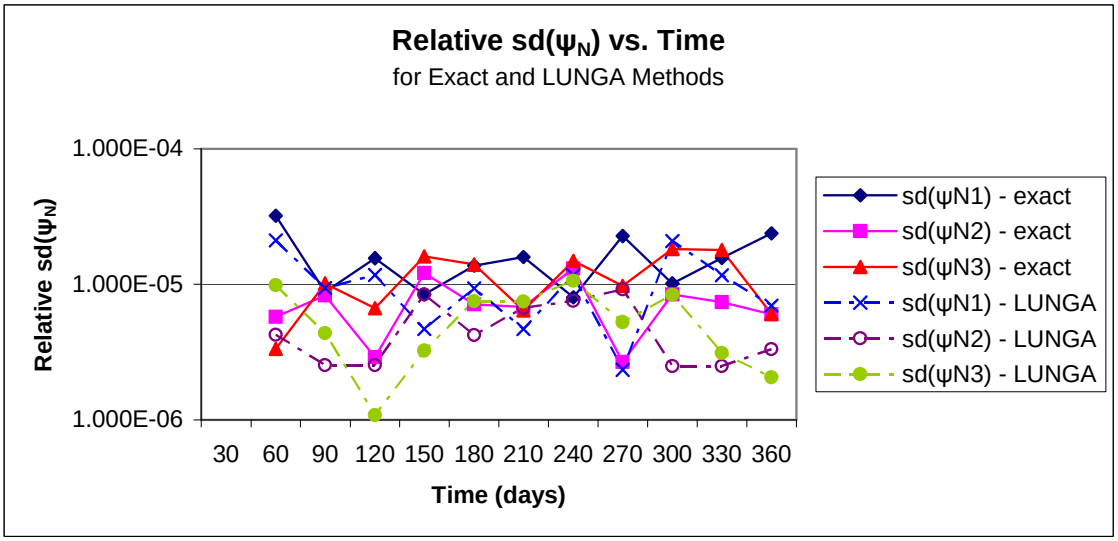

Figure 48. Relative sd(ψ_N) with thermal neutron spectrum and thermal cross section normalization for Example 3.

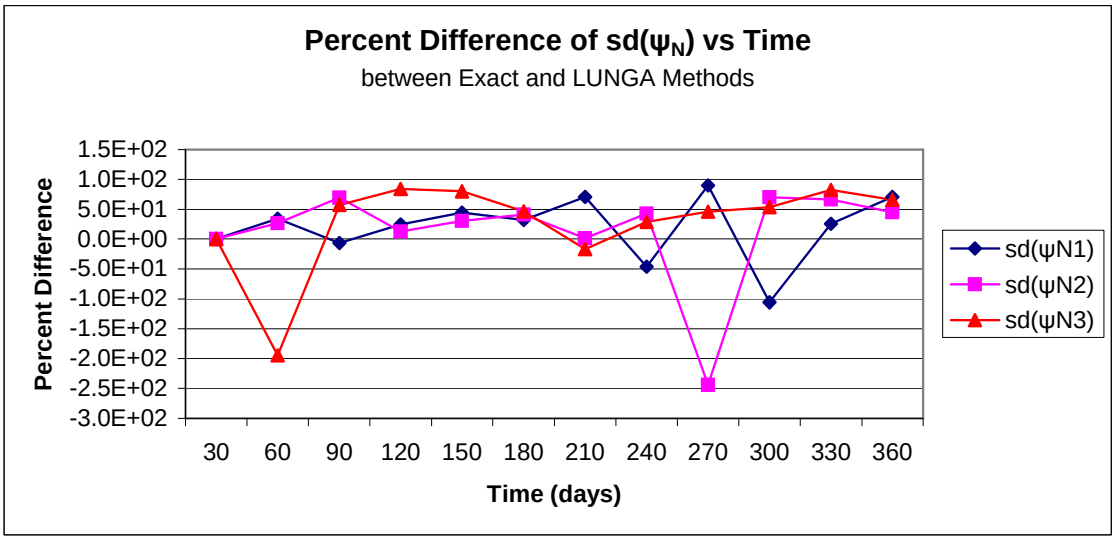

Figure 49. Percent difference of relative sd(ψ_N) with thermal neutron spectrum and thermal cross section normalization for Example 3.

Example 3 is further investigated with a higher reactor power level with a thermal neutron spectrum, thermal normalization of the cross sections, and the extended equations. The reactor power level is set at 55 MW for this variation. A higher reactor power is used to see if the LUNGA method holds as the power level is increased, and to see if the standard deviation in the number densities behaves as seen in previous literature [22]. Figure 50 show the relative standard deviation of the number densities and Figure 51 depicts the percent difference of the relative standard deviation of the number densities. Figure 50 and Figure 51 demonstrate that the exact and LUNGA methods agree very well with each other with much less than 1 percent difference between the two methods in calculating the standard deviation of the number densities. Figure 52 presents the relative standard deviation of the ψ_N term and Figure 53 shows the percent difference in the relative standard deviation of the ψ_N term. As seen in Figure 52 and Figure 53, like the other variations of Example 3, the percent difference between the two methods for

calculating the relative standard deviation of the ψ_N term is large, but the LUNGA method exhibits the same trends as the exact method.

Figure 46 (power level of 27.39MW) and Figure 50 (power level of 55MW) indicate that as burnup increases so does the standard deviation of the number densities. Larger standard deviations in the number densities with increasing burnup values are also seen in previous literature [22]. Figure 47 and Figure 51 illustrate that the percent difference between the LUNGA and exact methods is about the same for the two different reactor power levels.

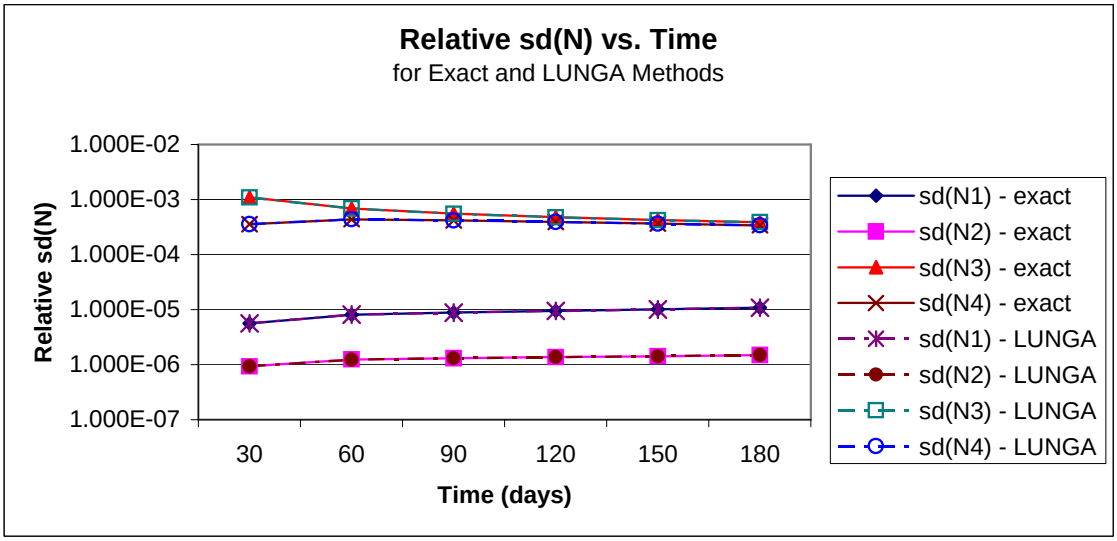

Figure 50. Relative sd(N) with a power level of 55MW for Example 3.

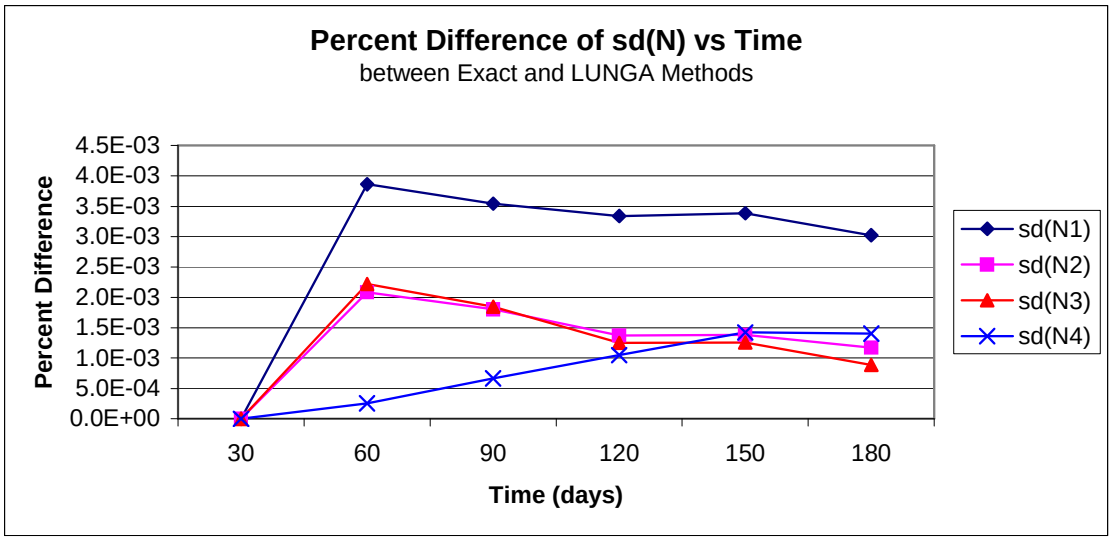

Figure 51. Percent deviation of relative sd(N) with a power level of 55MW for Example 3.

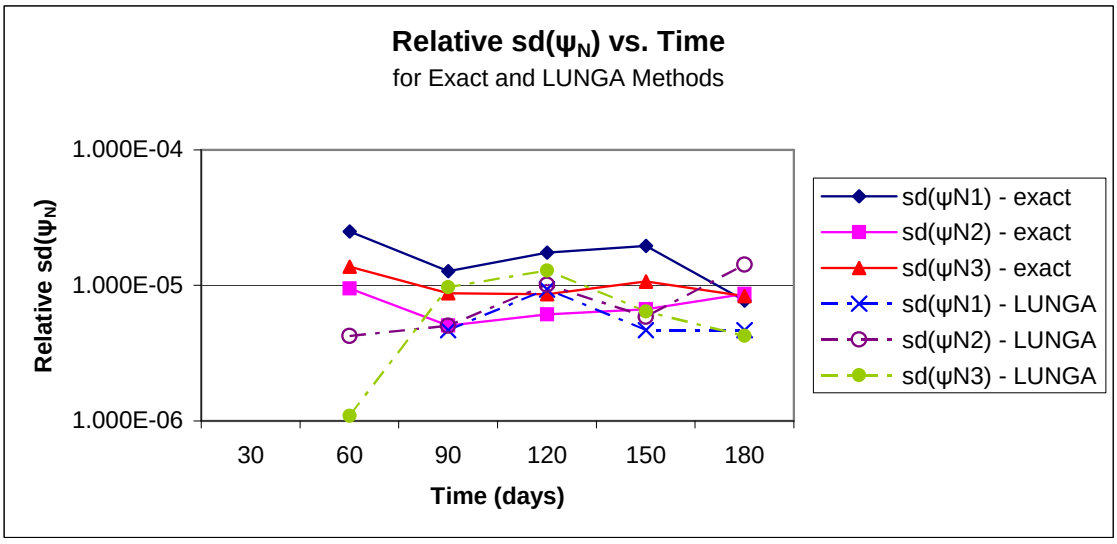

Figure 52. Relative sd(ψ_N) with a power level of 55MW for Example 3.

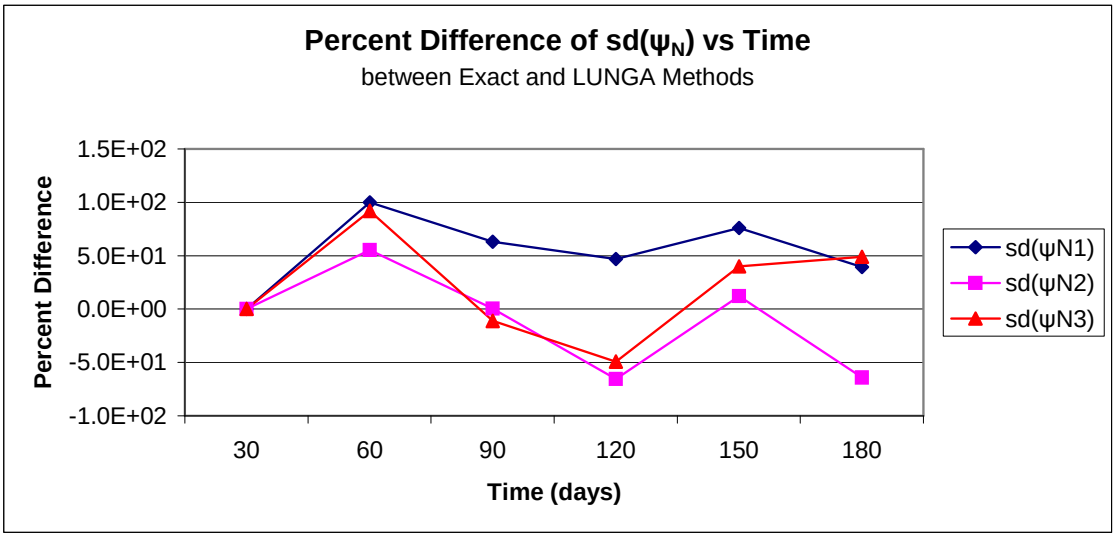

Figure 53. Percent difference of relative sd(ψ_N) with a power level of 55MW for Example 3.

Example 3 is briefly investigated using the central difference method instead of the forward difference method to calculate the derivatives of the flux shape with respect to a nuclide (the ψ_N term). The variation is examined with a thermal neutron spectrum with thermal normalization of the cross sections and the extended equations. The investigation shows there is little to gain by using the central difference method instead of the forward difference method. The central difference method should yield a more accurate answer but also requires twice as many simulations as the forward difference method. Table 14 and Table 15 present a comparison of the relative standard deviation in the nuclide number densities and the relative standard deviation in the ψ_N term respectively. As seen in Table 14, there is really no benefit of using the central difference method compared to the forward difference method. Both difference schemes calculate basically the same standard deviation in the nuclide number densities, and the differences between the exact and LUNGA methods are nearly the same for each difference scheme

(much less than 1 percent difference between the two difference schemes). Table 15 shows no real benefit for using the central difference scheme compared to the forward difference scheme to calculate the standard deviation of the ψ_N term, as both schemes produce on order the same percent difference between the exact and LUNGA methods in calculating the standard deviation of the ψ_N term.

Table 14. Comparison of forward and central difference schemes of the relative sd(N) for Example 3.

Example 3: relative sd(N) comparison for forward and central difference scheme								
		time (days)	30	60	90	120	150	180
real	forward difference	$sd(N_1)$	2.810E-06	3.938E-06	4.837E-06	5.717E-06	6.501E-06	7.248E-06
		$sd(N_2)$	4.630E-07	6.382E-07	7.619E-07	8.838E-07	9.847E-07	1.075E-06
		$sd(N_3)$	1.092E-03	7.092E-04	5.557E-04	4.828E-04	4.293E-04	3.908E-04
		$sd(N_4)$	2.280E-04	3.255E-04	3.267E-04	3.135E-04	2.969E-04	2.818E-04
	central difference	$sd(N_1)$	2.810E-06	3.937E-06	4.837E-06	5.717E-06	6.501E-06	7.248E-06
		$sd(N_2)$	4.630E-07	6.382E-07	7.619E-07	8.838E-07	9.847E-07	1.075E-06
		$sd(N_3)$	1.092E-03	7.092E-04	5.557E-04	4.828E-04	4.293E-04	3.908E-04
		$sd(N_4)$	2.280E-04	3.255E-04	3.267E-04	3.135E-04	2.969E-04	2.818E-04
approximate		$sd(N_1)$	2.810E-06	3.937E-06	4.837E-06	5.717E-06	6.501E-06	7.248E-06
		$sd(N_2)$	4.630E-07	6.382E-07	7.619E-07	8.838E-07	9.847E-07	1.075E-06
		$sd(N_3)$	1.092E-03	7.092E-04	5.557E-04	4.828E-04	4.293E-04	3.908E-04
		$sd(N_4)$	2.280E-04	3.255E-04	3.267E-04	3.135E-04	2.969E-04	2.818E-04
percent difference with forward and approximate (%)		$sd(N_1)$	0.0E+00	3.5E-03	2.5E-03	2.1E-03	1.9E-03	1.8E-03
		$sd(N_2)$	0.0E+00	-4.8E-04	3.7E-04	4.6E-04	1.4E-03	1.6E-03
		$sd(N_3)$	0.0E+00	-4.4E-04	5.3E-04	5.5E-04	1.6E-03	1.8E-03
		$sd(N_4)$	0.0E+00	4.2E-04	7.8E-05	5.6E-05	4.1E-04	4.6E-04
percent difference with central and approximate (%)		$sd(N_1)$	0.0E+00	-7.6E-04	-7.8E-04	-8.5E-04	-3.6E-04	-2.1E-04
		$sd(N_2)$	0.0E+00	-7.3E-04	-3.4E-04	-1.6E-04	-3.0E-04	-1.2E-04
		$sd(N_3)$	0.0E+00	-7.1E-04	-2.6E-04	-7.5E-05	-3.5E-04	-1.6E-04
		$sd(N_4)$	0.0E+00	-9.4E-05	-2.9E-04	-3.8E-04	-3.5E-04	-2.1E-04

Table 15. Comparison of forward and central difference schemes of the relative sd(ψ_N) for Example 3.

Example 3: relative sd(ψ_N) comparison for forward and central difference scheme								
		time (days)	30	60	90	120	150	180
real	forward difference	sd(ψ_{N1})	0.000E+00	3.208E-05	8.797E-06	1.556E-05	8.418E-06	1.372E-05
		sd(ψ_{N2})	0.000E+00	5.739E-06	8.273E-06	2.896E-06	1.212E-05	7.113E-06
		sd(ψ_{N3})	0.000E+00	3.342E-06	1.013E-05	6.658E-06	1.606E-05	1.401E-05
	central difference	sd(ψ_{N1})	0.000E+00	1.809E-05	3.606E-06	6.306E-06	1.435E-05	1.175E-05
		sd(ψ_{N2})	0.000E+00	1.277E-06	4.637E-06	3.860E-06	3.717E-07	8.338E-07
		sd(ψ_{N3})	0.000E+00	3.807E-06	6.397E-06	4.134E-06	2.410E-06	1.059E-05
approximate		sd(ψ_{N1})	0.000E+00	2.112E-05	9.373E-06	1.172E-05	4.675E-06	9.334E-06
		sd(ψ_{N2})	0.000E+00	4.235E-06	2.535E-06	2.528E-06	8.431E-06	4.202E-06
		sd(ψ_{N3})	0.000E+00	9.835E-06	4.365E-06	1.083E-06	3.238E-06	7.500E-06
percent difference with forward and approximate (%)		sd(ψ_{N1})	0.0E+00	3.4E+01	-6.6E+00	2.5E+01	4.4E+01	3.2E+01
		sd(ψ_{N2})	0.0E+00	2.6E+01	6.9E+01	1.3E+01	3.0E+01	4.1E+01
		sd(ψ_{N3})	0.0E+00	-1.9E+02	5.7E+01	8.4E+01	8.0E+01	4.6E+01
percent difference with central and approximate (%)		sd(ψ_{N1})	0.0E+00	-1.7E+01	-1.6E+02	-8.6E+01	6.7E+01	2.1E+01
		sd(ψ_{N2})	0.0E+00	-2.3E+02	4.5E+01	3.5E+01	-2.2E+03	-4.0E+02
		sd(ψ_{N3})	0.0E+00	-1.6E+02	3.2E+01	7.4E+01	-3.4E+01	2.9E+01

5.4 Example 3 with Multiple Materials

Example 3 with multiple materials is an extension of Example 3, and is examined to investigate the effects of multiple materials (different fuel pins types) in the system. Example 3 with multiple materials is investigated with a thermal neutron spectrum, thermal normalization of the cross sections, and the extended equations. Table 16 displays the number densities and the relative standard deviation of the number densities calculated using the LUNGA method.

Table 16. Relative sd(N) calculated with the LUNGA method for Example 3 with multiple materials.

Example 3 with multiple materials with 30 day time steps for material 1; solved with MC method								
		Time step	Step1	Step2	Step3	Step4	Step5	Step6
		N_1	2.374E+23	2.278E+23	2.184E+23	2.093E+23	2.004E+23	1.917E+23
		N_2	4.634E+24	4.630E+24	4.626E+24	4.622E+24	4.618E+24	4.614E+24
		N_3	2.794E+21	5.728E+21	8.438E+21	1.094E+22	1.323E+22	1.534E+22
		N_4	2.971E+14	7.595E+14	1.307E+15	1.886E+15	2.466E+15	3.029E+15
Approximate	Relative	$sd(N_1)$	7.916E-05	1.147E-04	1.423E-04	1.650E-04	1.869E-04	2.064E-04
		$sd(N_2)$	2.006E-06	2.877E-06	3.518E-06	4.059E-06	4.567E-06	5.014E-06
		$sd(N_3)$	2.382E-03	1.547E-03	1.194E-03	9.890E-04	8.574E-04	7.574E-04
		$sd(N_4)$	2.457E-03	1.849E-03	1.479E-03	1.215E-03	1.032E-03	8.875E-04
		$Var(\psi_{N1})$	0.000E+00	4.143E-12	7.366E-12	4.597E-13	1.483E-10	2.426E-10
		$Var(\psi_{N2})$	0.000E+00	1.632E-11	1.625E-11	1.620E-11	1.609E-09	2.574E-10
		$Var(\psi_{N3})$	0.000E+00	3.042E-11	3.200E-10	1.862E-10	9.075E-11	4.556E-11
Example 3 with multiple materials with 30 day time steps for material 2; solved with MC method								
		Time step	Step1	Step2	Step3	Step4	Step5	Step6
		N_1	1.412E+23	1.344E+23	1.278E+23	1.214E+23	1.153E+23	1.094E+23
		N_2	4.732E+24	4.727E+24	4.723E+24	4.719E+24	4.715E+24	4.711E+24
		N_3	2.946E+21	5.986E+21	8.740E+21	1.124E+22	1.351E+22	1.556E+22
		N_4	2.786E+14	7.748E+14	1.365E+15	1.983E+15	2.589E+15	3.164E+15
Approximate	Relative	$sd(N_1)$	1.207E-04	1.707E-04	2.107E-04	2.443E-04	2.769E-04	3.065E-04
		$sd(N_2)$	2.313E-06	3.269E-06	4.018E-06	4.637E-06	5.226E-06	5.747E-06
		$sd(N_3)$	2.640E-03	1.674E-03	1.285E-03	1.054E-03	9.037E-04	7.876E-04
		$sd(N_4)$	3.330E-03	2.333E-03	1.794E-03	1.436E-03	1.194E-03	1.009E-03
		$Var(\psi_{N1})$	0.000E+00	4.771E-13	2.970E-10	1.221E-10	2.976E-10	4.741E-11
		$Var(\psi_{N2})$	0.000E+00	0.000E+00	2.610E-10	6.487E-11	0.000E+00	6.443E-11
		$Var(\psi_{N3})$	0.000E+00	1.267E-10	3.898E-11	1.255E-10	6.175E-12	6.119E-12

Figure 54 and Figure 55 display a comparison of the relative standard deviation of the number densities for Example 3 and Example 3 with multiple materials. Since Example 3 with multiple materials is an extension of Example 3 the trends should be similar to one another. Figure 54 and Figure 55 illustrate that the trend of the relative standard deviation of the nuclides in material 1 and material 2 for Example 3 with multiple materials are very similar to the trends for Example 3.

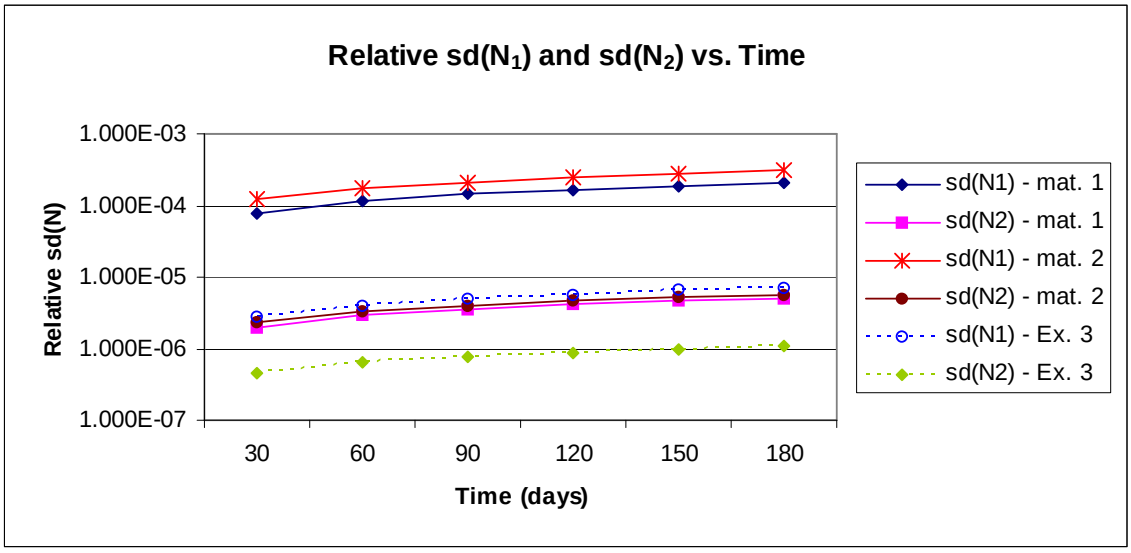

Figure 54. Relative sd(N_1) and sd(N_2) calculated with the LUNGA method for Example 3 and Example 3 with multiple materials.

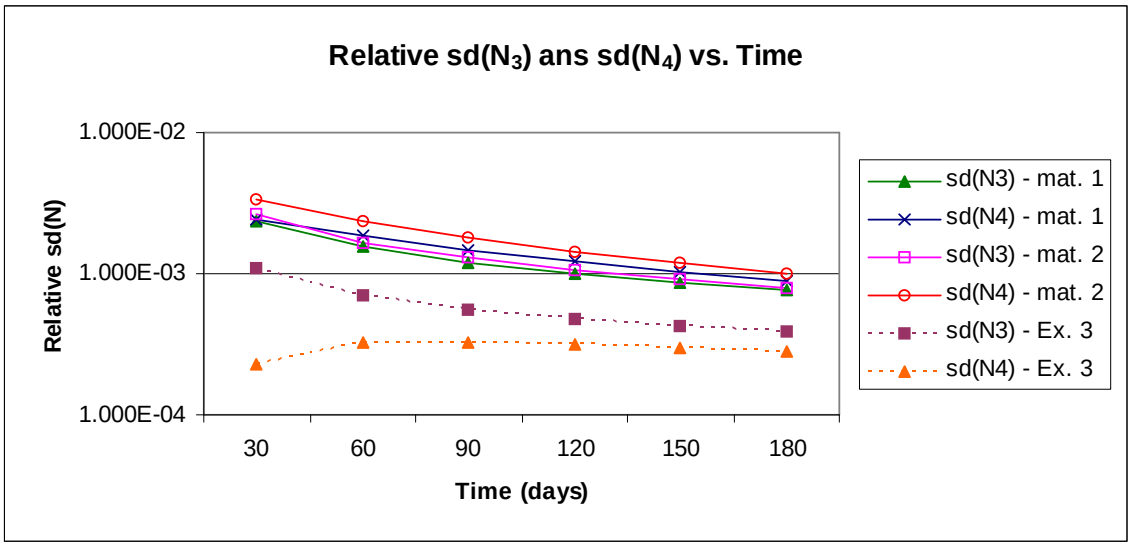

Figure 55. Relative sd(N_3) and sd(N_4) calculated with the LUNGA method for Example 3 and Example 3 with multiple materials.

5.5 Discussion of the ψ_N Term

The variance in the flux shape (ψ) is composed of two terms, the statistical component (ψ_S – from the Monte Carlo simulation) and the nuclide component (ψ_N – from the changes in the number densities). The variance of the ψ_N term contributes to part of the variance in the flux shape and is defined by

$\text{var}(\psi_N) = E\left[(\Delta\psi_N)^2\right] = \left(\frac{\partial\psi}{\partial\overline{N}}\right)^T COV\left[\overline{N}, \overline{N}^T\right]\left(\frac{\partial\psi}{\partial\overline{N}}\right)$ where $COV\left[\overline{N}, \overline{N}^T\right]$ is the nuclide covariance matrix. The ψ_N term comes from the uncertainty in the flux shape due to the uncertainty in the number densities and is defined by $\Delta\psi_N = \frac{\partial\psi}{\partial\overline{N}}\Delta\overline{N}$ where $\overline{N}$ is a vector of all nuclides in the system. In order to solve for the ψ_N term, the change in the flux shape must be found for a change in each nuclide in the system. That means finding the derivatives of the flux shape with respect to each nuclide in the system which takes time, or tabulating the derivatives in some kind of file.

The LUNGA method presented in this research calculates the $\Delta\psi_N$ term in a way that reduces the number of Monte Carlo simulations needed to describe the term, and requires only one additional Monte Carlo simulation per mixture being depleted (area of interest). The following equation used in the LUNGA method, in this research, to approximately calculate the $\Delta\psi_N$ term is $\sigma_{\psi_N} \approx \Delta\psi_N = \psi' - \psi$. The solutions for the flux shape come from the equations $B\left(\overline{N} + \Delta\overline{N}\right)\psi' = 0$ and $B\left(\overline{N}\right)\psi = 0$ where $\overline{N}$ is a vector of all the nuclides in the system and B is the Boltzman operator. Example 2 and Example 3 show how the ψ_N term behaved in two different systems. The two examples provide different insights about approximating the variance of the ψ_N term.

Example 2 shows that the LUNGA method worked very well in calculating the variance of the ψ_N term. The percent difference between the LUNGA and exact methods is less than 1 percent for a time step of 250-days (see Figure 23) and less than one half of 1 percent for a time step of 2-days (see Figure 27). Example 2 also shows the approximation agreeing very well with the exact method for a statistical uncertainty up to 25 percent; the percent difference in the ψ_N term for that case is under 2 percent as seen in Figure 19. However, Example 3 reveals that the LUNGA method did not work well in calculating the variance of the ψ_N term compared to the exact method. The percent difference between the LUNGA method and the exact method is generally around 100 percent as seen in Figure 31 and Figure 41.

In Example 2 the LUNGA method works very well in calculating the variance of the ψ_N term, but in Example 3 the LUNGA method did not work well in calculating the variance of the ψ_N term. This appears to be a problem; however, investigating the ψ_N term more closely reveals that the variance of the ψ_N term makes a very small contribution to the variances of the number densities. The contributions to the variance of the number densities are calculated using both Example 2 and Example 3. Table 17 for Example 2, and Table 18 and Table 19 for Example 3 present the percent contributions of the different terms to the variance in the number densities.

Table 17. Percent contribution of terms in var(N1) and var(N2) for Example 2.

Contribution of ψ_N, ψ_s, and var(N) and COV(N,N') terms in var(N)					
	Time step	Step1	Step2	Step3	Step4
	Time (days)	2.5E+02	5.0E+02	7.5E+02	1.0E+03
Percent contribution of var(ψ_N) in var(N)	var(N_1)	0.0E+00	2.4E-08	2.6E-07	7.3E-07
	var(N_2)	0.0E+00	2.4E-08	2.4E-07	5.8E-07
Percent contribution of var(ψ_s) in var(N)	var(N_1)	1.0E+02	5.0E+01	3.3E+01	2.5E+01
	var(N_2)	1.0E+02	5.0E+01	3.1E+01	2.0E+01
Percent contribution of var(N) and COV(N,N') in var(N)	var(N_1)	0.0E+00	5.0E+01	6.7E+01	7.5E+01
	var(N_2)	0.0E+00	5.0E+01	6.9E+01	8.0E+01

Table 18. Percent contribution of terms in var(N) with fast neutron spectrum for Example 3.

Contribution of ψ_N, ψ_s, and var(N) and COV(N,N') in var(N) for Fast Spectrum						
	Time (days)	30	60	90	120	150
Percent contribution of var(ψ_s) in var(N)	var(N_1) (U^{235})	1.0E+02	4.8E+01	2.7E+01	2.4E+01	2.0E+01
	var(N_2) (U^{238})	1.0E+02	5.1E+01	3.2E+01	2.2E+01	2.5E+01
	var(N_3) (Pu^{239})	1.0E+02	4.9E+01	2.8E+01	2.4E+01	2.1E+01
	var(N_4) (Eu^{155})	1.0E+02	5.7E+01	3.8E+01	3.1E+01	3.4E+01
Percent contribution of var(ψ_N) in var(N)	var(N_1) (U^{235})	0.0E+00	7.8E-04	9.1E-05	7.1E-04	3.9E-05
	var(N_2) (U^{238})	0.0E+00	8.7E-03	1.2E-03	2.0E-03	1.1E-03
	var(N_3) (Pu^{239})	0.0E+00	2.0E-03	2.9E-04	9.4E-04	2.5E-04
	var(N_4) (Eu^{155})	0.0E+00	4.8E-03	8.9E-04	2.0E-03	1.2E-03
Percent contribution of var(N) and COV(N,N') in var(N)	var(N_1) (U^{235})	0.0E+00	5.2E+01	7.3E+01	7.6E+01	8.0E+01
	var(N_2) (U^{238})	0.0E+00	4.9E+01	6.8E+01	7.8E+01	7.5E+01
	var(N_3) (Pu^{239})	0.0E+00	5.1E+01	7.2E+01	7.6E+01	7.9E+01
	var(N_4) (Eu^{155})	0.0E+00	4.3E+01	6.2E+01	6.9E+01	6.6E+01

Table 19. Percent contribution of terms in var(N) with thermal neutron spectrum for Example 3.

Contribution of ψ_N, ψ_s, and var(N) and COV(N,N') in var(N) for Thermal Spectrum					
	Time (days)	30	60	90	120
Percent contribution of var(ψ_s) in var(N)	var(N_1) (U^{235})	1.0E+02	4.8E+01	3.2E+01	2.6E+01
	var(N_2) (U^{238})	1.0E+02	4.9E+01	3.1E+01	2.7E+01
	var(N_3) (Pu^{239})	1.0E+02	5.1E+01	3.5E+01	3.2E+01
	var(N_4) (Eu^{155})	1.0E+02	5.8E+00	3.9E+00	5.0E+00
Percent contribution of var(ψ_N) in var(N)	var(N_1) (U^{235})	0.0E+00	5.4E-03	7.3E-04	8.1E-04
	var(N_2) (U^{238})	0.0E+00	1.8E-03	2.7E-04	7.0E-05
	var(N_3) (Pu^{239})	0.0E+00	1.7E-03	2.8E-04	7.6E-05
	var(N_4) (Eu^{155})	0.0E+00	6.6E-04	7.4E-05	5.7E-05
Percent contribution of var(N) and COV(N,N') in var(N)	var(N_1) (U^{235})	0.0E+00	5.2E+01	6.8E+01	7.4E+01
	var(N_2) (U^{238})	0.0E+00	5.1E+01	6.9E+01	7.3E+01
	var(N_3) (Pu^{239})	0.0E+00	4.9E+01	6.5E+01	6.8E+01
	var(N_4) (Eu^{155})	0.0E+00	9.4E+01	9.6E+01	9.5E+01
	Time (days)	150	180	210	240
Percent contribution of var(ψ_s) in var(N)	var(N_1) (U^{235})	2.0E+01	1.7E+01	1.4E+01	1.3E+01
	var(N_2) (U^{238})	2.1E+01	1.8E+01	1.6E+01	1.5E+01
	var(N_3) (Pu^{239})	2.5E+01	2.2E+01	2.0E+01	2.0E+01
	var(N_4) (Eu^{155})	5.8E+00	6.5E+00	7.3E+00	8.8E+00
Percent contribution of var(ψ_N) in var(N)	var(N_1) (U^{235})	3.0E-04	3.8E-04	1.7E-04	4.8E-04
	var(N_2) (U^{238})	4.2E-04	4.0E-04	4.4E-04	6.7E-04
	var(N_3) (Pu^{239})	6.4E-04	4.7E-04	6.0E-04	9.0E-04
	var(N_4) (Eu^{155})	7.2E-05	1.5E-04	1.9E-04	3.9E-04
Percent contribution of var(N) and COV(N,N') in var(N)	var(N_1) (U^{235})	8.0E+01	8.3E+01	8.6E+01	8.7E+01
	var(N_2) (U^{238})	7.9E+01	8.2E+01	8.4E+01	8.5E+01
	var(N_3) (Pu^{239})	7.5E+01	7.8E+01	8.0E+01	8.0E+01
	var(N_4) (Eu^{155})	9.4E+01	9.3E+01	9.3E+01	9.1E+01

As an additional investigation into the ψ_N term, Example 3 is analyzed by omitting the ψ_N term in the LUNGA method. Table 20 reveals the relative standard deviation and the percent difference in the relative standard deviation of the nuclide number densities with and without including the ψ_N term in the LUNGA method. As seen in Table 20, the

relative standard deviation in the number densities is about the same regardless of whether or not the ψ_N term is included. Not including the ψ_N term yields slightly less accurate results than including the ψ_N term as compared to the exact method which is also noticed in Table 20. This helps reinforce how small a contributor the ψ_N term is to the standard deviation of the number densities.

Table 20. Relative sd(N) and percent difference of sd(N) with no ψ_N term in LUNGA method for Example 3.

Example 3: relative sd(N) and percent difference in relative sd(N) with UO_2 fuel							
	time (days)	30	60	90	120	150	180
real method (atoms/cm^3)	sd(N_1)	2.810E-06	3.938E-06	4.837E-06	5.717E-06	6.501E-06	7.248E-06
	sd(N_2)	4.630E-07	6.382E-07	7.619E-07	8.838E-07	9.847E-07	1.075E-06
	sd(N_3)	1.092E-03	7.092E-04	5.557E-04	4.828E-04	4.293E-04	3.908E-04
	sd(N_4)	2.280E-04	3.255E-04	3.267E-04	3.135E-04	2.969E-04	2.818E-04
approximate method with ψ_N (atoms/cm^3)	sd(N_1)	2.810E-06	3.937E-06	4.837E-06	5.717E-06	6.501E-06	7.248E-06
	sd(N_2)	4.630E-07	6.382E-07	7.619E-07	8.838E-07	9.847E-07	1.075E-06
	sd(N_3)	1.092E-03	7.092E-04	5.557E-04	4.828E-04	4.293E-04	3.908E-04
	sd(N_4)	2.280E-04	3.255E-04	3.267E-04	3.135E-04	2.969E-04	2.818E-04
approximate method without ψ_N (atoms/cm^3)	sd(N_1)	2.810E-06	3.937E-06	4.837E-06	5.717E-06	6.501E-06	7.247E-06
	sd(N_2)	4.630E-07	6.382E-07	7.619E-07	8.838E-07	9.847E-07	1.075E-06
	sd(N_3)	1.092E-03	7.092E-04	5.556E-04	4.828E-04	4.293E-04	3.908E-04
	sd(N_4)	2.280E-04	3.255E-04	3.267E-04	3.135E-04	2.969E-04	2.818E-04
percent difference between real and approximate with ψ_N (%)	sd(N_1)	0.0E+00	3.5E-03	2.5E-03	2.1E-03	1.9E-03	1.8E-03
	sd(N_2)	0.0E+00	-4.8E-04	3.7E-04	4.6E-04	1.4E-03	1.6E-03
	sd(N_3)	0.0E+00	-4.4E-04	5.3E-04	5.5E-04	1.6E-03	1.8E-03
	sd(N_4)	0.0E+00	4.2E-04	7.8E-05	5.6E-05	4.1E-04	4.6E-04
percent difference between real and approximate without ψ_N (%)	sd(N_1)	0.0E+00	6.2E-03	4.7E-03	4.1E-03	3.6E-03	3.4E-03
	sd(N_2)	0.0E+00	4.3E-04	1.1E-03	1.0E-03	2.0E-03	2.3E-03
	sd(N_3)	0.0E+00	4.1E-04	1.2E-03	1.1E-03	2.3E-03	2.5E-03
	sd(N_4)	0.0E+00	7.5E-04	5.3E-04	6.3E-04	1.0E-03	1.1E-03

Table 17 to Table 20 show that the main contributions to the variance in the number densities come from the variance of the ψ_S term (statistical component of the flux shape) and the variance and covariances of the number densities themselves. For Example 2, the contribution from these terms are 6 to 7 orders of magnitude greater than the contribution

from the ψ_N term (nuclide component of the flux shape). For Example 3, the contribution from these terms are 3 to 5 orders of magnitude greater than the contribution from the ψ_N term. The contribution from the ψ_N term to the variance in the number densities is very, very small. Therefore, the ψ_N term is not as significant a contributor to the variance in the number densities as the ψ_S term or the variance and covariances of the number densities themselves.

CHAPTER 6

VALIDATION OF THE LUNGA METHOD

Validation of the LUNGA method for calculating the standard deviation in the nuclide number densities is not an easy task. There are limited journal articles to compare the research to, and the authors of the articles do not give an in-depth discussion about the operating conditions of their system simulation. Therefore, replication of the system in the journal articles was attempted with little knowledge of those systems. A large number of Monte Carlo simulations could be run and the results compared, but this takes time and computing resources.

Validation was accomplished by comparing the results of 100 different Monte Carlo simulations to the results of both Example 3 and Example 3 with multiple materials using the LUNGA method. Verification was done by indirectly comparing the results of Example 3 to the results found in previous journal articles. An indirect comparison to the journal articles is judged as a good method to help validate the research, since the simulations in the journal articles could not be reproduced exactly, because of the limited amount of information presented in the journal articles about the setup of the simulations.

6.1 Validation of Example 3

Validation of the LUNGA method for calculating the standard deviation in the nuclide number densities is done by running 100 different Monte Carlo simulations each with a different starting random number. Each simulation consisted of 250 generations (skipped 50 generations) with 2,000 neutrons per generation for a total of 400,000

particles. This is selected for two reasons: first, it is the number of particles used in the article by Shim and second, it shows convergence of infinite medium multiplication factor (k_{inf}) and the nuclide number densities, and creates a difference in the fluxes that is seen in the number densities. A higher particle count would lead to less statistical uncertainty in the flux and, therefore, less uncertainty in the nuclide number densities.

The nuclide number densities using the derived equations are verified with the nuclide number densities from the Monte Carlo solution (T5-DEPL sequence) and deterministic solution (T-DEPL sequence) from SCALE and are presented in Table 22 and Table 23. Table 22 and Table 23 indicate some discrepancy in the number densities between the derived equations and SCALE. With further investigation it was found that the main discrepancy in the number densities is due to omitting ^{239}U and ^{239}Np in nuclide chain equations. Therefore, the original equations for Example 3 were expanded to include ^{239}U and ^{239}Np. To help limit differences between the original equations and the expanded equations, no uncertainty was included in the ^{239}U and ^{239}Np isotopes. As seen in Table 22 and Table 23, these extended equations nearly duplicate the nuclide number densities calculated by the SCALE computer code. Some of the difference between the derived expanded equations and SCALE was contributed to the exclusion of other nuclides in the decay and capture chains [15]. Also the difference in how the nuclide transmutation equations were solved, SCALE using a more rigorous solution method, contributed to some of the differences in the values [15]. Some of the differences between the derived expanded equations and SCALE were also contributed to the small differences in some of the constants used in the calculations that are specified in Table 21.

Table 21. Differences of internal constants between SCALE and the derived equations.

Differences between derived equations and SCALE							
		Derived equations		SCALE		Percent difference (%)	
Power conversion constant (MW/(MeV/s))			1.60E-13		1.60219E-13		1.4E-01
Recoverable energy (MeV)		fission	capture	fission	capture	fission	capture
Nuclide	U^{235}	194.02	6.545	194.02	6.5451	0.0E+00	1.5E-03
	U^{238}	198.12	4.804	198.122	4.804	1.0E-03	0.0E+00
	Pu^{239}	200.05	6.533	200.05	6.533	0.0E+00	0.0E+00
	Eu^{155}	0	6.49	0	6.49	0.0E+00	0.0E+00
	O^{16}	0	4.143	0	4.143	0.0E+00	0.0E+00
	H^{1}	0	2.225	0	2.2246	0.0E+00	-1.8E-02

Table 22. Percent difference of the number densities between MC solution of SCALE and derived equations.

Percent difference in the number densities between SCALE with MC solution and derived equations												
Time (days)	30	60	90	120	150	180	210	240	270	300	330	360
Original equations with fast spectrum and total cross section normalization												
N_1 (U^{235})	1.2E-02	1.6E-02	1.4E-02	6.5E-03	1.5E-02	1.7E-03	8.0E-03	-8.7E-03	-5.2E-03	2.1E-03	-1.4E-02	-2.4E-03
N_2 (U^{238})	1.0E-02	1.6E-03	3.2E-03	4.4E-03	-5.4E-03	-4.7E-03	-4.1E-03	-3.6E-03	-1.4E-02	-1.4E-02	-1.4E-02	-1.4E-02
N_3 (Pu^{239})	-1.3E+01	-6.5E+00	-4.4E+00	-3.3E+00	-2.7E+00	-2.3E+00	-2.0E+00	-1.8E+00	-1.6E+00	-1.5E+00	-1.3E+00	-1.2E+00
N_4 (Eu^{155})	-9.7E+00	-7.1E+00	-5.7E+00	-4.7E+00	-3.9E+00	-3.4E+00	-3.0E+00	-2.7E+00	-2.4E+00	-2.2E+00	-2.0E+00	-1.8E+00
Original equations with fast spectrum and thermal cross section normalization												
N_1 (U^{235})	1.2E-02	1.6E-02	1.4E-02	6.5E-03	1.5E-02	1.7E-03	8.0E-03	-8.7E-03	-5.2E-03	2.1E-03	-1.4E-02	-2.4E-03
N_2 (U^{238})	1.0E-02	1.6E-03	3.2E-03	4.4E-03	-5.4E-03	-4.7E-03	-4.1E-03	-3.6E-03	-1.4E-02	-1.4E-02	-1.4E-02	-1.4E-02
N_3 (Pu^{239})	-1.3E+01	-6.5E+00	-4.4E+00	-3.3E+00	-2.7E+00	-2.3E+00	-2.0E+00	-1.8E+00	-1.6E+00	-1.5E+00	-1.3E+00	-1.2E+00
N_4 (Eu^{155})	-9.7E+00	-7.1E+00	-5.7E+00	-4.7E+00	-3.9E+00	-3.4E+00	-3.0E+00	-2.7E+00	-2.4E+00	-2.2E+00	-2.0E+00	-1.8E+00
Extended equations with fast spectrum and thermal cross section normalization												
N_1 (U^{235})	1.2E-02	2.0E-02	2.1E-02	1.7E-02	2.9E-02	1.7E-02	2.6E-02	1.0E-02	1.9E-02	2.7E-02	1.6E-02	2.8E-02
N_2 (U^{238})	1.0E-02	1.8E-03	3.5E-03	4.9E-03	-4.8E-03	-3.9E-03	-3.2E-03	-2.7E-03	-1.3E-02	-1.3E-02	-1.2E-02	-1.2E-02
N_3 (Pu^{239})	-1.2E-01	-3.5E-01	-3.9E-01	-3.5E-01	-3.2E-01	-2.8E-01	-2.6E-01	-2.6E-01	-2.7E-01	-2.6E-01	-2.5E-01	-2.4E-01
N_4 (Eu^{155})	-4.9E-01	-8.4E-01	-1.0E+00	-1.1E+00	-1.1E+00	-1.1E+00	-1.1E+00	-9.6E-01	-9.0E-01	-8.2E-01	-7.9E-01	-7.4E-01
Extended equations thermal spectrum and thermal cross section normalization												
N_1 (U^{235})	-2.3E-03	-3.4E-03	-1.0E-02	-8.7E-04	-1.8E-02	-1.8E-02	-2.1E-02	-2.8E-02	-3.7E-02	-4.9E-02	-3.8E-02	-5.4E-02
N_2 (U^{238})	5.8E-03	6.5E-03	7.5E-03	8.5E-03	-1.0E-03	4.2E-04	2.0E-03	3.7E-03	5.7E-03	-2.7E-03	-2.1E-04	2.5E-03
N_3 (Pu^{239})	2.1E-01	1.1E-03	-6.8E-02	-4.5E-02	-1.0E-01	-1.1E-01	-4.6E-02	-2.5E-02	2.0E-02	-5.4E-02	-6.8E-02	-6.2E-02
N_4 (Eu^{155})	3.0E-01	2.0E-01	1.3E-01	7.6E-03	1.9E-02	-2.5E-02	-6.0E-02	-9.7E-02	-7.6E-02	-3.0E-02	-4.3E-02	-6.1E-02

Table 23. Percent difference of the number densities between deterministic solution of SCALE and derived equations.

Percent difference in the number densities between SCALE with deterministic solution and derived equations												
Time (days)	30	60	90	120	150	180	210	240	270	300	330	360
Original equations with fast spectrum and total cross section normalization												
N_1 (U^{235})	1.2E-02	1.6E-02	1.4E-02	6.5E-03	1.5E-02	1.7E-03	8.0E-03	1.4E-02	-5.2E-03	2.1E-03	-1.4E-02	-2.4E-03
N_2 (U^{238})	1.0E-02	1.6E-03	3.2E-03	4.4E-03	-5.4E-03	-4.7E-03	-4.1E-03	-3.6E-03	-1.4E-02	-1.4E-02	-1.4E-02	-1.4E-02
N_3 (Pu^{239})	-1.3E+01	-6.4E+00	-4.3E+00	-3.3E+00	-2.6E+00	-2.2E+00	-1.9E+00	-1.7E+00	-1.5E+00	-1.4E+00	-1.3E+00	-1.2E+00
N_4 (Eu^{155})	-9.7E+00	-7.2E+00	-5.7E+00	-4.7E+00	-3.9E+00	-3.4E+00	-3.0E+00	-2.7E+00	-2.4E+00	-2.2E+00	-2.0E+00	-1.9E+00
Original equations with fast spectrum and thermal cross section normalization												
N_1 (U^{235})	1.2E-02	1.6E-02	1.4E-02	6.5E-03	1.5E-02	1.7E-03	8.0E-03	1.4E-02	-5.2E-03	2.1E-03	-1.4E-02	-2.4E-03
N_2 (U^{238})	1.0E-02	1.6E-03	3.2E-03	4.4E-03	-5.4E-03	-4.7E-03	-4.1E-03	-3.6E-03	-1.4E-02	-1.4E-02	-1.4E-02	-1.4E-02
N_3 (Pu^{239})	-1.3E+01	-6.4E+00	-4.3E+00	-3.3E+00	-2.6E+00	-2.2E+00	-1.9E+00	-1.7E+00	-1.5E+00	-1.4E+00	-1.3E+00	-1.2E+00
N_4 (Eu^{155})	-9.7E+00	-7.2E+00	-5.7E+00	-4.7E+00	-3.9E+00	-3.4E+00	-3.0E+00	-2.7E+00	-2.4E+00	-2.2E+00	-2.0E+00	-1.9E+00
Extended equations with fast spectrum and thermal cross section normalization												
N_1 (U^{235})	1.2E-02	2.0E-02	2.1E-02	1.7E-02	2.9E-02	1.7E-02	2.6E-02	3.3E-02	1.9E-02	2.7E-02	1.6E-02	2.8E-02
N_2 (U^{238})	1.0E-02	1.8E-03	3.5E-03	4.9E-03	-4.8E-03	-3.9E-03	-3.2E-03	-2.7E-03	-1.3E-02	-1.3E-02	-1.2E-02	-1.2E-02
N_3 (Pu^{239})	-6.5E-02	-2.7E-01	-2.7E-01	-3.0E-01	-2.9E-01	-2.5E-01	-2.4E-01	-2.1E-01	-2.1E-01	-1.9E-01	-1.9E-01	-1.7E-01
N_4 (Eu^{155})	-5.4E-01	-8.8E-01	-1.0E+00	-1.1E+00	-1.1E+00	-1.1E+00	-1.1E+00	-9.9E-01	-9.3E-01	-8.7E-01	-8.1E-01	-7.8E-01
Extended equations thermal spectrum and thermal cross section normalization												
N_1 (U^{235})	-2.3E-03	-3.4E-03	-1.0E-02	-8.7E-04	-1.8E-02	-1.8E-02	-2.1E-02	-2.8E-02	-3.7E-02	-4.9E-02	-6.4E-02	-5.4E-02
N_2 (U^{238})	5.8E-03	6.5E-03	7.5E-03	8.5E-03	-1.0E-03	4.2E-04	2.0E-03	3.7E-03	5.7E-03	-2.7E-03	-2.1E-04	2.5E-03
N_3 (Pu^{239})	2.8E-01	1.4E-01	9.0E-02	1.1E-01	9.0E-02	5.2E-02	9.8E-02	1.5E-01	1.4E-01	8.7E-02	6.3E-02	6.0E-02
N_4 (Eu^{155})	3.4E-01	2.2E-01	1.3E-01	1.3E-01	1.1E-01	8.5E-02	6.0E-02	3.1E-02	5.7E-02	8.7E-02	8.0E-02	8.3E-02

Verification continues with investigating the criticality (k_{inf}) of the system in Example 3, which is calculated with both Monte Carlo and deterministic solutions from SCALE. Figure 56 and Figure 57 show the criticality constant for both the fast and thermal neutron spectrums and illustrate that the derived equations can calculate the criticality of the system very accurately, generally with around a 0.10 percent difference.

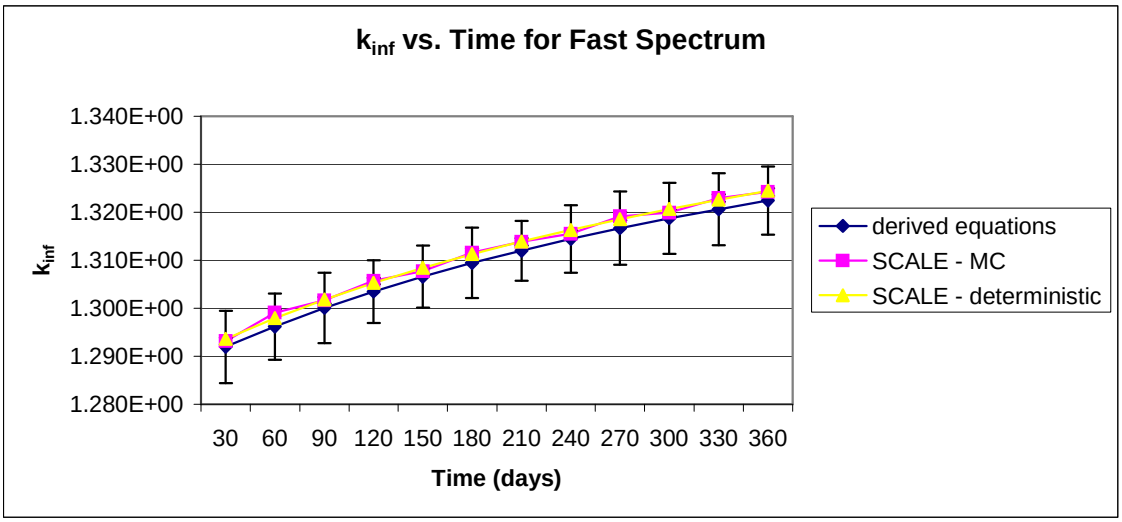

Figure 56. Criticality constant of a fast reactor system in Example 3.

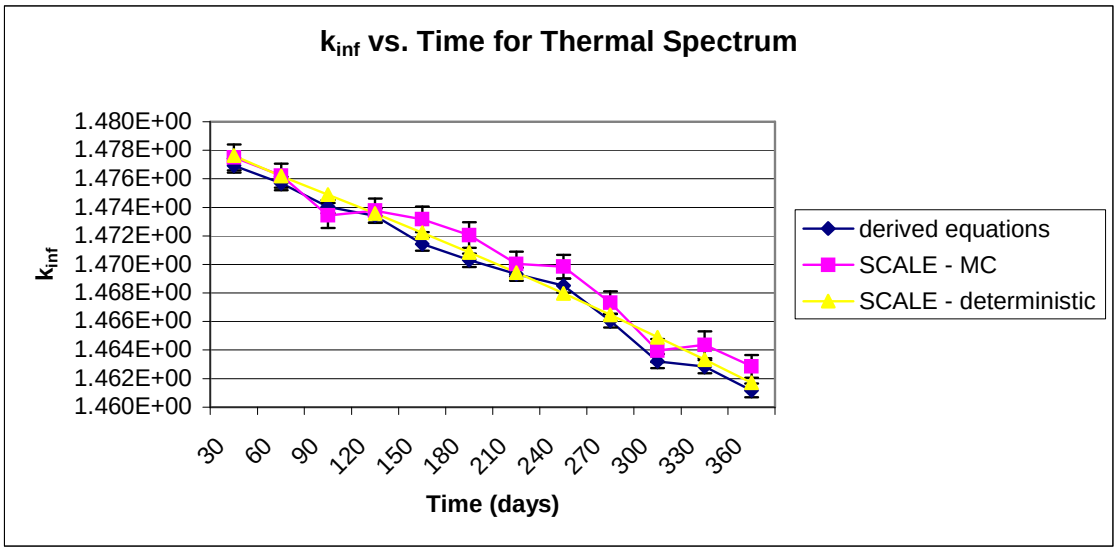

Figure 57. Criticality constant of a thermal reactor system in Example 3.

This part of the verification concludes with a statistical analysis of the 100 Monte Carlo simulations and the LUNGA method (1 simulation). The means and standard deviations are found for the 100 Monte Carlo simulations that are then compared to the LUNGA method. The number densities are observed to fit a normal distribution, which was seen in previous literature [7]. There is a probability of 95 percent that a random variable takes a value within two standard deviations of its mean with a normal distribution and that is observed in this research. The statistical analysis is done using a two-sample t-test with a two-sided 99 percent confidence interval. In the analysis, the null hypothesis is that the means are equal and the alternate hypothesis is that the means are not equal. The null hypothesis is accepted when the absolute value of the t-statistic is less than or equal to the critical point and rejected the rest of the time.

The two methods agree with 99 percent confidence for k_{inf} and the nuclide number densities when the neutron spectrum was dominated by both the fast and thermal energy

ranges. Table 24 to Table 29 present a summary of the statistical analysis conducted in this research. Table 24 and Table 25 show the results of the analysis for the standard deviation in the number densities and Table 28 displays the results of the analysis for the standard deviation in k_{inf} when the energy spectrum is dominated by the fast neutron spectrum. Table 26 and Table 27 specify the results of the analysis for the standard deviation in the number densities and Table 29 exhibits the results of the analysis for the standard deviation in k_{inf} when the energy spectrum is dominated by the thermal neutron spectrum.

Table 30 to Table 33 present the relative standard deviations in both the number densities and in the criticality constant for Example 3. Table 30 shows the relative standard deviation in the number densities and Table 32 displays the relative standard deviation in k_{inf} when the energy spectrum is dominated by the fast neutron spectrum. Table 31 expresses the relative standard deviation in the number densities and Table 33 shows the relative standard deviation in k_{inf} when the energy spectrum is dominated by the thermal neutron spectrum.

Differences between the two methods result from many different factors including: slight differences in the flux shape and cross sections, the limitation of LUNGA method, and rounding errors. The T5-DEPL sequence uses a predictor/corrector process that depletes the mixture to the midpoint of the cycle then does another transport calculation with these number densities to calculate the flux and to weight the cross sections, which are then used in the final depletion calculation. This difference yields slightly different flux shapes and one-group effective cross sections, which has an impact on the output number densities. It is illustrated in Table 22 and Table 23 that the LUNGA method does

not duplicate the SCALE results exactly. Precision in the data handling and the rounding of the data also affect the output number densities, and where and when data is rounded has been seen to affect the statistics of the number densities.

Table 24. Summary of statistical analysis of N_1 and N_2 with fast neutron spectrum for Example 3.

Statistical analysis for verification of the approximate method (base simulation) and 100 MC simulations for fast neutron spectrum							
	Time (days)	30	60	90	120	150	180
N_1	mean (100 simulations)	4.864E+23	4.786E+23	4.709E+23	4.633E+23	4.559E+23	4.485E+23
	mean (base simulation)	4.864E+23	4.786E+23	4.709E+23	4.633E+23	4.559E+23	4.485E+23
	pooled var	2.539E+37	7.111E+37	1.171E+38	1.701E+38	2.203E+38	2.848E+38
	t-stat	-2.120E-01	3.896E-02	-9.571E-03	-5.902E-02	1.625E-01	1.357E-01
	accept/reject	accept	accept	accept	accept	accept	accept
	99% CI (μ_{base}-μ_{100})	(-1.44E+19,1.226E+19)	(-2.198E+19,2.264E+19)	(-2.873E+19,2.853E+19)	(-3.527E+19,3.372E+19)	(-3.684E+19,4.169E+19)	(-4.234E+19,4.694E+19)
N_2	mean (100 simulations)	9.266E+24	9.257E+24	9.248E+24	9.239E+24	9.229E+24	9.220E+24
	mean (base simulation)	9.266E+24	9.257E+24	9.248E+24	9.239E+24	9.229E+24	9.220E+24
	pooled var	8.153E+36	1.560E+37	2.861E+37	3.532E+37	4.266E+37	5.296E+37
	t-stat	-3.069E-01	-1.536E+00	-1.449E+00	-1.267E+00	-1.230E+00	-5.438E-01
	accept/reject	accept	accept	accept	accept	accept	accept
	99% CI (μ_{base}-μ_{100})	(-8.434E+18,6.672E+18)	(-1.655E+19,4.35E+18)	(-2.194E+19,6.358E+18)	(-2.329E+19,8.154E+18)	(-2.535E+19,9.203E+18)	(-2.323E+19,1.527E+19)
	Time (days)	210	240	270	300	330	360
N_1	mean (100 simulations)	4.413E+23	4.342E+23	4.271E+23	4.202E+23	4.133E+23	4.066E+23
	mean (base simulation)	4.413E+23	4.342E+23	4.271E+23	4.202E+23	4.133E+23	4.066E+23
	pooled var	3.407E+38	3.709E+38	4.374E+38	5.408E+38	5.924E+38	6.640E+38
	t-stat	-2.600E-02	8.618E-02	-1.861E-01	3.390E-02	-3.206E-01	-2.721E-01
	accept/reject	accept	accept	accept	accept	accept	accept
	99% CI (μ_{base}-μ_{100})	(-4.931E+19,4.834E+19)	(-4.927E+19,5.261E+19)	(-5.924E+19,5.141E+19)	(-6.072E+19,6.231E+19)	(-7.222E+19,5.654E+19)	(-7.521E+19,6.112E+19)
N_2	mean (100 simulations)	9.211E+24	9.202E+24	9.193E+24	9.184E+24	9.175E+24	9.166E+24
	mean (base simulation)	9.211E+24	9.202E+24	9.193E+24	9.184E+24	9.175E+24	9.166E+24
	pooled var	6.907E+37	8.458E+37	9.786E+37	1.073E+38	1.172E+38	1.293E+38
	t-stat	-1.007E-01	-2.292E-01	-1.496E-01	-1.775E-01	-4.364E-01	-2.876E-01
	accept/reject	accept	accept	accept	accept	accept	accept
	99% CI (μ_{base}-μ_{100})	(-2.283E+19,2.114E+19)	(-2.644E+19,2.221E+19)	(-2.765E+19,2.468E+19)	(-2.925E+19,2.556E+19)	(-3.338E+19,2.389E+19)	(-3.337E+19,2.679E+19)

Table 25. Summary of statistical analysis of N_3 and N_4 with fast neutron spection for Example 3.

Statistical analysis for verification of the approximate method (base simulation) and 100 MC simulations for fast neutron spectrum							
	Time (days)	30	60	90	120	150	180
N_3	mean (100 simulations)	5.583E+21	1.173E+22	1.769E+22	2.349E+22	2.915E+22	3.466E+22
	mean (base simulation)	5.585E+21	1.173E+22	1.770E+22	2.350E+22	2.915E+22	3.467E+22
	pooled var	1.591E+37	4.179E+37	7.282E+37	1.017E+38	1.282E+38	1.635E+38
	t-stat	3.262E-01	7.012E-01	7.492E-01	6.671E-01	4.664E-01	1.455E-01
	accept/reject	accept	accept	accept	accept	accept	accept
	99% CI (μ_{base}-μ_{100})	(-9.242E+18,1.186E+19)	(-1.254E+19,2.165E+19)	(-1.615E+19,2.9E+19)	(-1.992E+19,3.344E+19)	(-2.464E+19,3.526E+19)	(-3.195E+19,3.569E+19)
N_4	mean (100 simulations)	2.100E+14	5.327E+14	9.284E+14	1.368E+15	1.830E+15	2.303E+15
	mean (base simulation)	2.100E+14	5.325E+14	9.284E+14	1.368E+15	1.830E+15	2.304E+15
	pooled var	2.104E+22	1.389E+23	3.479E+23	6.388E+23	9.253E+23	1.105E+24
	t-stat	1.847E-01	-4.240E-01	-1.091E-01	2.135E-01	6.702E-02	6.729E-01
	accept/reject	accept	accept	accept	accept	accept	accept
	99% CI (μ_{base}-μ_{100})	(-3.567E+11,4.106E+11)	(-1.144E+12,8.269E+11)	(-1.625E+12,1.496E+12)	(-1.943E+12,2.286E+12)	(-2.48E+12,2.609E+12)	(-2.069E+12,3.491E+12)
	Time (days)	210	240	270	300	330	360
N_3	mean (100 simulations)	4.005E+22	4.533E+22	5.048E+22	5.554E+22	6.048E+22	6.534E+22
	mean (base simulation)	4.006E+22	4.533E+22	5.049E+22	5.554E+22	6.049E+22	6.534E+22
	pooled var	2.107E+38	2.426E+38	2.920E+38	3.380E+38	3.608E+38	3.878E+38
	t-stat	3.652E-02	2.228E-02	1.603E-01	5.294E-02	3.921E-01	3.456E-01
	accept/reject	accept	accept	accept	accept	accept	accept
	99% CI (μ_{base}-μ_{100})	(-3.787E+19,3.893E+19)	(-4.085E+19,4.155E+19)	(-4.245E+19,4.796E+19)	(-4.765E+19,4.961E+19)	(-4.276E+19,5.773E+19)	(-4.525E+19,5.893E+19)
N_4	mean (100 simulations)	2.777E+15	3.246E+15	3.708E+15	4.160E+15	4.602E+15	5.032E+15
	mean (base simulation)	2.778E+15	3.247E+15	3.709E+15	4.161E+15	4.602E+15	5.033E+15
	pooled var	1.274E+24	1.566E+24	1.594E+24	2.267E+24	2.629E+24	2.876E+24
	t-stat	1.045E+00	4.383E-01	6.180E-01	2.531E-01	-5.928E-02	2.847E-01
	accept/reject	accept	accept	accept	accept	accept	accept
	99% CI (μ_{base}-μ_{100})	(-1.801E+12,4.171E+12)	(-2.759E+12,3.861E+12)	(-2.556E+12,4.124E+12)	(-3.6E+12,4.366E+12)	(-4.386E+12,4.192E+12)	(-4.001E+12,4.971E+12)

Table 26. Summary of statistical analysis of N_1 and N_2 with thermal neutron spectrum for Example 3.

Statistical analysis for verification of the approximate method (base simulation) and 100 MC simulations for thermal neutron spectrum							
	Time (days)	30	60	90	120	150	180
N_1	mean (100 simulations)	4.845E+23	4.747E+23	4.650E+23	4.555E+23	4.461E+23	4.368E+23
	mean (base simulation)	4.845E+23	4.747E+23	4.650E+23	4.555E+23	4.461E+23	4.368E+23
	pooled var	1.696E+36	2.700E+36	3.978E+36	4.485E+36	6.451E+36	8.787E+36
	t-stat	-9.026E-01	1.535E+00	1.805E+00	2.075E+00	1.750E+00	1.437E+00
	accept/reject	accept	accept	accept	accept	accept	accept
	99% CI (μ_{base}-μ_{100})	(-4.626E+18,2.264E+18)	(-1.812E+18,6.881E+18)	(-1.657E+18,8.894E+18)	(-1.186E+18,1.002E+19)	(-2.251E+18,1.119E+19)	(-3.562E+18,1.212E+19)
N_2	mean (100 simulations)	9.271E+24	9.267E+24	9.263E+24	9.259E+24	9.255E+24	9.251E+24
	mean (base simulation)	9.271E+24	9.267E+24	9.263E+24	9.259E+24	9.255E+24	9.251E+24
	pooled var	1.864E+37	4.750E+37	7.174E+37	9.799E+37	1.375E+38	1.756E+38
	t-stat	5.307E-03	-3.704E-01	-7.752E-01	-2.003E-01	-2.449E-01	-1.657E-01
	accept/reject	accept	accept	accept	accept	accept	accept
	99% CI (μ_{base}-μ_{100})	(-1.14E+19,1.144E+19)	(-2.08E+19,1.566E+19)	(-2.9E+19,1.581E+19)	(-2.818E+19,2.419E+19)	(-3.39E+19,2.813E+19)	(-3.726E+19,3.284E+19)
	Time (days)	210	240	270	300	330	360
N_1	mean (100 simulations)	4.276E+23	4.185E+23	4.095E+23	4.007E+23	3.919E+23	3.833E+23
	mean (base simulation)	4.276E+23	4.185E+23	4.096E+23	4.007E+23	3.919E+23	3.833E+23
	pooled var	1.100E+37	1.344E+37	1.400E+37	1.664E+37	1.966E+37	2.383E+37
	t-stat	1.190E+00	1.065E+00	2.957E-01	-1.291E-01	1.129E-01	3.432E-01
	accept/reject	accept	accept	accept	accept	accept	accept
	99% CI (μ_{base}-μ_{100})	(-4.806E+18,1.274E+19)	(-5.774E+18,1.362E+19)	(-8.785E+18,1.101E+19)	(-1.132E+19,1.026E+19)	(-1.123E+19,1.223E+19)	(-1.123E+19,1.46E+19)
N_2	mean (100 simulations)	9.247E+24	9.243E+24	9.238E+24	9.234E+24	9.230E+24	9.226E+24
	mean (base simulation)	9.247E+24	9.243E+24	9.238E+24	9.234E+24	9.230E+24	9.226E+24
	pooled var	2.078E+38	2.611E+38	3.264E+38	3.832E+38	4.163E+38	4.481E+38
	t-stat	2.948E-01	1.068E+00	1.239E+00	6.895E-01	5.949E-01	4.645E-01
	accept/reject	accept	accept	accept	accept	accept	accept
	99% CI (μ_{base}-μ_{100})	(-3.386E+19,4.24E+19)	(-2.541E+19,6.008E+19)	(-2.529E+19,7.029E+19)	(-3.822E+19,6.534E+19)	(-4.177E+19,6.617E+19)	(-4.611E+19,6.588E+19)

Table 27. Summary of statistical analysis of N_3 and N_4 with thermal neutron spectrum for Example 3.

Statistical analysis for verification of the approximate method (base simulation) and 100 MC simulations for thermal neutron spectrum							
	Time (days)	30	60	90	120	150	180
N_3	mean (100 simulations)	3.017E+21	6.306E+21	9.468E+21	1.251E+22	1.543E+22	1.823E+22
	mean (base simulation)	3.018E+21	6.307E+21	9.470E+21	1.251E+22	1.543E+22	1.823E+22
	pooled var	1.221E+37	3.295E+37	5.277E+37	6.953E+37	9.440E+37	1.165E+38
	t-stat	2.082E-01	7.981E-02	3.879E-01	-1.190E-01	-8.396E-02	-1.054E-01
	accept/reject	accept	accept	accept	accept	accept	accept
	99% CI (μ_{base}-μ_{100})	(-8.513E+18,9.976E+18)	(-1.472E+19,1.565E+19)	(-1.638E+19,2.205E+19)	(-2.305E+19,2.106E+19)	(-2.652E+19,2.488E+19)	(-2.969E+19,2.74E+19)
N_4	mean (100 simulations)	2.612E+14	6.332E+14	1.088E+15	1.601E+15	2.154E+15	2.732E+15
	mean (base simulation)	2.612E+14	6.331E+14	1.088E+15	1.601E+15	2.154E+15	2.732E+15
	pooled var	4.275E+21	5.924E+22	2.120E+23	4.737E+23	7.325E+23	1.124E+24
	t-stat	5.812E-01	-2.669E-01	-2.601E-01	1.930E-01	-6.516E-03	-9.641E-03
	accept/reject	accept	accept	accept	accept	accept	accept
	99% CI (μ_{base}-μ_{100})	(-1.348E+11,2.111E+11)	(-7.091E+11,5.785E+11)	(-1.338E+12,1.098E+12)	(-1.687E+12,1.954E+12)	(-2.269E+12,2.258E+12)	(-2.814E+12,2.794E+12)
	Time (days)	210	240	270	300	330	360
N_3	mean (100 simulations)	2.093E+22	2.351E+22	2.599E+22	2.838E+22	3.066E+22	3.285E+22
	mean (base simulation)	2.092E+22	2.350E+22	2.597E+22	2.837E+22	3.065E+22	3.284E+22
	pooled var	1.300E+38	1.589E+38	1.983E+38	2.285E+38	2.449E+38	2.526E+38
	t-stat	-5.318E-01	-1.335E+00	-1.432E+00	-7.905E-01	-6.572E-01	-5.606E-01
	accept/reject	accept	accept	accept	accept	accept	accept
	99% CI (μ_{base}-μ_{100})	(-3.626E+19,2.407E+19)	(-5.025E+19,1.643E+19)	(-5.751E+19,1.699E+19)	(-5.199E+19,2.797E+19)	(-5.173E+19,3.106E+19)	(-5.099E+19,3.308E+19)
N_4	mean (100 simulations)	3.324E+15	3.921E+15	4.517E+15	5.107E+15	5.687E+15	6.255E+15
	mean (base simulation)	3.324E+15	3.922E+15	4.517E+15	5.106E+15	5.685E+15	6.253E+15
	pooled var	1.625E+24	2.049E+24	2.523E+24	3.114E+24	3.978E+24	4.886E+24
	t-stat	2.312E-01	5.315E-01	7.899E-02	-9.359E-01	-9.656E-01	-9.960E-01
	accept/reject	accept	accept	accept	accept	accept	accept
	99% CI (μ_{base}-μ_{100})	(-3.076E+12,3.668E+12)	(-3.022E+12,4.551E+12)	(-4.076E+12,4.328E+12)	(-6.328E+12,3.008E+12)	(-7.211E+12,3.34E+12)	(-8.059E+12,3.634E+12)

Table 28. Summary of statistical analysis of the criticality constant of a fast reactor system in Example 3.

Statistical analysis for verification of the approximate method (base simulation) and 100 MC simulations for k_{eff} for fast neutron specturm						
Time (days)	30	60	90	120	150	180
mean (100 simulations)						
mean (base simulation)	1.292E+00	1.296E+00	1.300E+00	1.303E+00	1.307E+00	1.309E+00
pooled var	5.794E-07	6.305E-07	4.099E-07	6.727E-07	5.686E-07	5.158E-07
t-stat	-2.394E+00	-9.392E-01	-1.454E+00	-1.061E+00	-1.455E+00	-1.418E+00
accept/reject	accept	accept	accept	accept	accept	accept
99% CI (μ_{base}-μ_{100})	-3.845E-03,1.821E-04	-2.85E-03,1.351E-03	-2.629E-03,7.58E-04	-3.044E-03,1.295E-03	-3.097E-03,8.922E-04	-2.923E-03,8.762E-04
Time (days)	210	240	270	300	330	360
mean (100 simulations)						
mean (base simulation)	1.312E+00	1.314E+00	1.317E+00	1.319E+00	1.321E+00	1.322E+00
pooled var	5.733E-07	5.782E-07	5.227E-07	6.241E-07	4.990E-07	6.336E-07
t-stat	-1.543E+00	-1.496E+00	-1.577E+00	-1.586E+00	-1.695E+00	-1.548E+00
accept/reject	accept	accept	accept	accept	accept	accept
99% CI (μ_{base}-μ_{100})	-3.177E-03,8.285E-04	-3.155E-03,8.681E-04	-3.058E-03,7.669E-04	-3.349E-03,8.302E-04	-3.072E-03,6.653E-04	-3.344E-03,8.672E-04

Table 29. Summary of statistical analysis of the criticality constant of a thermal reactor system in Example 3.

Statistical analysis for verification of the approximate method (base simulation) and 100 MC simulations for k_{eff} for thermal neutron spectrum						
Time (days)	30	60	90	120	150	180
mean (100 simulations)	1.47697E+00	1.47577E+00	1.47434E+00	1.47320E+00	1.47170E+00	1.47023E+00
mean (base simulation)	1.477E+00	1.476E+00	1.474E+00	1.473E+00	1.471E+00	1.470E+00
pooled var	6.043E-07	6.580E-07	7.300E-07	9.010E-07	5.762E-07	7.754E-07
t-stat	-6.782E-02	-1.099E-01	-3.528E-01	2.291E-01	-3.575E-01	7.822E-02
accept/reject	accept	accept	accept	accept	accept	accept
99% CI (μ_{base}-μ_{100})	(-2.109E-03,2.003E-03)	(-2.235E-03,2.056E-03)	(-2.563E-03,1.957E-03)	(-2.292E-03,2.729E-03)	(-2.281E-03,1.735E-03)	(-2.26E-03,2.398E-03)
Time (days)	210	240	270	300	330	360
mean (100 simulations)	1.46887E+00	1.46743E+00	1.46577E+00	1.46422E+00	1.46281E+00	1.46113E+00
mean (base simulation)	1.469E+00	1.469E+00	1.466E+00	1.463E+00	1.463E+00	1.461E+00
pooled var	6.060E-07	7.934E-07	9.489E-07	6.545E-07	7.622E-07	7.389E-07
t-stat	5.725E-01	1.215E+00	2.882E-01	-1.227E+00	2.151E-02	4.810E-02
accept/reject	accept	accept	accept	accept	accept	accept
99% CI (μ_{base}-μ_{100})	(-1.611E-03,2.507E-03)	(-1.268E-03,3.444E-03)	(-2.295E-03,2.859E-03)	(-3.138E-03,1.142E-03)	(-2.29E-03,2.328E-03)	(-2.232E-03,2.315E-03)

Table 30. Relative sd(N) with fast neutron spectrum for Example 3.

Relative standard deviation of N for fast neutron specturm													
	Time (days)	30	60	90	120	150	180	210	240	270	300	330	360
N_1	100 simulations	1.036E-05	1.762E-05	2.298E-05	2.815E-05	3.256E-05	3.762E-05	4.183E-05	4.436E-05	4.897E-05	5.534E-05	5.888E-05	6.338E-05
	approximate method	1.065E-05	1.818E-05	2.076E-05	2.669E-05	2.875E-05	3.504E-05	3.861E-05	4.029E-05	4.198E-05	4.585E-05	6.712E-05	6.918E-05
N_2	100 simulations	3.082E-07	4.267E-07	5.784E-07	6.433E-07	7.076E-07	7.893E-07	9.023E-07	9.994E-07	1.076E-06	1.128E-06	1.180E-06	1.241E-06
	approximate method	2.091E-07	7.679E-07	8.446E-07	9.634E-07	1.045E-06	1.261E-06	1.474E-06	1.482E-06	1.480E-06	1.592E-06	1.602E-06	1.617E-06
N_3	100 simulations	7.143E-04	5.513E-04	4.823E-04	4.293E-04	3.884E-04	3.688E-04	3.624E-04	3.437E-04	3.385E-04	3.310E-04	3.140E-04	3.014E-04
	approximate method	6.888E-04	6.806E-04	4.959E-04	4.493E-04	3.849E-04	3.892E-04	3.792E-04	3.369E-04	3.031E-04	2.967E-04	3.371E-04	3.140E-04
N_4	100 simulations	6.907E-04	6.995E-04	6.353E-04	5.844E-04	5.256E-04	4.564E-04	4.065E-04	3.855E-04	3.405E-04	3.619E-04	3.523E-04	3.370E-04
	approximate method	8.886E-04	1.277E-03	7.184E-04	6.527E-04	5.605E-04	6.738E-04	7.029E-04	4.852E-04	3.671E-04	4.771E-04	3.593E-04	3.412E-04

Table 31. Relative sd(N) with thermal neutron spectrum for Example 3.

Relative standard deviation of N for thermal neutron spectrum													
	Time (days)	30	60	90	120	150	180	210	240	270	300	330	360
N_1	100 simulations	2.688E-06	3.461E-06	4.289E-06	4.650E-06	5.694E-06	6.787E-06	7.757E-06	8.760E-06	9.136E-06	1.018E-05	1.131E-05	1.274E-05
	approximate method	2.810E-06	8.484E-06	9.642E-06	1.105E-05	1.196E-05	1.298E-05	1.377E-05	1.517E-05	1.603E-05	1.845E-05	1.963E-05	2.053E-05
N_2	100 simulations	4.657E-07	7.437E-07	9.144E-07	1.069E-06	1.267E-06	1.432E-06	1.559E-06	1.748E-06	1.956E-06	2.120E-06	2.211E-06	2.295E-06
	approximate method	4.630E-07	9.499E-07	1.082E-06	1.182E-06	1.358E-06	1.523E-06	1.695E-06	1.933E-06	2.073E-06	2.196E-06	2.236E-06	2.275E-06
N_3	100 simulations	1.158E-03	9.103E-04	7.673E-04	6.667E-04	6.298E-04	5.919E-04	5.449E-04	5.360E-04	5.417E-04	5.327E-04	5.104E-04	4.838E-04
	approximate method	1.092E-03	1.036E-03	7.707E-04	6.260E-04	5.973E-04	5.589E-04	5.404E-04	5.492E-04	5.310E-04	5.022E-04	4.593E-04	4.251E-04
N_4	100 simulations	2.504E-04	3.844E-04	4.233E-04	4.299E-04	3.974E-04	3.880E-04	3.835E-04	3.651E-04	3.517E-04	3.455E-04	3.507E-04	3.534E-04
	approximate method	2.280E-04	3.909E-04	4.134E-04	4.176E-04	4.033E-04	3.862E-04	3.719E-04	3.701E-04	3.508E-04	3.439E-04	3.302E-04	3.264E-04

Table 32. Relative sd(k_{inf}) of a fast reactor system in Example 3.

Relative standard deviation of k_{eff} for fast neutron specturm												
Time (days)	30	60	90	120	150	180	210	240	270	300	330	360
100 simulations	5.883E-04	6.122E-04	4.921E-04	6.288E-04	5.766E-04	5.480E-04	5.766E-04	5.780E-04	5.486E-04	5.985E-04	5.344E-04	6.013E-04
approximate method	4.235E-04	4.041E-04	3.576E-04	3.816E-04	3.926E-04	3.640E-04	3.971E-04	3.539E-04	3.441E-04	3.969E-04	3.766E-04	3.604E-04

Table 33. Relative sd(k_{inf}) of a thermal reactor system Example 3.

Relative standard deviation of k_{eff} for thermal neutron spectrum												
Time (days)	30	60	90	120	150	180	210	240	270	300	330	360
100 simulations	5.263E-04	5.497E-04	5.795E-04	6.443E-04	5.158E-04	5.989E-04	5.300E-04	6.070E-04	6.646E-04	5.525E-04	5.968E-04	5.883E-04
approximate method	3.311E-04	3.178E-04	3.056E-04	3.297E-04	3.198E-04	3.202E-04	3.204E-04	3.344E-04	3.355E-04	3.361E-04	3.135E-04	3.236E-04

6.2 Verification of Example 3

Validation of Example 3 concludes with indirectly verifying results of Example 3 using the LUNGA method and comparing them with the results found in previous literature. Verification with previous literature is based on trends found in journal articles with the majority of the verification coming from the article by Shim [19].

Since there are limited amounts of data and results available in the Shim article, indirect verification means inspecting the trends of ^{235}U in Example 3 and comparing them to the trends in the article [19]. First the system in the Shim article is recreated with the information given, and KENO V.a is used to calculate fluxes. The derived equations from Example 3 using the LUNGA method are then used to propagate the uncertainties from the fluxes. The system in the Shim article is composed of UO_2 fuel with a ^{235}U weight percent of 4.95 [19]. Table 34 shows that the equations correctly predict the ^{235}U number density with less than a 1 percent difference between them.

Table 34. Comparison of ^{235}U number density between Shim article and derived equations from Example 3.

Comparison of U^{235} number density between Shim article and derived equations					
	Research by Shim			Derived equations (Example 3)	
Effective full power days	Number density of U^{235} (atoms/b*cm)	sd of U^{235} (atoms/b*cm)	relative sd of U^{235}	Number density of U^{235} (atoms/b*cm)	Percent difference (%)
0	1.131E-03			1.131E-03	
1	1.128E-03	3.042E-08	2.697E-05	1.128E-03	-2.8E-02
10	1.104E-03	3.171E-07	2.872E-04	1.104E-03	-3.6E-02
30	1.050E-03	7.599E-07	7.237E-04	1.052E-03	-2.4E-01
60	9.751E-04	1.349E-06	1.383E-03	9.778E-04	-2.8E-01
90	9.025E-04	1.774E-06	1.966E-03	9.064E-04	-4.3E-01
120	8.358E-04	2.059E-06	2.464E-03	8.380E-04	-2.6E-01

Next, it is shown that the calculated contributions to the standard deviation of ^{235}U using the equations in the LUNGA method for the Shim simulation follow the same trends presented in the Shim article [19]. Figure 58 presents the standard deviation of ^{235}U calculated with the LUNGA equations from Example 3, and Figure 59 exhibits the standard deviation of ^{235}U given in the Shim article [19]. Figure 58 and Figure 59 illustrate that the trends for the standard deviation of ^{235}U are the same. Figure 58 and Figure 59 also indicate that the behavior of the trends in the figures is also the same (even the time at which the contribution from the ^{235}U number density becomes greater than the contribution from the flux is the same – around 70 days) [19]. The magnitudes of the standard deviation in the ^{235}U number density will be different because the Shim article included uncertainty in the group cross sections and this research did not include any uncertainty in the group cross sections.

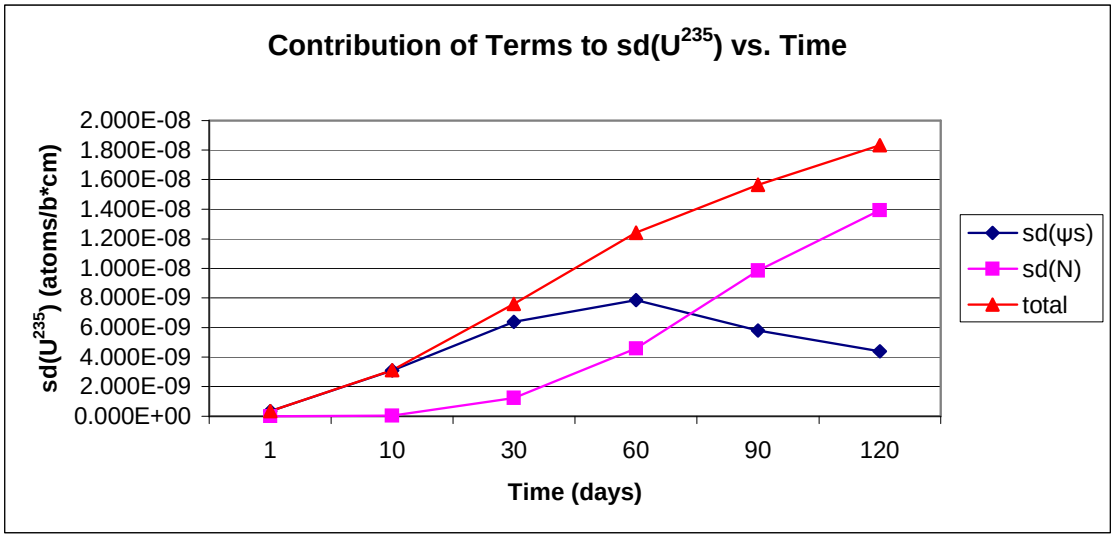

Figure 58. Contribution of terms in sd(^{235}U) calculated with LUNGA equations from Example 3 for the simulation in the Shim article.

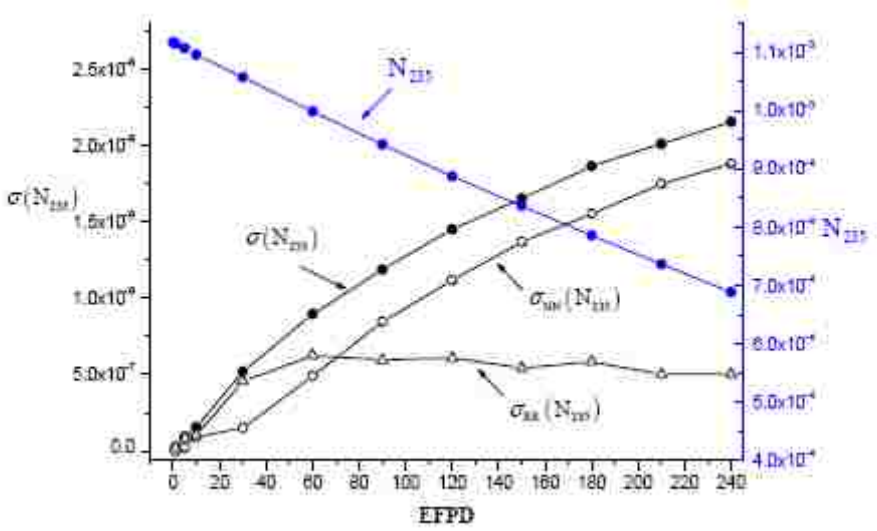

Figure 59. Contribution of terms in sd(^{235}U) from Shim article [19].

Finally, it is demonstrated that the trends of Example 3 also follow the trends shown in the Shim article. The trends of Example 3 are shown in Figure 60 and can be compared to the trends in Figure 59 from the article by Shim [19]. Since Example 3 is a system composed of UO_2 fuel like the Shim article, we expect the trends will resemble each other but not necessarily be the same since the two systems are different. Figure 60 indicates that the trends in the standard deviation of U^{235} are very similar to the trends illustrated in Figure 59. The contribution from the flux is the dominating term in the initial time steps, and then the contribution from the U^{235} number density becomes the dominating term in later time steps which is seen in the Shim article [19]. The contribution from the flux also flattens out as time goes on which was also seen in the Shim article, while the contribution from the U^{235} number density increases steadily with time [19].

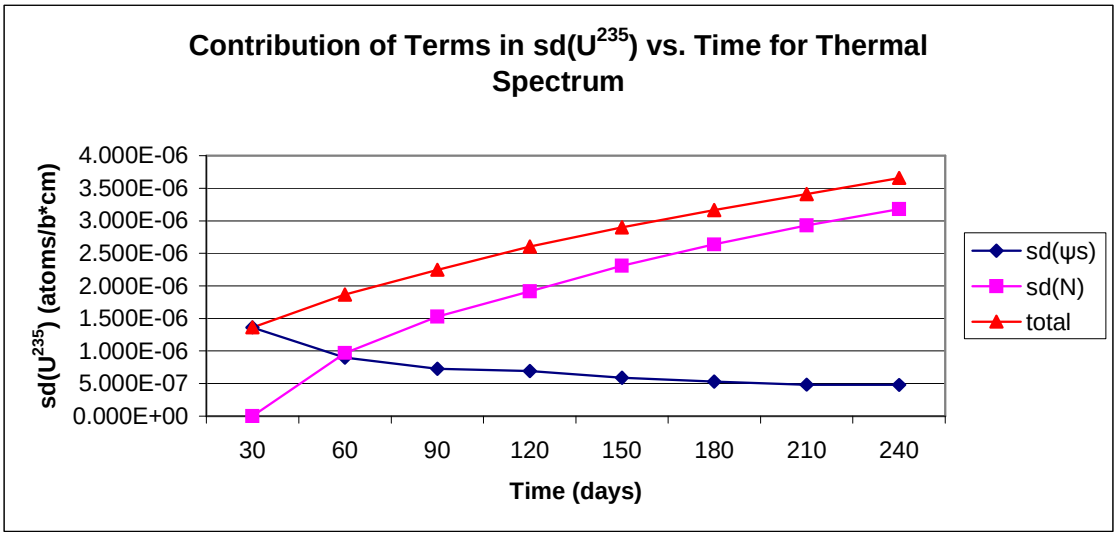

Figure 60. Contribution of terms in sd(^{235}U) for Example 3.

In the journal article by Tohjoh, the relative standard deviation of ^{235}U and ^{238}U increased with increasing values of the reactor burnup for a BWR fuel assembly [22]. In this research, the calculated relative standard deviation of ^{235}U and ^{238}U also increased with increasing values of reactor burnup for both the fast and thermal neutron systems.

In the article by Garcia-Herranz, the authors demonstrate that the calculated uncertainty in the nuclide concentrations from 1 Monte Carlo simulation is very similar to the calculated uncertainty in the nuclide concentrations from multiple Monte Carlo simulations, which is also seen in this research [7]. Table 30, Table 31, Table 39, and Table 40 show that the calculated uncertainty in the number densities from 1 Monte Carlo simulation is similar to the calculated uncertainty in the number densities from 100 Monte Carlo simulations.

6.3 Validation of Example 3 with Multiple Materials

The nuclide number densities of Example 3 with multiple materials using the derived equations are verified with the nuclide number densities from the Monte Carlo solution and the deterministic solution from SCALE. The percent difference between the derived equations and the SCALE solutions is given in Table 35. Like Example 3, there is some discrepancy in the number densities between the derived equations and SCALE; however, the difference is generally less than 1.0 percent.

Table 35. Percent difference of nuclide number densities between derived equations and SCALE for Example 3 with multiple materials.

Percent difference in number densities between SCALE solutions and derived equations						
Time (days)	30	60	90	120	150	180
SCALE with MC solution and derived equations						
material 1						
N_1 (U^{235})	-3.1E-02	-2.7E-02	-1.3E-01	-7.3E-02	-1.3E-01	-2.1E-01
N_2 (U^{238})	5.5E-03	2.2E-03	-1.9E-04	-1.8E-03	-2.8E-03	-3.1E-03
N_3 (Pu^{239})	7.9E-01	5.6E-01	5.1E-01	4.3E-01	3.5E-01	3.8E-01
N_4 (Eu^{155})	1.1E+00	8.3E-01	6.0E-01	5.8E-01	5.9E-01	4.9E-01
material 2						
N_1 (U^{235})	-9.5E-03	-1.8E-02	-3.1E-02	-5.6E-02	-7.4E-02	-1.1E-01
N_2 (U^{238})	1.2E-02	1.3E-02	1.4E-02	1.7E-02	2.0E-02	-1.9E-02
N_3 (Pu^{239})	4.1E-01	1.7E-01	1.5E-01	1.2E-01	8.1E-02	7.1E-02
N_4 (Eu^{155})	3.7E-01	5.4E-02	9.3E-02	1.1E-01	5.7E-02	5.0E-02
SCALE with deterministic solution and derived equations						
material 1						
N_1 (U^{235})	-3.1E-02	-1.1E-01	-2.2E-01	-2.6E-01	-3.8E-01	-4.7E-01
N_2 (U^{238})	5.5E-03	2.2E-03	-1.9E-04	-1.8E-03	-2.8E-03	-3.1E-03
N_3 (Pu^{239})	3.6E-01	1.1E-01	-3.0E-02	-1.7E-01	-2.4E-01	-2.7E-01
N_4 (Eu^{155})	1.9E+00	1.4E+00	1.1E+00	9.7E-01	8.3E-01	6.9E-01
material 2						
N_1 (U^{235})	4.7E-02	8.6E-02	1.1E-01	1.4E-01	1.7E-01	1.8E-01
N_2 (U^{238})	1.2E-02	1.3E-02	1.4E-02	1.7E-02	2.0E-02	2.4E-02
N_3 (Pu^{239})	-6.8E-01	-7.7E-01	-7.3E-01	-7.2E-01	-6.9E-01	-6.9E-01
N_4 (Eu^{155})	-1.1E+00	-1.4E+00	-1.2E+00	-1.1E+00	-1.0E+00	-9.1E-01

Validation continues with investigating the criticality constant (k_{inf}) of the system in Example 3 with multiple materials, which is calculated with both Monte Carlo and deterministic solutions from SCALE. Figure 61, which presents the criticality constant for Example 3 with multiple materials, shows that the derived equations can calculate the criticality of the system very accurately with generally less than a 0.10 percent difference in the criticality value.

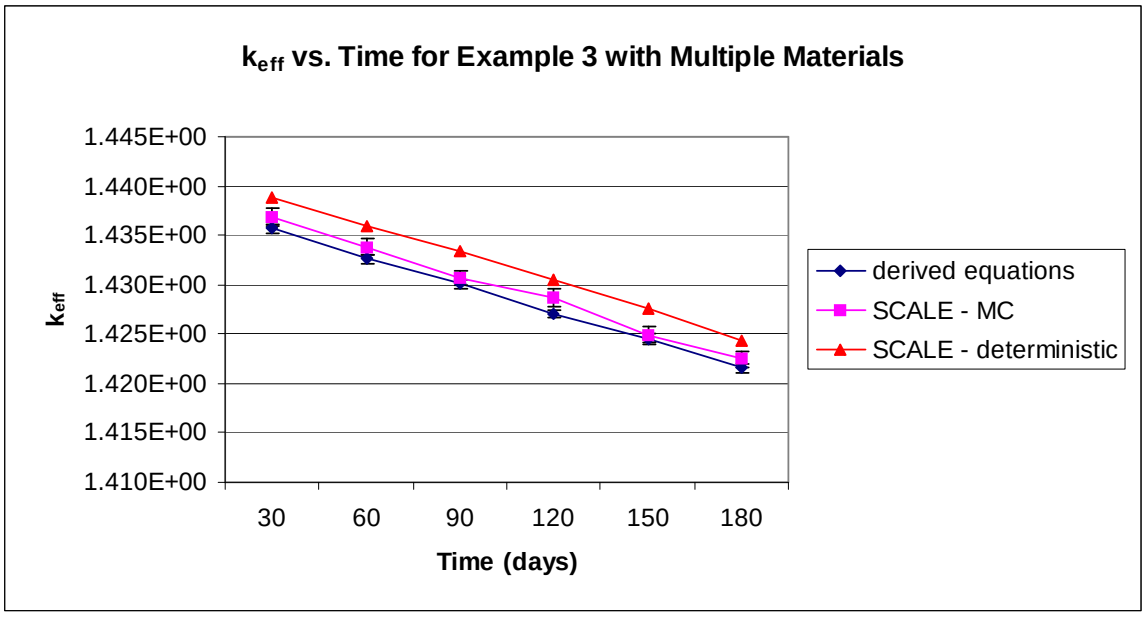

Figure 61. Criticality constant for Example 3 with multiple materials.

Validation of Example 3 with multiple materials concludes, as is done in Example 3, with a statistical analysis of 100 Monte Carlo simulations and the LUNGA method. The statistical analysis of Example 3 with multiple materials is the same as the analysis for Example 3. All of the parameters from the validation of Example 3 apply here; the only difference is that now Example 3 has multiple materials in the simulation consisting of two different fuel pins (multiple materials) with varying initial enrichments. Table 36 to

Table 38 present a summary of the statistical analysis of Example 3 with multiple materials conducted in this research. Table 36 and Table 37 show the results of the analysis for the standard deviation in the number densities for material 1 and material 2 respectively, and Table 38 displays the results of the analysis for the standard deviation in k_{inf}. The two methods, the LUNGA method and the analysis of 100 Monte Carlo simulations, agreed with 99 percent confidence for the number densities and k_{inf} as seen in Table 36 to Table 38.

Table 39 and Table 40 depict the relative standard deviations in the number densities for material 1 and material 2 for Example 3 with multiple materials for the LUNGA method and the 100 Monte Carlo simulations. Table 41 specifies the relative standard deviation in k_{inf} for Example 3 with multiple materials.

Table 36. Statistical analysis of nuclides in material 1 for Example 3 with multiple materials.

Statistical analysis for verification of the approximate method (base simulation) and 100 MC simulations for material 1 for thermal neutron spectrum							
	Time (days)	30	60	90	120	150	180
N_1	mean (100 simulations)	2.374E+23	2.278E+23	2.184E+23	2.093E+23	2.004E+23	1.917E+23
	mean (base simulation)	2.374E+23	2.278E+23	2.184E+23	2.093E+23	2.004E+23	1.917E+23
	pooled var	1.132E+38	2.301E+38	2.960E+38	3.981E+38	4.369E+38	5.169E+38
	t-stat	3.503E-01	4.562E-01	-7.783E-01	-9.259E-01	-1.010E+00	-1.209E+00
	accept/reject	accept	accept	accept	accept	accept	accept
	99% CI (μ_{base}-μ_{100})	(-2.44E+19,3.189E+19)	(-3.317E+19,4.708E+19)	(-5.897E+19,3.205E+19)	(-7.134E+19,3.421E+19)	(-7.65E+19,3.408E+19)	(-8.777E+19,3.251E+19)
N_2	mean (100 simulations)	4.634E+24	4.630E+24	4.626E+24	4.622E+24	4.618E+24	4.614E+24
	mean (base simulation)	4.634E+24	4.630E+24	4.626E+24	4.622E+24	4.618E+24	4.614E+24
	pooled var	2.979E+37	6.612E+37	9.099E+37	1.256E+38	1.689E+38	2.099E+38
	t-stat	1.303E+00	1.591E+00	1.248E+00	8.163E-01	9.302E-01	1.503E+00
	accept/reject	accept	accept	accept	accept	accept	accept
	99% CI (μ_{base}-μ_{100})	(-7.291E+18,2.158E+19)	(-8.506E+18,3.451E+19)	(-1.327E+19,3.72E+19)	(-2.045E+19,3.883E+19)	(-2.223E+19,4.653E+19)	(-1.644E+19,6.021E+19)
N_3	mean (100 simulations)	2.793E+21	5.730E+21	8.441E+21	1.094E+22	1.324E+22	1.535E+22
	mean (base simulation)	2.788E+21	5.721E+21	8.432E+21	1.093E+22	1.323E+22	1.533E+22
	pooled var	1.580E+37	3.903E+37	4.903E+37	6.292E+37	7.676E+37	9.332E+37
	t-stat	-1.229E+00	-1.435E+00	-1.238E+00	-8.095E-01	-1.032E+00	-1.779E+00
	accept/reject	accept	accept	accept	accept	accept	accept
	99% CI (μ_{base}-μ_{100})	(-1.543E+19,5.605E+18)	(-2.554E+19,7.514E+18)	(-2.723E+19,9.812E+18)	(-2.743E+19,1.453E+19)	(-3.226E+19,1.409E+19)	(-4.283E+19,8.278E+18)
N_4	mean (100 simulations)	2.964E+14	7.590E+14	1.306E+15	1.885E+15	2.465E+15	3.028E+15
	mean (base simulation)	2.961E+14	7.582E+14	1.306E+15	1.885E+15	2.465E+15	3.028E+15
	pooled var	1.415E+23	6.897E+23	1.424E+24	2.243E+24	2.533E+24	3.173E+24
	t-stat	-6.914E-01	-1.016E+00	-8.079E-02	-3.150E-01	-2.297E-01	9.977E-02
	accept/reject	accept	accept	accept	accept	accept	accept
	99% CI (μ_{base}-μ_{100})	(-1.257E+12,7.337E+11)	(-3.045E+12,1.349E+12)	(-3.253E+12,3.059E+12)	(-4.436E+12,3.488E+12)	(-4.577E+12,3.842E+12)	(-4.533E+12,4.89E+12)

Table 37. Statistical analysis of nuclides in material 2 for Example 3 with multiple materials.

Statistical analysis for verification of the approximate method (base simulation) and 100 MC simulations for material 2 for thermal neutron spectrum							
	Time (days)	30	60	90	120	150	180
N_1	mean (100 simulations)	1.412E+23	1.344E+23	1.278E+23	1.214E+23	1.153E+23	1.094E+23
	mean (base simulation)	1.412E+23	1.344E+23	1.278E+23	1.214E+23	1.153E+23	1.094E+23
	pooled var	1.034E+38	2.021E+38	2.684E+38	3.494E+38	3.700E+38	4.197E+38
	t-stat	-4.664E-01	-7.243E-01	3.868E-01	5.191E-01	6.122E-01	7.593E-01
	accept/reject	accept	accept	accept	accept	accept	accept
	99% CI (μ_{base}-μ_{100})	(-3.167E+19,2.214E+19)	(-4.795E+19,2.725E+19)	(-3.697E+19,4.971E+19)	(-3.969E+19,5.919E+19)	(-3.905E+19,6.272E+19)	(-3.856E+19,6.982E+19)
N_2	mean (100 simulations)	4.732E+24	4.727E+24	4.723E+24	4.719E+24	4.715E+24	4.711E+24
	mean (base simulation)	4.732E+24	4.727E+24	4.723E+24	4.719E+24	4.715E+24	4.711E+24
	pooled var	3.639E+37	6.931E+37	1.242E+38	1.578E+38	1.763E+38	2.245E+38
	t-stat	3.128E-01	7.824E-01	1.407E+00	1.538E+00	1.714E+00	1.609E+00
	accept/reject	accept	accept	accept	accept	accept	accept
	99% CI (μ_{base}-μ_{100})	(-1.406E+19,1.785E+19)	(-1.548E+19,2.857E+19)	(-1.372E+19,4.524E+19)	(-1.382E+19,5.265E+19)	(-1.225E+19,5.8E+19)	(-1.541E+19,6.385E+19)
N_3	mean (100 simulations)	2.941E+21	5.984E+21	8.743E+21	1.125E+22	1.351E+22	1.557E+22
	mean (base simulation)	2.940E+21	5.979E+21	8.734E+21	1.124E+22	1.350E+22	1.556E+22
	pooled var	1.893E+37	3.683E+37	6.101E+37	6.923E+37	7.118E+37	8.235E+37
	t-stat	-2.907E-01	-7.113E-01	-1.114E+00	-1.250E+00	-1.393E+00	-1.135E+00
	accept/reject	accept	accept	accept	accept	accept	accept
	99% CI (μ_{base}-μ_{100})	(-1.278E+19,1.024E+19)	(-2.039E+19,1.172E+19)	(-2.941E+19,1.192E+19)	(-3.246E+19,1.156E+19)	(-3.413E+19,1.05E+19)	(-3.435E+19,1.366E+19)
N_4	mean (100 simulations)	2.771E+14	7.730E+14	1.366E+15	1.984E+15	2.591E+15	3.167E+15
	mean (base simulation)	2.772E+14	7.733E+14	1.364E+15	1.981E+15	2.588E+15	3.163E+15
	pooled var	2.449E+23	1.177E+24	2.200E+24	3.663E+24	4.074E+24	4.174E+24
	t-stat	2.572E-01	2.688E-01	-1.210E+00	-1.219E+00	-1.281E+00	-1.590E+00
	accept/reject	accept	accept	accept	accept	accept	accept
	99% CI (μ_{base}-μ_{100})	(-1.181E+12,1.437E+12)	(-2.577E+12,3.163E+12)	(-5.726E+12,2.12E+12)	(-7.407E+12,2.718E+12)	(-7.938E+12,2.74E+12)	(-8.668E+12,2.141E+12)

Table 38. Statistical analysis of criticality constant for Example 3 with multiple materials.

Statistical analysis for verification of the approximate method (base simulation) and 100 MC simulations for k_{eff} of Example 3 with multiple materials						
Time (days)	30	60	90	120	150	180
mean (100 simulations)						
mean (base simulation)	1.436E+00	1.433E+00	1.430E+00	1.427E+00	1.425E+00	1.422E+00
pooled var	8.195E-07	7.804E-07	4.797E-07	6.023E-07	6.891E-07	6.844E-07
t-stat	-4.080E-01	-4.962E-01	-7.724E-01	-9.649E-01	-4.857E-01	-2.091E-01
accept/reject	accept	accept	accept	accept	accept	accept
99% CI (μ_{base}-μ_{100})	-2.766E-03,2.023E-03	-2.777E-03,1.896E-03	-2.37E-03,1.294E-03	-2.805E-03,1.3E-03	-2.601E-03,1.791E-03	-2.362E-03,2.014E-03

Table 39. Relative sd(N) in material 1 for Example 3 with multiple materials.

Relative standard deviation of N for material 1 for thermal neutron spectrum							
	Time (days)	30	60	90	120	150	180
N_1	100 simulations	4.482E-05	6.660E-05	7.877E-05	9.532E-05	1.043E-04	1.186E-04
	approximate method	7.916E-05	1.147E-04	1.423E-04	1.650E-04	1.869E-04	2.064E-04
N_2	100 simulations	1.178E-06	1.756E-06	2.062E-06	2.424E-06	2.814E-06	3.140E-06
	approximate method	2.006E-06	2.877E-06	3.518E-06	4.059E-06	4.567E-06	5.014E-06
N_3	100 simulations	1.424E-03	1.090E-03	8.296E-04	7.252E-04	6.618E-04	6.293E-04
	approximate method	2.382E-03	1.547E-03	1.194E-03	9.890E-04	8.574E-04	7.574E-04
N_4	100 simulations	1.269E-03	1.094E-03	9.135E-04	7.944E-04	6.456E-04	5.883E-04
	approximate method	2.457E-03	1.849E-03	1.479E-03	1.215E-03	1.032E-03	8.875E-04

Table 40. Relative sd(N) in material 2 for Example 3 with multiple materials.

Relative standard deviation of N for material 2 for thermal neutron spectrum							
	Time (days)	30	60	90	120	150	180
N_1	100 simulations	7.202E-05	1.058E-04	1.282E-04	1.539E-04	1.668E-04	1.873E-04
	approximate method	1.207E-04	1.707E-04	2.107E-04	2.443E-04	2.769E-04	3.065E-04
N_2	100 simulations	1.275E-06	1.761E-06	2.360E-06	2.662E-06	2.816E-06	3.180E-06
	approximate method	2.313E-06	3.269E-06	4.018E-06	4.637E-06	5.226E-06	5.747E-06
N_3	100 simulations	1.479E-03	1.014E-03	8.934E-04	7.399E-04	6.243E-04	5.830E-04
	approximate method	2.640E-03	1.674E-03	1.285E-03	1.054E-03	9.037E-04	7.876E-04
N_4	100 simulations	1.786E-03	1.404E-03	1.086E-03	9.648E-04	7.792E-04	6.452E-04
	approximate method	3.330E-03	2.333E-03	1.794E-03	1.436E-03	1.194E-03	1.009E-03

Table 41. Relative sd(k_{inf}) for Example 3 with multiple materials.

Relative standard deviation of k_{eff} of Example 3 with multiple materials						
Time (days)	30	60	90	120	150	180
100 simulations	6.304E-04	6.164E-04	4.841E-04	5.435E-04	5.826E-04	5.819E-04
approximate method	3.174E-04	3.203E-04	3.109E-04	3.080E-04	3.126E-04	3.034E-04

CHAPTER 7

SUMMARY AND CONCLUSIONS

This research derives a formula that calculates the standard deviation in the nuclide number densities based on propagating the statistical uncertainty introduced when using the Monte Carlo method to solve the neutron transport equations in coupled Monte Carlo depletion computer codes. The formula derived calculates the standard deviation in the nuclide number densities with the aid of the LUNGA method, which is also derived in this research.

The variance in the flux shape (ψ) is composed of two terms, the statistical component (ψ_S – from the Monte Carlo simulation) and the nuclide component (ψ_N – from the changes in the number densities). In order to exactly solve for the ψ_N term, the change in the flux shape must be found for a change in each nuclide in the system, which means calculating the derivatives of the flux shape with respect to each nuclide in the system. A method that could reduce the number of Monte Carlo simulations needed to describe the ψ_N term would help save time and computing resources. This resulted in the development of the LUNGA method to approximate the variance in the ψ_N term.

The LUNGA method developed in this research approximated the variance of the ψ_N term in a way that drastically decreases the computing time and resources needed to perform the simulations needed to calculate the standard deviation in the nuclide number densities. Use of the LUNGA method, allows users to find the standard deviation in the nuclide number densities by performing only one additional simulation per area of interest instead of one additional simulation for every nuclide (forward difference

method) or two additional simulations for every nuclide (central difference method), which would be needed for the exact method. As an example, when the system of interest contains 1,000 nuclides using the exact method, users would have to run the 1,000 base simulations plus 1,000 simulations to find the derivatives of each nuclide for the $\Delta\psi_N$ term for a total of 2,000 simulations. Using the LUNGA method users would run the same 1,000 base simulations in addition to 1 simulation to find the approximate variance of the ψ_N term for a total of 1,001 simulations, which effectively reduces the number of Monte Carlo simulations by half.

The example problems (Example 2 and Example 3) used in this research demonstrate that the LUNGA method is valid for computing the standard deviation in the nuclide number densities and k_{inf}. The LUNGA method exhibits a percent difference of less than 1 percent compared to the exact method in calculating the standard deviation in the nuclide number densities and k_{inf}.

The LUNGA method is not as capable at calculating the variance of the ψ_N term as wanted, which was seen as a problem until further investigation of the ψ_N term revealed that its contribution to the standard deviation in the number densities was small compared to other terms in the equations for the standard deviation in the number densities. Example 2 illustrates that the LUNGA method agreed very well with the exact method in calculating the variance of the ψ_N term with generally only a 2 percent difference between the two methods. Example 3 on the other hand, demonstrates that the LUNGA method did not agree well with the exact method in calculating the variance of the ψ_N term with around 100 percent difference in the two methods for most of the time steps. However, both Example 2 and Example 3 indicate that the contribution from the ψ_N term

to the variance in the number densities is minute compared to the contribution from the ψ_S term and the variance and covariances of the number densities themselves. Further investigation of the ψ_N term revealed that its contribution to the variance of the number densities was anywhere from 3 to 7 orders of magnitude less than the contribution from the ψ_S term or the variance and covariance of the number densities. Therefore, the ψ_N term is not as significant a contributor to the variance in the number densities as the ψ_S term or the variance and covariances of the number densities themselves.

The LUNGA method and the statistics of 100 Monte Carlo simulations agree with 99 percent confidence in calculating the standard deviation in the nuclide number densities and k_{inf} with neutron energies in both the fast and the thermal energy spectrums using the examples problems (Example 3 and Example 3 with multiple materials) in this research. The trends of the standard deviation in the number densities for Example 3 also match the trends published in previous literature, which provided an indirect verification of the LUNGA method.

Monte Carlo methods are a powerful and proven tool for the nuclear engineering community. Coupled Monte Carlo depletion methods add the power of the Monte Carlo method with a depletion code. Monte Carlo methods are based on probabilities and therefore have stochastic uncertainties and propagated uncertainties in the results of a Monte Carlo depletion calculation. However, these propagated uncertainties are not reported to the user. The LUNGA method and the methodology described in this research provides users a way to calculate the standard deviation in the nuclide number densities and k_{inf} based on the statistical uncertainty, introduce by using the Monte Carlo method, and the propagation of the statistical uncertainty in coupled Monte Carlo

depletion calculations. The knowledge of the standard deviation in the nuclide number densities and k_{inf} will give users more confidence in the results from using coupled Monte Carlo depletion calculations and will also give users the ability to use this method in addition to deterministic depletion methods.

CHAPTER 8

FUTURE RECOMMENDATIONS

The LUNGA method can calculate the variance of the ψ_N term. However, since the LUNGA method was generally around 100 percent different from the exact method in calculating the variance of the ψ_N term, the first recommendation for this research would be to investigate if there is an approach that would provide better agreement between the LUNGA method and the exact method when calculating the variance of the ψ_N term. This could possibly be done by grouping certain nuclides together and finding the derivates of the flux shape with respect to all nuclides in a given group, instead of all nuclides at once (LUNGA method presented in this research) or all individual nuclides (exact method). Grouping some nuclides together is plausible because some of the derivates have the potential to go to zero, which is touched on in this research. This requires finding the derivates of the flux shape with respect to a group of nuclides, but since some nuclides are grouped together, as in the LUNGA method, it could drastically reduce the number of required simulations compared to the exact method. This could provide better accuracy for the ψ_N term than with the LUNGA method.

The next recommendation for this research would be to expand the system of multiple materials to a larger lattice of fuel pins, which would more correctly represent a real reactor core. This system would need to be tested to make sure the LUNGA method is still capable of calculating the standard deviations of the number densities and k_{inf}. The research done in this paper has been with an infinite lattice of a single pin type (Example 3), and with two fuel pins with different enrichments (Example 3 with multiple

materials). The equations derived in this research for Example 3 with multiple materials should be valid for any number of different fuel pins; the difference is that the power normalization would have to be calculated for each pin type, which would then be used to normalize the flux shape for each pin type.

Another recommendation for this research would be to program the equations in FORTRAN so that the LUNGA method could be used with the SCALE computer code. This would allow for the LUNGA method to be tested with a complete problem domain, and then the results could possibly be compared to the results from computer codes developed in other countries.

The final improvement to this research would be to investigate using the method coupled with a segmented fuel pin in the axial direction. This could possibly create a mapping of the variance in the nuclide number densities in the system. The equations derived in this work would serve as a starting point, but would need to be modified to take into account the segmentation of the fuel pin.

APPENDIX 1

LIST OF ABBREVIATIONS

BWR	Boiling Water Reactor
COV	Covariance
DOE	Department of Energy
GNEP	Global Nuclear Energy Partnership
GWd/MTU	Gigawatt-days/Metric Ton Uranium
HTGR	High Temperature Gas-cooled Reactor
k_{inf}	Infinite Medium Multiplication Factor
LANL	Los Alamos National Laboratory
LUNGA	Linear Uncertainty Nuclide Group Approximation
LWR	Light Water Reactor
MC	Monte Carlo
MCNP	Monte Carlo N-Particle
MCNPX	Monte Carlo N-Particle eXtended
ORIGEN-S	Oak Ridge Isotope GENeration
ORNL	Oak Ridge National Laboratory
PWR	Pressurized Water Reactor
SCALE	Standardized Computer Analyses for Licensing Evaluations
SD	Standard Deviation
VAR	Variance

APPENDIX 2

LIST OF SYMBOLS AND NOTATION

ψ	flux shape
ψ_S	statistical uncertainty in the flux shape
ψ_N	number density uncertainty in the flux shape; the uncertainty in the flux shape due to a change in the number densities
ψ_{Ng}	number density uncertainty in the flux shape in energy group g
Φ	neutron flux
σ	cross section
σ_{kx}	effective one-group cross sections as in the SCALE manual where x is the type of cross section for nuclide k
σ_x^k	effective one-group cross sections where x is the type of cross section for nuclide k
σ_{xj}^k	group cross sections where x is the type of cross section for nuclide k and group j
N_{i0}	initial number density of nuclide i
N_i	number density of nuclide i
ΔX	a change in the variable X
$E[(\Delta X)^2]$	expectation of $(\Delta X)^2$ where E is the expectation operator
sd(X)	standard deviation of variable X
cov(X,X')	covariance between X and X'
var(X)	variance of variable X

APPENDIX 3

EXPANDED EQUATIONS FOR ΔN FOR EXAMPLE 2

Shown here are the expanded equations for a change in the number densities for Example 2. The variance of the number densities is found by taking the expected value of the square of the change in the number densities; e.g. $\mathrm{var}(N_1) = E\left[(\Delta N_1)^2\right]$ and $\mathrm{var}(N_2) = E\left[(\Delta N_2)^2\right]$.

$$\Delta N_1 = \frac{e^{-\Phi \cdot t \cdot (\psi_1 \cdot \sigma_{1a1} + \psi_2 \cdot \sigma_{1a2})} \cdot \left(\psi_2 + \Phi \cdot t \cdot \psi_2^{\,2} \cdot \sigma_{1a2} + \Phi \cdot t \cdot \psi_1 \cdot \psi_2 \cdot \sigma_{1a1}\right)}{\psi_2} \cdot \Delta N_{10}$$

$$+ \left[-N_{10} \cdot \Phi \cdot t \cdot \sigma_{1a1} \cdot e^{-\Phi \cdot t \cdot (\psi_1 \cdot \sigma_{1a1} + \psi_2 \cdot \sigma_{1a2})}\right] \cdot \Delta\psi_1$$

$$+ \frac{N_{10} \cdot \Phi \cdot t \cdot \psi_1 \cdot \sigma_{1a1} \cdot e^{-\Phi \cdot t \cdot (\psi_1 \cdot \sigma_{1a1} + \psi_2 \cdot \sigma_{1a2})}}{\psi_2} \cdot \Delta\psi_2$$

$$\Delta N_2 = n2n_1 \cdot \Delta N_{20} + n2n_2 \cdot \Delta N_{10} + n2n_3 \cdot \Delta\psi_1 + n2n_4 \cdot \Delta\Phi + n2n_5 \cdot \Delta\psi_2$$

where

$$n2n_1 = e^{-t\cdot\left(\Lambda+\Phi\cdot\psi_2\cdot\sigma_{2c2}\right)}$$

$$n2n_2 = \frac{\gamma\cdot\Phi\cdot\psi_2\cdot\sigma_{1f2}\cdot\left[e^{-\Phi\cdot t\cdot\left(\psi_1\cdot\sigma_{1a1}+\psi_2\cdot\sigma_{1a2}\right)} - e^{-t\cdot\left(\Lambda+\Phi\cdot\psi_2\cdot\sigma_{2c2}\right)}\right]}{\Lambda - \Phi\cdot\left(\psi_1\cdot\sigma_{1a1} + \psi_2\cdot\sigma_{1a2}\right) + \Phi\cdot\psi_2\cdot\sigma_{2c2}}$$

$$n2n_3 = \frac{\gamma\cdot N_{10}\cdot\Phi^2\cdot\psi_2\cdot\sigma_{1a1}\cdot\sigma_{1f2}\cdot\left[e^{-\Phi\cdot t\cdot\left(\psi_1\cdot\sigma_{1a1}+\psi_2\cdot\sigma_{1a2}\right)} - e^{-t\cdot\left(\Lambda+\Phi\cdot\psi_2\cdot\sigma_{2c2}\right)}\right]}{\left[\Lambda - \Phi\cdot\left(\psi_1\cdot\sigma_{1a1} + \psi_2\cdot\sigma_{1a2}\right) + \Phi\cdot\psi_2\cdot\sigma_{2c2}\right]^2}$$

$$- \frac{\gamma\cdot N_{10}\cdot\Phi^2\cdot t\cdot\psi_2\cdot\sigma_{1a1}\cdot\sigma_{1f2}\cdot e^{-\Phi\cdot t\cdot\left(\psi_1\cdot\sigma_{1a1}+\psi_2\cdot\sigma_{1a2}\right)}}{\Lambda - \Phi\cdot\left(\psi_1\cdot\sigma_{1a1} + \psi_2\cdot\sigma_{1a2}\right) + \Phi\cdot\psi_2\cdot\sigma_{2c2}}$$

$$n2n_4 = \frac{\gamma \cdot N_{10} \cdot \psi_2 \cdot \sigma_{1f2} \cdot \left[e^{-\Phi \cdot t \cdot \left(\psi_1 \cdot \sigma_{1a1} + \psi_2 \cdot \sigma_{1a2} \right)} - e^{-t \cdot \left(\Lambda + \Phi \cdot \psi_2 \cdot \sigma_{2c2} \right)} \right]}{\Lambda - \Phi \cdot \left(\psi_1 \cdot \sigma_{1a1} + \psi_2 \cdot \sigma_{1a2} \right) + \Phi \cdot \psi_2 \cdot \sigma_{2c2}}$$

$$- N_{20} \cdot t \cdot \psi_2 \cdot \sigma_{2c2} \cdot e^{-t \cdot \left(\Lambda + \Phi \cdot \psi_2 \cdot \sigma_{2c2} \right)}$$

$$- \frac{\gamma \cdot N_{10} \cdot \Phi \cdot \psi_2 \cdot \sigma_{1f2} \cdot \left[t \cdot e^{-\Phi \cdot t \cdot \left(\psi_1 \cdot \sigma_{1a1} + \psi_2 \cdot \sigma_{1a2} \right)} \cdot \left(\psi_1 \cdot \sigma_{1a1} + \psi_2 \cdot \sigma_{1a2} \right) - t \cdot \psi_2 \cdot \sigma_{2c2} \cdot e^{-t \cdot \left(\Lambda + \Phi \cdot \psi_2 \cdot \sigma_{2c2} \right)} \right]}{\Lambda - \Phi \cdot \left(\psi_1 \cdot \sigma_{1a1} + \psi_2 \cdot \sigma_{1a2} \right) + \Phi \cdot \psi_2 \cdot \sigma_{2c2}}$$

$$+ \frac{\gamma \cdot N_{10} \cdot \Phi \cdot \psi_2 \cdot \sigma_{1f2} \cdot \left[e^{-\Phi \cdot t \cdot \left(\psi_1 \cdot \sigma_{1a1} + \psi_2 \cdot \sigma_{1a2} \right)} - e^{-t \cdot \left(\Lambda + \Phi \cdot \psi_2 \cdot \sigma_{2c2} \right)} \right] \cdot \left(\psi_1 \cdot \sigma_{1a1} + \psi_2 \cdot \sigma_{1a2} - \psi_2 \cdot \sigma_{2c2} \right)}{\left[\Lambda - \Phi \cdot \left(\psi_1 \cdot \sigma_{1a1} + \psi_2 \cdot \sigma_{1a2} \right) + \Phi \cdot \psi_2 \cdot \sigma_{2c2} \right]^2}$$

$$n2n_5 = \frac{\gamma \cdot N_{10} \cdot \Phi \cdot \sigma_{1f2} \cdot \left[e^{-\Phi \cdot t \cdot \left(\psi_1 \cdot \sigma_{1a1} + \psi_2 \cdot \sigma_{1a2} \right)} - e^{-t \cdot \left(\Lambda + \Phi \cdot \psi_2 \cdot \sigma_{2c2} \right)} \right]}{\Lambda - \Phi \cdot \left(\psi_1 \cdot \sigma_{1a1} + \psi_2 \cdot \sigma_{1a2} \right) + \Phi \cdot \psi_2 \cdot \sigma_{2c2}} - N_{20} \cdot \Phi \cdot t \cdot \sigma_{2c2} \cdot e^{-t \cdot \left(\Lambda + \Phi \cdot \psi_2 \cdot \sigma_{2c2} \right)}$$

$$- \frac{\gamma \cdot N_{10} \cdot \Phi \cdot \psi_2 \cdot \sigma_{1f2} \cdot \left[\Phi \cdot t \cdot \sigma_{1a2} \cdot e^{-\Phi \cdot t \cdot \left(\psi_1 \cdot \sigma_{1a1} + \psi_2 \cdot \sigma_{1a2} \right)} - \Phi \cdot t \cdot \sigma_{2c2} \cdot e^{-t \cdot \left(\Lambda + \Phi \cdot \psi_2 \cdot \sigma_{2c2} \right)} \right]}{\Lambda - \Phi \cdot \left(\psi_1 \cdot \sigma_{1a1} + \psi_2 \cdot \sigma_{1a2} \right) + \Phi \cdot \psi_2 \cdot \sigma_{2c2}}$$

$$+ \frac{\gamma \cdot N_{10} \cdot \Phi \cdot \psi_2 \cdot \sigma_{1f2} \cdot \left[e^{-\Phi \cdot t \cdot \left(\psi_1 \cdot \sigma_{1a1} + \psi_2 \cdot \sigma_{1a2} \right)} - e^{-t \cdot \left(\Lambda + \Phi \cdot \psi_2 \cdot \sigma_{2c2} \right)} \right] \cdot \left(\Phi \cdot \sigma_{1a2} - \Phi \cdot \sigma_{2c2} \right)}{\left[\Lambda - \Phi \cdot \left(\psi_1 \cdot \sigma_{1a1} + \psi_2 \cdot \sigma_{1a2} \right) + \Phi \cdot \psi_2 \cdot \sigma_{2c2} \right]^2}$$

APPENDIX 4

DETAILED EQUATIONS FOR FIRST ORDER PERTURBATION THEORY FOR EXAMPLE 1 AND EXAMPLE 2

The following equations are used to investigate the acceptability of using first order perturbation theory in determining the variance of the number densities by perturbing only the number densities; therefore, the following equations only include a change in the number density values.

Equations for Example 1

A change in the flux comes from a change in the flux normalization equation as follows:

$$\Phi = \frac{P}{N_0 \sigma_f} \Rightarrow P = \psi_0 N_0 \Phi \sigma_f$$

$$\Delta P = 0 = \frac{\partial P}{\partial \psi_0}\Delta\psi_0 + \frac{\partial P}{\partial N_0}\Delta N_0 + \frac{\partial P}{\partial \Phi}\Delta\Phi + \frac{\partial P}{\partial \sigma_f}\Delta\sigma_f$$

$$\Rightarrow \Delta\Phi = -\frac{\Phi}{N_0}\Delta N_0$$

where $\frac{\partial P}{\partial \sigma_f}\Delta\sigma_f$ is equal to zero because this research did not take into account uncertainty in the cross section values themselves and $\frac{\partial P}{\partial \psi_0}\Delta\psi_0$ equals zero because in investigating the use of first order perturbation theory we are only interested in a change in the number density. Transmutation is done under a constant power restraint; therefore, there is no change in the power during a time step ($\Delta P = 0$). The equation for the change in the nuclide number density is given by the following:

$$\Delta N = \frac{\partial N}{\partial N_0}\Delta N_0 + \frac{\partial N}{\partial \Phi}\Delta\Phi = \frac{\partial N}{\partial N_0}\Delta N_0 + \frac{\partial N}{\partial \Phi}\left(-\frac{\Phi}{N_0}\Delta N_0\right) = \left[e^{-\sigma_a \Phi t_f} + \sigma_a \Phi t_f e^{-\sigma_a \Phi t_f}\right]\Delta N_0$$

The variance of the nuclide is given by

$$\mathrm{var}(N) = E[(\Delta N)^2] = \left[e^{-\sigma_a \Phi t_f} + \sigma_a \Phi t_f e^{-\sigma_a \Phi t_f}\right]^2 \mathrm{var}(N_0).$$

Equations for Example 2

A change in the flux comes from a change in the flux normalization equation as follows:

$$\Phi = \frac{P}{N_{10}\sigma_{f2}^1 \psi_2} \Rightarrow P = N_{10}\sigma_{f2}^1 \psi_2 \Phi$$

$$\Delta P = 0 = \frac{\partial P}{\partial \psi_2}\Delta\psi_2 + \frac{\partial P}{\partial N_{10}}\Delta N_{10} + \frac{\partial P}{\partial \Phi}\Delta\Phi + \frac{\partial P}{\partial \sigma_{f2}^1}\Delta\sigma_{f2}^1$$

$$\Rightarrow \Delta\Phi = -\frac{\Phi}{N_{10}}\Delta N_{10}$$

where $\frac{\partial P}{\partial \sigma_{f2}^1}\Delta\sigma_{f2}^1$ equals zero because this research did not take into account uncertainty in the cross section values themselves and $\frac{\partial P}{\partial \psi_2}\Delta\psi_2$ equals zero because in investigating the use of first order perturbation theory we are only interested in a change in the number density. There is no uncertainty in the group cross sections; however, uncertainty in the effective cross sections comes from the uncertainty in the flux when the group cross sections are collapsed to the effective group cross sections.

The equation for the change in the nuclide number density is given by the following:

$$\Delta N_1 = \frac{\partial N_1}{\partial N_{10}}\Delta N_{10} + \frac{\partial N_1}{\partial \Phi}\Delta\Phi = \frac{\partial N_1}{\partial N_{10}}\Delta N_{10} + \frac{\partial N_1}{\partial \Phi}\left(-\frac{\Phi}{N_{10}}\Delta N_{10}\right)$$

$$\Delta N_2 = \frac{\partial N_2}{\partial N_{20}}\Delta N_{20} + \frac{\partial N_2}{\partial N_{10}}\Delta N_{10} + \frac{\partial N_2}{\partial \Phi}\Delta\Phi = \frac{\partial N_2}{\partial N_{20}}\Delta N_{20} + \frac{\partial N_2}{\partial N_{10}}\Delta N_{10} + \frac{\partial N_2}{\partial \Phi}\left(-\frac{\Phi}{N_{10}}\Delta N_{10}\right)$$

After taking the derivatives, rearranging terms, and simplifying, the equations for a change in the nuclide number density become:

$$\Delta N_1(t) = \left\{e^{-\zeta} + N_1(0)e^{-\zeta}\left[\frac{\sigma_{a1}^1\sigma_{a2}^1 Pt}{\sigma_{s1-2}^1 N_1^2\sigma_{f2}^1} + \frac{2\sigma_{a1}^1\sigma_{c2}^2 PtN_2}{\sigma_{s1-2}^1\sigma_{f2}^1 N_1^3} + \frac{\sigma_{a2}^1 Pt}{\sigma_{f2}^1 N_1^2}\right]\right\}\Delta N_1(0)$$
$$-\left\{N_1(0)e^{-\zeta}\left(\frac{\sigma_{a1}^1\sigma_{c2}^1 Pt}{\sigma_{s1-2}^1\sigma_{f2}^1 N_1^2}\right)\right\}\Delta N_2(0)$$

$$\Delta N_2(t) = \left\{\begin{array}{l} N_2(0)e^{-\mu t}\left(\frac{\sigma_{c2}^2 Pt}{\sigma_{f2}^1 N_1^2}\right) \\ -\frac{\gamma P}{\zeta^2}\left[-\frac{P\sigma_{c2}^2}{\sigma_{f2}^1 N_1^2} + \frac{\sigma_{a1}^1\sigma_{a2}^1 P}{\sigma_{s1-2}^1\sigma_{f2}^1 N_1^2} + \frac{2\sigma_{a1}^1 N_2\sigma_{c2}^2 P}{\sigma_{s1-2}^1\sigma_{f2}^1 N_1^3} + \frac{\sigma_{a2}^1 P}{\sigma_{f2}^1 N_1^2}\right] * \left[e^{-\zeta} - e^{-\mu t}\right] \\ +\frac{\gamma P}{\zeta}\left[e^{-\zeta} * \left[\frac{\sigma_{a1}^1\sigma_{a2}^1 Pt}{\sigma_{s1-2}^1\sigma_{f2}^1 N_1^2} + \frac{2\sigma_{a1}^1 N_2\sigma_{c2}^2 Pt}{\sigma_{s1-2}^1\sigma_{f2}^1 N_1^3} + \frac{\sigma_{a2}^1 Pt}{\sigma_{f2}^1 N_1^2}\right] - e^{-\mu t}\left(\frac{\sigma_{c2}^2 Pt}{\sigma_{f2}^1 N_1^2}\right)\right] \end{array}\right\}\Delta N_1(0)$$
$$+\left\{\begin{array}{l} e^{-\mu t} + \frac{\gamma P}{\zeta^2}\frac{\sigma_{a1}^1\sigma_{c2}^2 P}{\sigma_{s1-2}^1 N_1^2\sigma_{f2}^1}\left[e^{-\zeta} - e^{-\mu t}\right] \\ -\frac{\gamma P}{\zeta}\left[e^{-\zeta}\left(\frac{\sigma_{a1}^1\sigma_{c2}^2 Pt}{\sigma_{s1-2}^1 N_1^2\sigma_{f2}^1}\right)\right] \end{array}\right\}\Delta N_2(0)$$

where $\zeta = \left(\frac{\sigma_{a1}^1\sigma_{a2}^1 Pt}{\sigma_{s1-2}^1 N_1\sigma_{f2}^1} + \frac{\sigma_{a1}^1\sigma_{c2}^2 PtN_2}{\sigma_{s1-2}^1\sigma_{f2}^1 N_1^2} + \frac{\sigma_{a2}^1 Pt}{N_1\sigma_{f2}^1}\right)$ and $\mu = \left(\frac{\sigma_{c2}^2 P}{N_1\sigma_{f2}^1} + \Lambda\right)$

The variances in the number densities are given by: $\text{var}(N_1) = E[(\Delta N_1)^2]$ and $\text{var}(N_2) = E[(\Delta N_2)^2]$.

APPENDIX 5

TRANSMUTATION EQUATIONS FOR EXAMPLE 3

The following two sets of equations are the nuclide transmutation equations used for Example 3. The original equations are presented first, and the extended equations, which are the equations used to more closely resemble SCALE are presented second.

Example 3 nuclide transmutation equations.

$$\text{U-235} \quad N_1 := N_{10} \cdot e^{-\Phi \cdot \sigma_{1a} \cdot t}$$

$$\text{U-238} \quad N_2 := N_{20} \cdot e^{-\Phi \cdot \sigma_{2a} \cdot t}$$

$$\text{Pu-239} \quad N_3 := N_{30} \cdot e^{-(\Phi \cdot \sigma_{3a} + \Lambda_3) \cdot t} + \frac{N_{20} \cdot \Phi \cdot \sigma_{2c}}{\Phi \cdot \sigma_{2a} - (\Phi \cdot \sigma_{3a} + \Lambda_3)} \cdot \left[e^{-(\Phi \cdot \sigma_{3a} + \Lambda_3) \cdot t} - e^{-\Phi \cdot \sigma_{2a} \cdot t} \right]$$

$$\text{Eu}-155 \quad N_4 := \frac{\gamma_2 \cdot \Phi \cdot \sigma_{2f} \cdot N_{20}}{\left[\Phi \cdot \sigma_{2a} - \left(\Phi \cdot \sigma_{4c} + \Lambda_4\right)\right]} \cdot \left[e^{-\left(\Phi \cdot \sigma_{4c} + \Lambda_4\right) \cdot t} - e^{-\Phi \cdot \sigma_{2a} \cdot t}\right] + N_{40} \cdot e^{-\left(\Phi \cdot \sigma_{4c} + \Lambda_4\right) \cdot t}$$

$$+ \frac{N_{10} \cdot \Phi \cdot \sigma_{1f} \cdot \gamma_4}{\Phi \cdot \sigma_{1a} - \left(\Phi \cdot \sigma_{4c} + \Lambda_4\right)} \cdot \left[e^{-\left(\Phi \cdot \sigma_{4c} + \Lambda_4\right) \cdot t} - e^{-\Phi \cdot \sigma_{1a} \cdot t}\right]$$

$$+ \frac{N_{30} \cdot \Phi \cdot \sigma_{3f} \cdot \gamma_3}{\left(\Phi \cdot \sigma_{3a} + \Lambda_3\right) - \left(\Phi \cdot \sigma_{4c} + \Lambda_4\right)} \cdot \left[e^{-\left(\Phi \cdot \sigma_{4c} + \Lambda_4\right) \cdot t} - e^{-\left(\Phi \cdot \sigma_{3a} + \Lambda_3\right) \cdot t}\right]$$

$$+ N_{20} \cdot \Phi^2 \cdot \sigma_{3f} \cdot \sigma_{2c} \cdot \gamma_3 \left[\begin{array}{l} \dfrac{1}{\left[\left(\Phi \cdot \sigma_{3a} + \Lambda_3\right) - \left(\Phi \cdot \sigma_{4c} + \Lambda_4\right)\right] \cdot \left[\left(\Phi \cdot \sigma_{2a}\right) - \left(\Phi \cdot \sigma_{4c} + \Lambda_4\right)\right]} \cdot e^{-\left(\Phi \cdot \sigma_{4c} + \Lambda_4\right) \cdot t} \\ + \dfrac{1}{\left[\left(\Phi \cdot \sigma_{4c} + \Lambda_4\right) - \left(\Phi \cdot \sigma_{3a} + \Lambda_3\right)\right] \cdot \left[\left(\Phi \cdot \sigma_{2a}\right) - \left(\Phi \cdot \sigma_{3a} + \Lambda_3\right)\right]} \cdot e^{-\left(\Phi \cdot \sigma_{3a} + \Lambda_3\right) \cdot t} \\ + \dfrac{1}{\left[\left(\Phi \cdot \sigma_{4c} + \Lambda_4\right) - \left(\Phi \cdot \sigma_{2a}\right)\right] \cdot \left[\left(\Phi \cdot \sigma_{3a} + \Lambda_3\right) - \left(\Phi \cdot \sigma_{2a}\right)\right]} \cdot e^{-\left(\Phi \cdot \sigma_{2a}\right) \cdot t} \end{array}\right]$$

Expanded nuclide transmutation equations with ^{239}U and ^{239}Np included in Example 3.

$$U-235 \qquad N_1 := N_{10}\cdot e^{-\Phi\cdot\sigma_{1a}\cdot t}$$

$$U-238 \qquad N_2 := N_{20}\cdot e^{-\Phi\cdot\sigma_{2a}\cdot t}$$

$$U-239 \qquad N_7 := N_{70}\cdot e^{-\Lambda_7\cdot t} + \frac{\Phi\cdot\sigma_{2c}\cdot N_{20}}{\left(\Phi\cdot\sigma_{2a}-\Lambda_7\right)}\cdot\left(e^{-\Lambda_7\cdot t} - e^{-\Phi\cdot\sigma_{2a}\cdot t}\right)$$

$$Np-239 \qquad N_5 := N_{50}\cdot e^{-\left(\Phi\cdot\sigma_{5a}+\Lambda_5\right)\cdot t} + \frac{\Lambda_7\cdot N_{70}}{\Lambda_7-\left(\Phi\cdot\sigma_{5a}+\Lambda_5\right)}\cdot\left[e^{-\left(\Phi\cdot\sigma_{5a}+\Lambda_5\right)\cdot t} - e^{-\Lambda_7\cdot t}\right]$$

$$+\ \Lambda_7\cdot\Phi\cdot\sigma_{2c}\cdot N_{20}\cdot\left[\frac{1}{\left[\Lambda_7-\left(\Phi\cdot\sigma_{5a}+\Lambda_5\right)\right]\cdot\left[\Phi\cdot\sigma_{2a}-\left(\Phi\cdot\sigma_{5a}+\Lambda_5\right)\right]}\cdot e^{-\left(\Phi\cdot\sigma_{5a}+\Lambda_5\right)\cdot t}\right.$$

$$+\ \frac{1}{\left[\left(\Phi\cdot\sigma_{5a}+\Lambda_5\right)-\Lambda_7\right]\cdot\left(\Phi\cdot\sigma_{2a}-\Lambda_7\right)}\cdot e^{-\Lambda_7\cdot t}$$

$$\left.+\ \frac{1}{\left[\left(\Phi\cdot\sigma_{5a}+\Lambda_5\right)-\Phi\cdot\sigma_{2a}\right]\cdot\left(\Lambda_7-\Phi\cdot\sigma_{2a}\right)}\cdot e^{-\Phi\cdot\sigma_{2a}\cdot t}\right]$$

$$\text{Pu}-239 \quad N_3 := N_{30}\cdot e^{-\left(\Phi\cdot\sigma_{3a}+\Lambda_3\right)\cdot t} + \frac{\Lambda_5\cdot N_{50}}{\left[\left(\Phi\cdot\sigma_{5a}+\Lambda_5\right)-\left(\Phi\cdot\sigma_{3a}+\Lambda_3\right)\right]}\cdot\left[e^{-\left(\Phi\cdot\sigma_{3a}+\Lambda_3\right)\cdot t} - e^{-\left(\Phi\cdot\sigma_{5a}+\Lambda_5\right)\cdot t}\right]$$

$$+ \Lambda_5\cdot\Lambda_7\cdot N_{70}\left[\frac{1}{\left[\left(\Phi\cdot\sigma_{5a}+\Lambda_5\right)-\left(\Phi\cdot\sigma_{3a}+\Lambda_3\right)\right]\cdot\left[\Lambda_7-\left(\Phi\cdot\sigma_{3a}+\Lambda_3\right)\right]}\cdot e^{-\left(\Phi\cdot\sigma_{3a}+\Lambda_3\right)\cdot t}\right.$$

$$+ \frac{1}{\left[\left(\Phi\cdot\sigma_{3a}+\Lambda_3\right)-\left(\Phi\cdot\sigma_{5a}+\Lambda_5\right)\right]\cdot\left[\Lambda_7-\left(\Phi\cdot\sigma_{5a}+\Lambda_5\right)\right]}\cdot e^{-\left(\Phi\cdot\sigma_{5a}+\Lambda_5\right)\cdot t}$$

$$\left. + \frac{1}{\left[\left(\Phi\cdot\sigma_{3a}+\Lambda_3\right)-\Lambda_7\right]\cdot\left[\left(\Phi\cdot\sigma_{5a}+\Lambda_5\right)-\Lambda_7\right]}\cdot e^{-\Lambda_7\cdot t}\right]$$

$$+ \Lambda_5\cdot\Lambda_7\cdot\Phi\cdot\sigma_{2c}\cdot N_{20}\left[\frac{1}{\left[\left(\Phi\cdot\sigma_{5a}+\Lambda_5\right)-\left(\Phi\cdot\sigma_{3a}+\Lambda_3\right)\right]\cdot\left[\Lambda_7-\left(\Phi\cdot\sigma_{3a}+\Lambda_3\right)\right]\cdot\left[\Phi\cdot\sigma_{2a}-\left(\Phi\cdot\sigma_{3a}+\Lambda_3\right)\right]}\cdot e^{-\left(\Phi\cdot\sigma_{3a}+\Lambda_3\right)\cdot t}\right.$$

$$+ \frac{1}{\left[\left(\Phi\cdot\sigma_{3a}+\Lambda_3\right)-\left(\Phi\cdot\sigma_{5a}+\Lambda_5\right)\right]\cdot\left[\Lambda_7-\left(\Phi\cdot\sigma_{5a}+\Lambda_5\right)\right]\cdot\left[\Phi\cdot\sigma_{2a}-\left(\Phi\cdot\sigma_{5a}+\Lambda_5\right)\right]}\cdot e^{-\left(\Phi\cdot\sigma_{5a}+\Lambda_5\right)\cdot t}$$

$$+ \frac{1}{\left[\left(\Phi\cdot\sigma_{3a}+\Lambda_3\right)-\Lambda_7\right]\cdot\left[\left(\Phi\cdot\sigma_{5a}+\Lambda_5\right)-\Lambda_7\right]\cdot\left(\Phi\cdot\sigma_{2a}-\Lambda_7\right)}\cdot e^{-\Lambda_7\cdot t}$$

$$\left. + \frac{1}{\left[\left(\Phi\cdot\sigma_{3a}+\Lambda_3\right)-\Phi\cdot\sigma_{2a}\right]\cdot\left[\left(\Phi\cdot\sigma_{5a}+\Lambda_5\right)-\Phi\cdot\sigma_{2a}\right]\cdot\left(\Lambda_7-\Phi\cdot\sigma_{2a}\right)}\cdot e^{-\left(\Phi\cdot\sigma_{2a}\right)\cdot t}\right]$$

This is the equation for ^{155}Eu including the terms on the following page.

$$
\begin{aligned}
Eu-155 \quad N_4 := {} & \frac{\gamma_2 \cdot \Phi \cdot \sigma_{2f} \cdot N_{20}}{\left[\Phi \cdot \sigma_{2a} - \left(\Phi \cdot \sigma_{4c} + \Lambda_4\right)\right]} \cdot \left[e^{-\left(\Phi \cdot \sigma_{4c} + \Lambda_4\right) \cdot t} - e^{-\Phi \cdot \sigma_{2a} \cdot t}\right] + N_{40} \cdot e^{-\left(\Phi \cdot \sigma_{4c} + \Lambda_4\right) \cdot t} \\
& + \frac{\gamma_4 \cdot \Phi \cdot \sigma_{1f} \cdot N_{10}}{\left[\Phi \cdot \sigma_{1a} - \left(\Phi \cdot \sigma_{4c} + \Lambda_4\right)\right]} \cdot \left[e^{-\left(\Phi \cdot \sigma_{4c} + \Lambda_4\right) \cdot t} - e^{-\Phi \cdot \sigma_{1a} \cdot t}\right] \\
& + \frac{\gamma_3 \cdot \Phi \cdot \sigma_{3f} \cdot N_{30}}{\left[\left(\Phi \cdot \sigma_{3a} + \Lambda_3\right) - \left(\Phi \cdot \sigma_{4c} + \Lambda_4\right)\right]} \cdot \left[e^{-\left(\Phi \cdot \sigma_{4c} + \Lambda_4\right) \cdot t} - e^{-\left(\Phi \cdot \sigma_{3a} + \Lambda_3\right) \cdot t}\right] \\
& + \gamma_3 \cdot \Phi \cdot \sigma_{3f} \cdot \Lambda_5 \cdot N_{50} \cdot \left[\begin{array}{l}
\dfrac{1}{\left[\left(\Phi \cdot \sigma_{3a} + \Lambda_3\right) - \left(\Phi \cdot \sigma_{4c} + \Lambda_4\right)\right] \cdot \left[\left(\Phi \cdot \sigma_{5a} + \Lambda_5\right) - \left(\Phi \cdot \sigma_{4c} + \Lambda_4\right)\right]} \cdot e^{-\left(\Phi \cdot \sigma_{4c} + \Lambda_4\right) \cdot t} \\
+ \dfrac{1}{\left[\left(\Phi \cdot \sigma_{4c} + \Lambda_4\right) - \left(\Phi \cdot \sigma_{3a} + \Lambda_3\right)\right] \cdot \left[\left(\Phi \cdot \sigma_{5a} + \Lambda_5\right) - \left(\Phi \cdot \sigma_{3a} + \Lambda_3\right)\right]} \cdot e^{-\left(\Phi \cdot \sigma_{3a} + \Lambda_3\right) \cdot t} \\
+ \dfrac{1}{\left[\left(\Phi \cdot \sigma_{4c} + \Lambda_4\right) - \left(\Phi \cdot \sigma_{5a} + \Lambda_5\right)\right] \cdot \left[\left(\Phi \cdot \sigma_{3a} + \Lambda_3\right) - \left(\Phi \cdot \sigma_{5a} + \Lambda_5\right)\right]} \cdot e^{-\left(\Phi \cdot \sigma_{5a} + \Lambda_5\right) \cdot t}
\end{array}\right]
\end{aligned}
$$

$$+ \gamma_3 \cdot \Phi \cdot \sigma_{3f} \cdot \Lambda_5 \cdot \Lambda_7 \cdot N_{70} \cdot \left[\begin{array}{l} \dfrac{1}{\left[(\Phi \cdot \sigma_{3a} + \Lambda_3) - (\Phi \cdot \sigma_{4c} + \Lambda_4)\right] \cdot \left[(\Phi \cdot \sigma_{5a} + \Lambda_5) - (\Phi \cdot \sigma_{4c} + \Lambda_4)\right] \cdot \left[\Lambda_7 - (\Phi \cdot \sigma_{4c} + \Lambda_4)\right]} \cdot e^{-(\Phi \cdot \sigma_{4c} + \Lambda_4) \cdot t} \\ + \dfrac{1}{\left[(\Phi \cdot \sigma_{4c} + \Lambda_4) - (\Phi \cdot \sigma_{3a} + \Lambda_3)\right] \cdot \left[(\Phi \cdot \sigma_{5a} + \Lambda_5) - (\Phi \cdot \sigma_{3a} + \Lambda_3)\right] \cdot \left[\Lambda_7 - (\Phi \cdot \sigma_{3a} + \Lambda_3)\right]} \cdot e^{-(\Phi \cdot \sigma_{3a} + \Lambda_3) \cdot t} \\ + \dfrac{1}{\left[(\Phi \cdot \sigma_{4c} + \Lambda_4) - (\Phi \cdot \sigma_{5a} + \Lambda_5)\right] \cdot \left[(\Phi \cdot \sigma_{3a} + \Lambda_3) - (\Phi \cdot \sigma_{5a} + \Lambda_5)\right] \cdot \left[\Lambda_7 - (\Phi \cdot \sigma_{5a} + \Lambda_5)\right]} \cdot e^{-(\Phi \cdot \sigma_{5a} + \Lambda_5) \cdot t} \\ + \dfrac{1}{\left[(\Phi \cdot \sigma_{4c} + \Lambda_4) - \Lambda_7\right] \cdot \left[(\Phi \cdot \sigma_{3a} + \Lambda_3) - \Lambda_7\right] \cdot \left[(\Phi \cdot \sigma_{5a} + \Lambda_5) - \Lambda_7\right]} \cdot e^{-\Lambda_7 \cdot t} \end{array} \right]$$

$$+ \gamma_3 \cdot \Phi^2 \cdot \sigma_{3f} \cdot \Lambda_5 \cdot \Lambda_7 \cdot \sigma_{2c} \cdot N_{20} \cdot \left[\begin{array}{l} \dfrac{1}{\left[(\Phi \cdot \sigma_{3a} + \Lambda_3) - (\Phi \cdot \sigma_{4c} + \Lambda_4)\right] \cdot \left[(\Phi \cdot \sigma_{5a} + \Lambda_5) - (\Phi \cdot \sigma_{4c} + \Lambda_4)\right] \cdot \left[\Lambda_7 - (\Phi \cdot \sigma_{4c} + \Lambda_4)\right] \cdot \left[\Phi \cdot \sigma_{2a} - (\Phi \cdot \sigma_{4c} + \Lambda_4)\right]} \cdot e^{-(\Phi \cdot \sigma_{4c} + \Lambda_4) \cdot t} \\ + \dfrac{1}{\left[(\Phi \cdot \sigma_{4c} + \Lambda_4) - (\Phi \cdot \sigma_{3a} + \Lambda_3)\right] \cdot \left[(\Phi \cdot \sigma_{5a} + \Lambda_5) - (\Phi \cdot \sigma_{3a} + \Lambda_3)\right] \cdot \left[\Lambda_7 - (\Phi \cdot \sigma_{3a} + \Lambda_3)\right] \cdot \left[\Phi \cdot \sigma_{2a} - (\Phi \cdot \sigma_{3a} + \Lambda_3)\right]} \cdot e^{-(\Phi \cdot \sigma_{3a} + \Lambda_3) \cdot t} \\ + \dfrac{1}{\left[(\Phi \cdot \sigma_{4c} + \Lambda_4) - (\Phi \cdot \sigma_{5a} + \Lambda_5)\right] \cdot \left[(\Phi \cdot \sigma_{3a} + \Lambda_3) - (\Phi \cdot \sigma_{5a} + \Lambda_5)\right] \cdot \left[\Lambda_7 - (\Phi \cdot \sigma_{5a} + \Lambda_5)\right] \cdot \left[\Phi \cdot \sigma_{2a} - (\Phi \cdot \sigma_{5a} + \Lambda_5)\right]} \cdot e^{-(\Phi \cdot \sigma_{5a} + \Lambda_5) \cdot t} \\ + \dfrac{1}{\left[(\Phi \cdot \sigma_{4c} + \Lambda_4) - \Lambda_7\right] \cdot \left[(\Phi \cdot \sigma_{3a} + \Lambda_3) - \Lambda_7\right] \cdot \left[(\Phi \cdot \sigma_{5a} + \Lambda_5) - \Lambda_7\right] \cdot (\Phi \cdot \sigma_{2a} - \Lambda_7)} \cdot e^{-\Lambda_7 \cdot t} \\ + \dfrac{1}{\left[(\Phi \cdot \sigma_{4c} + \Lambda_4) - \Phi \cdot \sigma_{2a}\right] \cdot \left[(\Phi \cdot \sigma_{3a} + \Lambda_3) - \Phi \cdot \sigma_{2a}\right] \cdot \left[(\Phi \cdot \sigma_{5a} + \Lambda_5) - \Phi \cdot \sigma_{2a}\right] \cdot (\Lambda_7 - \Phi \cdot \sigma_{2a})} \cdot e^{-(\Phi \cdot \sigma_{2a}) \cdot t} \end{array} \right]$$

APPENDIX 6

SAMPLE OF MONTE CARLO SIMULATION DECK

The following is an example of an input deck used to run SCALE with the Monte Carlo method being called to calculate the flux shape. The deck is an illustration for Example 3 in this research.

```
=shell
 copy c:\scale6\data\xn238v6 ft88f001
end
=malocs
0$$ 88 89
1$$ 238 3 a5 1 e t
4$$ 27r1 172r2 39r3
t
end
=csas25  parm=nitawl
Test problem
'example 3 with KENO
'3 group 4 nuclide example
'5.0 wt% U-235
ft89f001
read comp
'fuel
u-235 1 0 0.494374214307702097132 end
u-238 1 0 9.27519969625904808055 end
np-239 1 0 0.000028747811392092781691048 end 'caprection
pm-149 1 0 2.4439437849901783552196e-7 end 'fp
h2o 3 1.0 end
end comp
read celldata
latticecell squarepitch pitch=1.25984 3 fuelr=0.47483 1 end
end celldata
'***************
'* begining of KENO model input
'***************
read parm
    cfx=yes gen=1100 nsk=100 npg=1000 flx=yes plt=yes
    xs1=yes xs2=yes
```

```
    rnd=3BAF0299538C6FE0
end parm
read geom
global unit 1
com='fuel rod'
cylinder 1 1 0.47483 365.8 0.0
cuboid   3 1 0.62992 -0.62992 0.62992 -0.62992 365.8 0.0
end geom
read bounds all=refl end bounds
end data
end model
'****************
'* end of KENO model input
'****************
end
=paleale
0$$ 89 0
1$$ 4
2$$ 1 0 0 0 0 0 0 0 0 0
7$$ 1 18 27 101 102 2 3 452 459 191r0
t
11$$ 92235 92238 93239 61149
t
end
=paleale
0$$ 0 04
1$$ 4
2$$ 1 0 0 0 0 0 0 0 0 0
4$$ 1 99r0
7$$ 1 18 27 101 102 2 3 452 459 191r0
t
11$$ 1092235 1092238 1093239 1061149
t
end
```

APPENDIX 7

CUSTOM BUILT LIBRARIES FOR SCALE SIMULATIONS

Custom decay and nuclear reaction libraries are built to use in SCALE for the validation part of this research. The libraries include only the nuclides of interest (^{235}U, ^{238}U, ^{239}Pu, and ^{155}Eu) and any needed supporting nuclides (like hydrogen and oxygen isotopes) for this research. The libraries are made in order to eliminate any basis between SCALE and the equations derived in this research.

APPENDIX 8

INFORMATIONAL FLOW CHARTS

The following flow charts are provided to help visualize the flow of information in the equations. Figure 62 shows the types of uncertainty and how the uncertainty is passed from one term to another. Figure 63 shows how the information advances in the calculation.

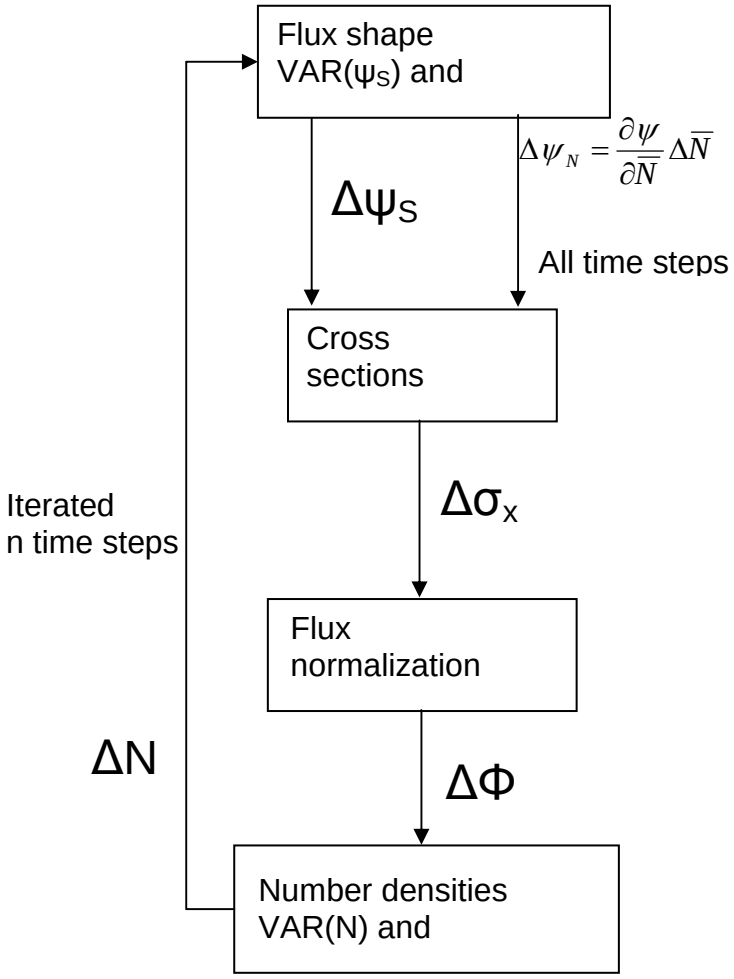

Figure 62. Uncertainty flow chart.

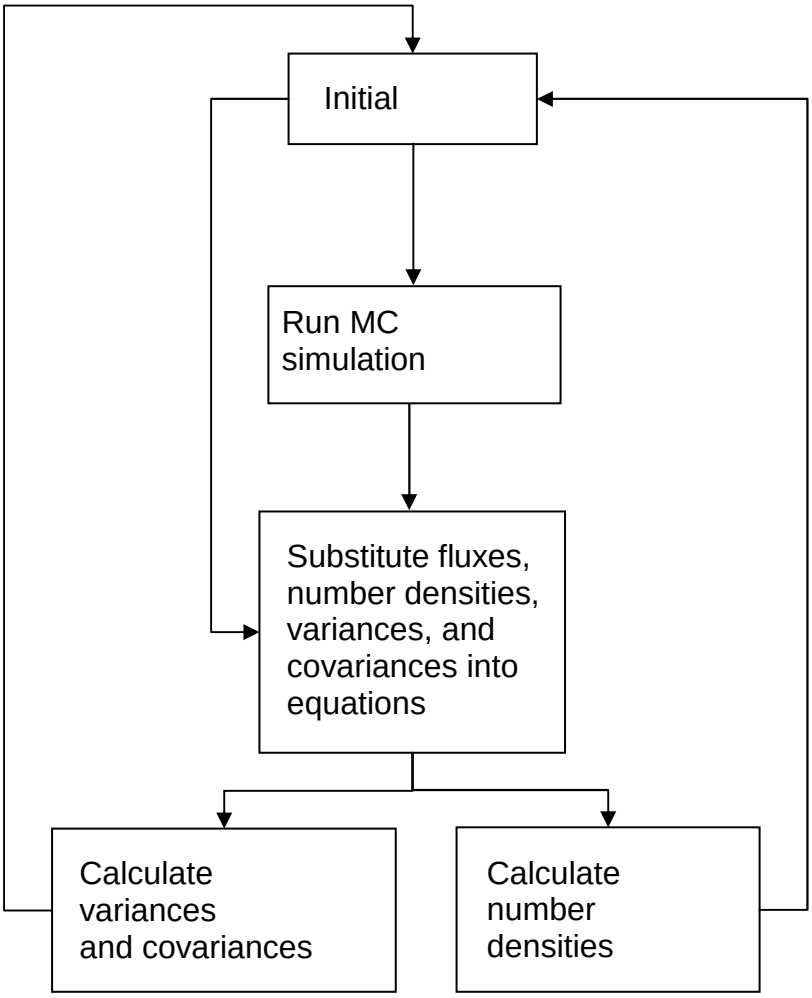

Figure 63. Calculational flow chart.

APPENDIX 9

NUMBER OF LIBRARIES PER CYCLE

The number of libraries per cycle was not fully discussed in this paper. The research focused on the methodology for the statistical uncertainty propagation. As the number of libraries per cycle can be very important in the reactor calculation, like when properties change rapidly, it is not as important in the statistical uncertainty propagation and is discussed here. In TRITON users can set the number of cross section libraries produced per cycle that can be used to force more cross section and concentration updates per cycle. This allows for greater refinement of the cross sections and the concentrations during the cycle depletion time step size by allowing more intermediate steps within each cycle, which results in more transport and depletion steps in each cycle [15]. The number of libraries per cycle will affect both Monte Carlo and deterministic calculations [22].

In this research, the statistical uncertainty propagation is calculated after each depletion time step. If the number of depletion calculations is increased during a cycle, then the statistical uncertainty propagation calculation is increased by that same number of calculations.

Table 42 shows the comparison of one 30-day time step (step4 at 120 days) and three 10-day time steps (from step3 at 90 days to step4 at 120 days). Table 42 shows that the calculated number densities are very close to each other and that the relative uncertainty in the number densities is of the same order of magnitude. Differences in the relative uncertainty of the nuclide number densities can be attributed to differences in the number

density distribution, changes in the mean of the distribution, and any shifts in the distribution [22].

Table 42. Different libraries per cycle.

Example 3 with different size time steps						
With 10 day time steps going from step 3 to step 4						With 30 time steps
Time (days)			100	110	120	120
Time step			Step3.1	Step3.2	Step4	Step4
		N_1	4.618E+23	4.587E+23	4.555E+23	4.555E+23
		N_2	9.262E+24	9.261E+24	9.259E+24	9.259E+24
		N_3	1.050E+22	1.151E+22	1.251E+22	1.251E+22
		N_4	1.254E+15	1.425E+15	1.602E+15	1.601E+15
		$sd(N_1)$	4.954E-06	5.088E-06	5.197E-06	5.717E-06
		$sd(N_2)$	7.746E-07	7.872E-07	7.974E-07	8.838E-07
		$sd(N_3)$	4.999E-04	4.546E-04	4.164E-04	4.828E-04
Approximate	Relative	$sd(N_4)$	3.202E-04	3.153E-04	3.096E-04	3.135E-04

LIST OF REFERENCES

1. Bowman, S.M. and D.F. Gill. 2006. Validation of Standardized Computer Analyses for Licensing Evaluation/TRITON Two-Dimensional and Three-Dimensional Models for Light Water Reactor Fuel. http://www.ornl.gov/~webworks/cppr/y2001/pres/124965.pdf.

2. DeHart, M. D. 1996. *Sensitivity and Parametric Evaluations of Significant Aspects of Burnup Credit for PWR Spent Fuel Packages*. Oak Ridge, TN: Oak Ridge National Laboratory. ORNL/TM-12973.

3. DeHart, M. D. and S.M. Bowman. 2006. *Improved Radiochemical Assay Analysis Using TRITON Depletion Sequences in SCALE*. IAEA Conference Paper.

4. DeHart, Mark D. and Lester M. Petrie. A Radioisotope Depletion Method Using Monte Carlo Transport with Variance Reduction and Error Propagation. http://www.ornl.gov/~webworks/cppr/y2001/pres/118835.pdf.

5. Diamond, David J. 2003. *Generation IV Nuclear Energy Systems: How They Got Here and Where They Are Going*. Brookhaven National Laboratory. Presented at the University of Tennessee, April 30, 2003.

6. Duderstadt, James J., and Louis J Hamilton. 1976. *Nuclear Reactor Analysis*. Ann Arbor, MI: John Wiley & Sons.

7. Garcia-Herranz, Nuria, et al. 2008. Propagation of Statistical and Nuclear Data Uncertainties in Monte Carlo Burn-up Calculations. *Annals of Nuclear Energy* 35: 714-730.

8. Hayter, Anthony J. 1996. *Probability and Statistics for Engineers and Scientists*. Boston: PWS Publishing Company.

9. Hendricks, Jon S. et al. 2008. *MCNPX 2.6.0 Extensions*. Los Alamos, New Mexico: Los Alamos National Laboratory. LA-UR-08-2216.

10. James, M.R., et al. 2007. *MCNPX – New Features Demonstrated: Burnup/Depletion and Delayed Gammas*. 13th UK Monte Carlo User Group Meeting (MCNEG 2007). Teddington, UK, March 28-29, 2007.

11. Japan Science and Technology Agency. 2006-2007. SWAT2: The Improved SWAT Code System by Incorporating the Continuous Energy Monte Carlo Code MVP. http://sciencelinks.jp/j-east/article/200403/000020040303A0828408.php.

12. KAPL Inc. 2002. *Nuclides and Isotopes Chart of the Nuclides 16th Edition*.

13. Lewis, E.E. and W.F. Miller Jr. 1984. *Computational Methods of Neutron Transport*. New York: John Wiley & Sons.

14. NEA. 2002. MCB1C, Monte-Carlo Continuous Energy Burnup Code. France: OECD Nuclear Energy Agency. http://www.nea.fr/abs/html/nea-1643.html.

15. Oak Ridge National Laboratory. 2009. *SCALE: A Modular Code System for Performing Standardized Computer Analyses for Licensing Evaluation Version 6 Vols. I–III*. Oak Ridge, TN: Oak Ridge National Laboratory. ORNL/TM-2005/39.

16. Oberhettinger, F., and L. Badii. 1973. *Tables of Laplace Transforms*. New York: Springer-Verlag.

17. Office of Nuclear Energy, Office of Advanced Scientific Computing Research, and U.S. Department of Energy. 2006. *Workshop on Simulation and Modeling for Advanced Nuclear Energy Systems*. Washington D.C.

18. SCK CEN. ALEPH: An Optimal Approach to Monte Carlo Burn-Up. http://www.sckcen.be/sckcen/ScientificReports/2006/4_br2/pdf/01_sr2006_wimhaeck.pdf (2006).

19. Shim, Hyung Jin, et al. 2008. Uncertainty Propagation in Monte Carlo Depletion Analysis. In *International Conference on the Physics of Reactors "Nuclear Power: A Sustainable Resource* held in Casino-Kursaal Conference Center Interlaken, Switzerland 14-19 September 2008.

20. Strang, Gilbert. 1976. *Linear Algebra and Its Applications*. New York: Academic Press, Inc.

21. Takeda, Toshikazu, Naoki Hirokawa, and Tomohiro Noda. 1999. Estimation of Error Propagation in Monte-Carlo Burnup Calculations. *Journal of Nuclear Science and Technology* 36, no. 9 (September): 738-745.

22. Tohjoh, Masayuki, et al. 2006. Effect of Error Propagation of Nuclide Number Densities on Monte Carlo Burn-up Calculations. *Annals of Nuclear Energy* 33: 1424-1436.

23. Turabian, Kate L. 1996. *A Manual for Writers of Term Papers, Theses, and Dissertations*. Chicago: The University of Chicago Press.

24. Wagner, J. C. Addressing the Axial Burnup Distribution in PWR Burnup Credit Criticality Safety Analyses. Oak Ridge National Laboratory. http://www.ornl.gov/sci/radiation_transport_criticality/WagnerPubs/wagner_ncsd2001_axial-burnup.pdf.

25. Wagner, J. C. and M. D. DeHart. 2000. *Review of Axial Burnup Distribution Considerations for Burnup Credit Calculations*. Oak Ridge, TN: Oak Ridge National Laboratory. ORNL/TM-1999/246.

26. Williams, M. L. 1979. *Perturbation and Sensitivity Theory for Reactor Burnup Analysis*. Oak Ridge, TN: Oak Ridge National Laboratory. ORNL/TM-7096.

27. X-5 Monte Carlo Team. 2003. *MCNP – A General Monte Carlo N-Particle Transport Code, Version 5*. Los Alamos, NM: Los Alamos National Laboratory. LA-UR-03-1987.

VITA

After graduating from high school, he entered The University of Texas at Austin in the Fall of 1999. Quentin received his Bachelor of Science in Mechanical Engineering in 2003 and his Master of Science Engineering in Mechanical Engineering in 2005, both with a technical area of Nuclear Engineering, from the University of Texas at Austin. After receiving his Masters, he decided to pursue a Doctoral Degree in Mechanical Engineering, with a specialization in Nuclear Engineering, and was invited to the University of Nevada, Las Vegas by Dr. Denis Beller. While attending UNLV, he met Dr. Charlotta Sanders, who helped him receive internships at Bechtel SAIC Company, LLC working on the Yucca Mountain Project, Holtec International, and Oak Ridge National Laboratory in the Nuclear Engineering Student Laboratory Synthesis (NESLS) program. After completing his Ph.D. program, Quentin plans to pursue a career in nuclear reactor research.

This dissertation was typed by the author.